Modulation of neuronal activity using magnetic nanoparticles and magnetic field stimulation – a computational modeling study

Nahid Taheri

Mestrado em Física Médica

Faculdade de Ciências da Universidade de Porto

Supervisor: Paulo de Castro Aguiar
Co-Supervisor: Joaquim Agostinho Moreira

Acknowledgments

I thank my dissertation advisors Dr. Paulo Aguiar and Dr. Joaquim Moreira. Their encouragement and advice has made the study and redaction of this thesis a very rewarding experience, with many challenges and hard work.

Additionally, I could not have accomplished what I have without the love and support of my family. I express my gratitude for their moral and financial support during my years of study. Finally, I would like to address special thanks to my husband for his assistance and encouragement.

Nahid Taheri

Abstract

This work focused on modeling and simulating the conditions in which external radio-frequency magnetic fields can be effectively and safely used to activate neurons expressing temperature sensitive transient receptor potential cation channels, subfamily V member 1 (TRPV1).

Advances in different fields of science such as nanotechnology and neuroscience leads to the pursuit of new methods to achieve neuronal stimulation/modulation. An innovative method for remote control of neuronal activity has recently been achieved through combination of magnetic nanoparticles and magnetic stimulation. Magnetic nanoparticles (e.g. iron oxide based) submitted to tuned magnetic fields convert the magnetic energy to local heat. The change in temperature is within the range that activates neuronal TRPV1 channels, which are one of the principal, ubiquitous, thermal sensors/transducers in the nervous system - thermal energy stimulates these channels and an action potential (AP) is produced (or facilitated) in the neural membrane. Although many studies have addressed the effect of temperature on neural ionic channels, the mechanism of temperature sensitivity is still obscure. More importantly, the details on the temperature-dependent dynamics of the interaction between (AP)s generating channels and TRPV1 channels are unknown.

The main goal of this study was to describe, in high biophysical detail, the neuronal membrane electrophysiological mechanisms behind AP generation by magneto-thermal stimulation. This implicated the development and simulation of biologically realistic models of neuronal membrane dynamics, including the contribution of temperature on the gating mechanism of the core membrane channels: sodium (Na_V), potassium (K_V), calcium (Ca_V) and TRPV1 channels. For the mathematical description of the channels' dynamics, we used the Hodgkin and Huxley conductance formalism/models. The dynamics of TRPV1 channels are directly gated by temperature, however they are also voltage dependent; on the other hand, sodium, potassium and calcium voltage-gated channels have their kinetics modulated by temperature; their synergistic interactions are far from understood. The NEURON simulation environment, a well-established computational tool for theoretical / *in silico* neuroscience, was used to develop and

simulate our models. Specific stimulation protocols were designed and applied to assess neuronal responses. With these stimulation protocols, we analyzed the combined behavior of the voltage-gated channels during electrical stimulations and at different temperatures (as produced by magneto-thermal stimulation).

In this work, we constructed the first computational model for TRPV1 channels. The results of simulations with this model were validated and a good match to experimental records was observed. With the goal of understanding the behavior of TRPV1 channels, several simulations were designed and interesting results were reached. As an example, results show that AP does not occur at temperatures higher than about 40^oC when TRPV1 channels are not expressed in the membrane. TRPV1 channels are responsible for generation of APs in the temperature range of 40^oC to 51^oC. Interestingly, a different trend for Ca_V channels gating was recorded at 43^oC which is an important temperature level for activation of TRPV1 channels. It can be concluded that Ca_V channels may have an important role in gating process of TRPV1s. The produced biophysical models of the neuronal membrane also allowed us to uncover the combined contributions of the temperature- and voltage-gated channels in the process of AP generation upon magneto-thermal stimulation. This allows optimization of future systems using this type of stimulation. Finally, a novel quantal model is put forward as an aid to explain the behavior of ionic channels when thermal stimulation changes the temperature of the system and cause neural impulses. Using basic rules of thermodynamics, the behavior of channels under thermal and electrical stimulation is formalized. It is suggested that this model can be applied to find the mechanisms of a wide range of channel type under a wide range of physical stimulation. In fact, it is indicated that channels use the easiest way to consume energy for gating. The gate to activate/deactivate uses any type of energy that matches well with the gating requirements (in the case of energy amount and frequency). Thereafter, this model is investigated for TRPV1 and voltage gated channels in general. This leads to mathematical equations describing the gating process when heat and/or current is 'injected' to the membrane. The constructed model shows that exposure of heat increases the entropy and enthalpy of the system to a threshold value which provides the required conditions for generation of TRPV1-caused spikes. The results of simulations with this model matches well experimental data. In addition, our model addresses key problems arising from the use of the temperature factor (Q_{10}) for the description of temperature dependence.

Key words: neuron, soma, TRPV1, Hodgkin and Huxley, ionic channel, temperature, Gibbs energy

Table of Contents

Abstract IV
Chapter 1 X
Introduction .....- 1 -
Chapter 2 .....- 5 -
Literature Review .....- 5 -
Heating of ionic channels by magnetic stimulation of nanoparticles .....- 5 -
Membrane potential .....- 6 -
Electrical circuits help explain neural functions .....- 9 -
Hodgkin and Huxley model for equivalent circuit of $\boldsymbol{NaV}$, $\boldsymbol{KV}$, $\boldsymbol{ClV}$ channels.....- 11 -
Action Potential .....- 13 -
Potassium current .....- 15 -
Sodium current .....- 18 -
Leak current .....- 19 -
Summary of HH model: .....- 19 -
Effect of temperature .....- 20 -
Voltage gated Calcium currents .....- 21 -
Transition State Theory .....- 22 -
TRP channels .....- 23 -
Effect of Magnetic field .....- 23 -
Basic principles .....- 23 -
NEURON software .....- 30 -
Creating a simple compartment .....- 30 -
Inserting the properties of the membrane .....- 32 -
Injection of current: .....- 32 -
How to run the simulation? .....- 34 -
Modeling by graphical interface .....- 34 -
Kirchhoff's law: .....- 35 -

Neuronal Network ..... - 37 -
Figures generation ..... - 40 -
Chapter 3 ..... - 41 -
Effect of temperature on voltage gated sodium, potassium and calcium channels ..- 41 -
Methods and Settings ..... - 41 -
Result 1: Membrane voltage versus time ..... - 42 -
Result 2: Gating parameters ..... - 45 -
Effect of thermal and electrical stimulation in VClamp condition ..... - 47 -
Result 1 : Effect of temperature on time constant ..... - 47 -
Result 2: Gate number versus temperature and voltage ..... - 48 -
Chapter 4 ..... - 51 -
A code for TRPV1 ..... - 51 -
Experiments on dependence of TRPV1 on membrane voltage ..... - 51 -
Results of simulations for voltage dependency of TRPV1 ..... - 52 -
Chapter 5 ..... - 58 -
Simulation: Role pf TRPV1 channels in membrane stimulations ..... - 58 -
Simulation settings ..... - 58 -
Result 1: Simulation of Pulses caused by alteration of temperature ..... - 59 -
Result 2: Membrane potential perturbations ..... - 60 -
Result 3: Contribution of $\boldsymbol{CaV, NaV, KV}$ channels in membrane potential variations ..- 63 -
Result 4: Threshold values ..... - 67 -
Result 5: Series of APs ..... - 68 -
Chapter 6 ..... - 71 -
A mathematical model for ionic channels ..... - 71 -
Theory and Facts ..... - 71 -
New Model ..... - 72 -
Calculations ..... - 73 -
Conditions ..... - 77 -

Model for TRPV1 and voltage gated sodium and potassium channels ..... - 77 -
Chapter 7 ..... - 81 -
Conclusions & Discussion ..... - 81 -
Conclusions ..... - 81 -
Discussion ..... - 83 -
Further research ..... - 84 -
References ..... - 85 -

List of Figures

2.1 Schematic illustration of nerve magnetic stimulation 6
2.2 Cell membrane and pumps 8
2.3 Consideration of membrane lipid as a capacitor 10
2.4 Consideration of ionic channel as a resistor 11
2.5 Voltage Clamp technique 12
2.6 HH circuit model 12
2.7 Stages of action potential 13
2.8 Time curse of potassium conductance 16
2.9 Adjusting the power of potassium gating number 17
2.10 Rate constants of potassium conductance as a function of voltage..... 17
2.11 Time curse of sodium conductance 18
2.12 Time evolution of membrane potential during the action potential 20
2.13 TMS technique 25
2.14 Magnetic stimulation of a culture in the form of a ring 26
2.15 Compartments of HH model in NEURON 30
2.16 Modeling in Neuron by graphical interface 34
2.17 Chain of components connected each other in NEURON 37
2.18 Construction of a complex network of nerves in NEURON 37
2.19 Connection of independent segments of soma and dendrites 38
3.1 Initial settings for our simulations with ICLAMP technique 42
3.2 Reaction of soma to the injection of current at various temperatures 43
3.3 Voltage difference, rate and duration of spikes at different temperatures 44
3.4 Changes of the spike durations (spike width) with temperature 44
3.5 fraction of gating number of Na_V and K_V at different temperatures 45
3.6 maximum percentage of gating numbers 46
3.7 Activation percentage versus membrane voltage 47
3.8 Time constant for m,h and n gates versus time 48
3.9 Fraction of m,h and n gates due to change in voltage and temperature 49
3.10 Fraction of activated gate numbers versus voltage an temperature(3-D) 50
4.1 Initial settings for simulation of the TRPV1 channels 53

4.2 Comparing the simulated function of TRPV1s with experimental records …….. 54
4.3 Simulation settings for measurement of effect of voltage changes on TRPV1 … 55
4.4 Effect of variation in the injected voltage to dynamics of TRPV1 channels ……. 56
4.5 Settings for simulation of opening probability of TRPV1s at different voltages and temperatures …… 57
4.6 Comparing opening probability-V of TRPV1 with experimental data …… 57
5.1 ICLAMP settings for TRPV1 and voltage gated channels …….. 59
5.2 Membrane voltage versus temperature with 0nA current injection ……. 59
5.3 V-time graph for electric stimulation of voltage gated channels ……..... 60
5.4 V-time graph for electric stimulation of voltage gated and TRPV1 channels …. 61
5.5 Details of V-time graph for the spikes at different temperatures ……... 62
5.6 proportion of activated m_∞ and $nTRPV1_\infty$ at different temperatures ……. 63
5.7 $m_\infty, h_\infty, n_\infty$ and $nTRPV1_\infty$ during curent injection at 36 and 40^oC …….. 64
5.8 $m_\infty, h_\infty, n_\infty$ and $nTRPV1_\infty$ during curent injection at 43 and 45^oC ……... 64
5.9 Percentage of considered $gate\text{-}number_\infty$ at different temperatures …… 65
5.10 Time constant for m, h,n and nTRPV1 gates in different temperatures ……. 66
5.11 Fraction of voltage gated and TRPV1 gating numbers at 40^oC ……. 67
5.12 V-time graph for voltage gated channels with and without TRPV1s at 55^oC …. 67
5.13 $I_{threshold}$-temperature with and without TRPV1s …….. 68
5.14 Graphs of V-t at different temperatures and injected currents ……. 69
5.15 firing rate of APs versus temperature …….. 70
6.1 (Logarithm of) Opening probability- temperature for Na_V, K_V and TRPV1s …… 80
6.2 (Logarithm of) Opening probability- voltage for Na_V, K_V and TRPV1s …… 80

List of Tables

2.1 Model parameters of neuron cell ……..... 27

2.2 Default properties of nerve a section …….. 31

2.3 Default properties of the pas channel …… 32

Chapter 1

Introduction

Neurons are the basic element of the nervous system. Despite of the different responses of the nervous system to various stimulations, similar fundamental mechanisms underlie their response to the physical inputs. Ionic channels are pores in lipid bilayer, which allow certain ions to pass in response to the changes in the neuron environment and generate electrical neural impulses. Studying the gating mechanism of these channels helps to understand the behavior of neurons in particular circumstances.

Several techniques are used in both research and clinical approaches to control the nerve behavior by modulating the activity of ionic channels. In electric stimulation, injection of a specific amount of current changes membrane potential. Since the voltage gated ionic channels depend strongly on the membrane voltage, they start to show reaction and generate APs. Therefore, electrical stimulation is capable to control the signaling process of neurons. Another technique used for signal controlling is named optogenetic, which involves the use of light to control the kinetics of ion flux through light-sensitive ion channels. However, since visible light does not penetrate deep into tissues, optical stimulation approach also requires implantation of an optical fiber. Therefore, despite of several advantages, these techniques are invasive because of the requirement of surgical implantations. In this thesis, we discuss an alternative non-invasive technique of magnetic stimulation and the roles it plays for gating the ionic channels.

In magneto thermo genetics technique, superparamagnetic ferrite nanoparticles are targeted to the membrane plasma expressing Transient Receptor Potential type V member 1 (TRPV1) channels. Application of magnetic field heats the nano-labeled membrane and so temperature sensitive TRPV1 channels are activated. In this technique, magnetic field is applied remotely to stimulate the nanomagnets attached to the neuron membrane. The applied magnetic field interacts very weakly with biological molecules but the depth of penetration is large. These properties results in noninvasive magnetic therapy techniques that are used for treatment of various neurological disorders. Contribution of several factors such as voltage, magnetic and particularly thermal stimulation results in generation of an action potential. One way to understand

the involvement of each stimulation factor is computing their effect on the conductance of ionic channels on a single nerve cell[1] .

Hodgkin and Huxley or HH mathematical model is one of the quantitative models that describes the behavior of the membrane potential under various conditions [2]. In this model, Voltage Clamp amplifier is used in space clamp configuration to study the current carried mostly by sodium and potassium ions. Since temperature has strong effect on the behavior of voltage gated channels, a temperature coefficient is used to quantify this dependence.

HH model can only be solved numerically, and although several software packages include the appropriate numerical methods to solve HH equations, Neuron software provides a flexible numerical environment for modeling and study of neuroscience including the possibility of using databases and software tools. The NMODEL language can be used to add new components by specification of reaction and diffusion systems[3]. This simulation environment is suitable for modeling individual neurons and neuron networks. NEURON software has tools to simulate the behavior of voltage gated channels at different membrane temperatures. In this work, this simulation environment, and its associated numerical methods are used to create biophysically detailed neuronal models and to assess the impact thermos-stimulation of magnetic nanoparticles. Namely, the profile, rate and threshold value of action potentials generated on a soma membrane are analyzed as a function of thermos/magnetic-stimulation parameters.

Studding the effect of temperature on dynamics of voltage gated channels provide a general perspective for function of Transient Receptor Potential (TRP) channels that are the main candidates responsible for generation of action potential caused by magnetic nanoparticles thermo stimulation. The mechanism of its interaction with biological cells is still unknown. Using NEURON software programming environment, we constructed a computational model for simulating voltage sensitivity of TRPV1 channels . Thereafter, several simulations are designed to evaluate the mechanism of TRPV1 channels during electrical stimulation at different initial temperatures on a single soma that includes voltage gated $Ca_V, Na_V \; and \; K_V$ channels on its membrane.

Furthermore, considering basic roles of thermodynamic, we present a mathematical model that suggests a unifying framework for the function of voltage gated and temperature sensitive channels. These expressions enable us to compare the contribution of thermal and electrical stimulation factors on voltage gated and temperature sensitive channels and find the mechanism of AP generated by temperature changes in the environment of TRPV1s. Since physical base roles are utilized in this

model, and the channels are considered as (an) energy barrier(s), it is possible to investigate this model for all types of ionic channels under all types of physical or even chemical stimulations.

The work presented here have the following main contributions:

1. Using HH model in NEURON to simulate the kinetics of ion flux through voltage-gated $Na_V, k_V\ and\ Ca_V$ channels when a specific amount of current is injected in the membrane. Then the results are analyzed in MATLAB.

2. Construction of the first computational model for behavior of TRPV1 channels under electric stimulation and at different initial temperatures.

3. Comparing the behavior of a soma under electric stimulation in the case that only voltage gated channels are inserted to the simulation and the case that TRPV1 channel model is added to the simulation construction.

5. Introdusing a mathematical model by basic thermodynamic roles that not only suggests a mathematical expression for temperature-caused gating of TRPV1 channels but also it is capable to include the expressions for effect of other types of stimuli on TRPV1 and other types of channels.

Overall, we studied the effect of temperature in two aspects: 1- numerical method that the results of simulations and model constructions are presented in chapters 3 to 5 and 2- suggestion of a mathematical model with physical perspective that is explained in chapter 6.

Chapter 2 reviews the general properties of neuron membrane and mathematical models for generation of spikes focusing on certain aspects of ionic channels, HH model,Goldman-Hodjkin-Kats (GHK)flux equation, TRP family and effect of electrical, thermal and magnetic stimulation on ionic channels.

In chapter 3, the results of simulations about different effects of temperature on voltage gated sodium, potassium and calcium channels is presented using NEURON software and MATLAB.

Chapter 4 presents the numerical model we instructed for voltage sensitivity of TRPV1 channels at different initial temperatures. It concludes the methods we used to reach this approach. At the end of this chapter, several simulations are designed to check if our model matches well with the experimental records of Voets et al [4].

Chapter 5 presents the results of simulations about the condition that TRPV1 model is inserted on a soma that includes voltage gated Na_V, K_V and Ca_V channels and is applied electric stimulation. This chapter compare the effect of electric exposure on soma at different initial temperatures.

Finally, in chapter6, several mathematical formulas are derived and a quantal model is generated to describe the mechanism of temperature-caused AP by TRPV1 channels. In addition, this model includes the effect of voltage on TRPV1 as well as voltage gated channels.

Chapter 2

Literature Review

In this chapter, we explain the method for remote activation of the ionic channels. Additionally, the action potential (AP), physiological concepts and several methods that can be used to evaluate the effect of this procedure is analyzed. These methods include expressions formechanism of voltage gated sodium and potassium channels, voltage gated calcium channels, Transient Receptor potential (TRP) channels under electrical, magnetic and thermal stimulation.

This chapter describes many of the publications relevant for this work.

Heating of ionic channels by magnetic stimulation of nanoparticles

In a new approach by Huang et al. a new method for magnetic stimulation of cells is suggested. Since the interaction of magnetic field with tissue is very low, exposure of this field alone cannot cause a noticeable effect on issue. However, targeting nanoparticles on neural membrane converts the magnetic field to local thermal energy, which is high enough to stimulate temperature-sensitive channels to generate neural impulse. Because of small side effect of magnetic stimulation on tissue and its large depth of penetration, it is a proper method to use in clinical procedures.

To produce an effective interaction, it is possible to label magnetic sensitive nano-particles to cell membrane, so that the nanoparticles translate the magnetic field to mechanical or thermal irritations. In an in vivo experiment presented by Huang et al. (Fig 2.1) superparamagnetic nanoparticles named Manganese ferrite($MnFe_2O_4$) with 6 nm diameter were labeled to the cell membrane expressing TRPV1 channels and heated using a RF magnetic field that resulted in increasing the temperature of the cells' membrane. At about 42^oC APs are recorded by fluorophores in molecular-scale.

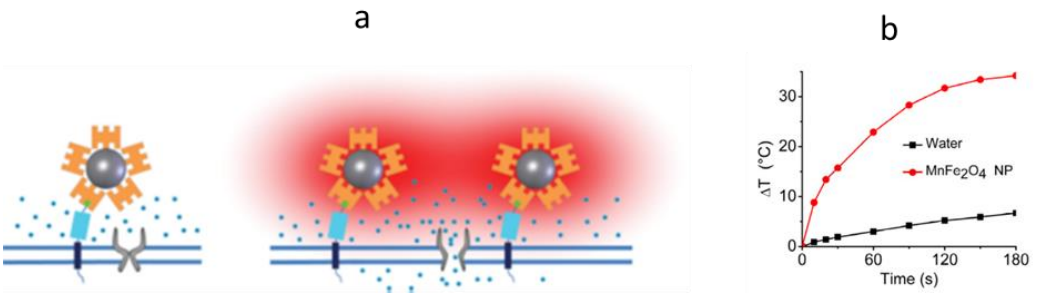

Fig 2.1 a)A schematic illustration to show the activation process of ionic channels by magnetic stimulation. The nanomagnets are labeled near the ionic channels and convert the magnetic field to local heat, which leads to increase the local temperature near the gates, and result is activation of the temperature sensitive ionic channels b) effect of magnetic stimulation on water is much smaller than the case it includes magnetic sensitive nanoparticles[1].

It is suggested that TRPV1 channels are the main responsible to generate AP in this method. Moreover, cells with the absence of TRPV1 channels did not generate spikes upon application of RF magnetic field. Therefore, it is concluded that activation of TRPV1 channels is triggered by heating of RF magnetic-field-induced nanoparticles.

In this experiment, hippocampal neurons that included uniform expression of TRPV1 channels were targeted by nanoparticles. Stimulation of the nanoparticles resulted in the local heating of the channels and changes in the membrane potential that was measured by ANNINE6 dye. When the membrane temperature reached about 40^oC an AP happened. Huang et al. concluded that this method can be used for remote stimulation of nerve cells in different future researches and clinical approaches.

In other experiment, during the magnetic stimulation of human embryonic kidney (HEK 293) cells the concentration of calcium ions inside the cell is recorded to increase as the result of Ca^{2+} flux. So it is suggested that TRPV1 channels may be activated by passing calcium ions through them.

To understand the contribution of electric, magnetic and thermal factors on excitation of different types of ionic channels, we will study the effect of these factors on a single nerve cell in the next chapters [1].

Membrane potential

Neurons are the signaling units of the body. Their capability for electrical excitation leads the process and transfer of signals rapidly over large distances. Electrical activation of the neurons is possible by action potential (AP), phenomenon in the cell membrane that is defined as the extreme change of the membrane potential due to flow of ions inside, and then, outside the cell through the ionic channels of the membrane.

The structure and function of nerve cells can be divided in four main parts:

1. Soma that is the body of the cell
2. Dendrites
3. Axon, long nerve fiber

Neural membrane consists a double layer of phospholipids impermeable to water and intra-extra cellular ionic solutions which causes excess of positive charges on the outside than the inside. Membrane rest potential is about -70 mV relative to the potential of the outside of the cell (consider $\boldsymbol{V_{out}} = 0$) and the cell is in polarized condition.

Membrane also consists of a number of ionic channels made up of proteins that transfer selective ion flow through the membrane. Change in potential or other parameters of the membrane irritate the channels to open and close. Ion flow occurs to keep the balance between the chemical driving force (concentration gradient) and electrical driving force (potential difference) inside and outside the cell. There are several types of channels in the membrane that each type is activated only by a specific ion flux. Usually the name of the channel is determined by the ion that the channel is permeable to it, for example, potassium channel only transfers K^+ions in-out side of the cell.

Studies show that nerve cells are permeable to Na^+, K^+ and Cl^- ions when they are at rest. The number of K^+ resting channels is much more than the other channels. So, the rest potential in the membrane is closer to the equilibrium potential of the K^+ions. K^+ions tend to move out of the cell because of their high concentration inside. But, the concentration of Na^+ ions is more than the outside, so they tend to flow inside the cell. This phenomenon may also happen for other types of ionic channels. The membrane has a steady rest potential, so the influx ions are balanced by the out-flux ions. Passive movements of ions reduce the rest potential, so to have a constant rest potential, ion leaks are prevented by Na^+- K^+ pump channels that pump the ions against their electrochemical gradients (flow two K^+ions in and three Na^+ ions out of the cell). An ATP is used to provide energy for each pump. Fig 2.2 illustrates the explained phenomenon.

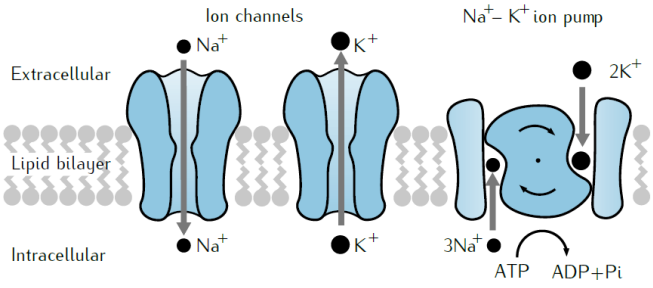

Fig2.2 Cell is isolated by impermeable lipid bilayer from its environment. There is a potential difference in out and inside of the membrane due to electrochemical gradients. This difference forces the sodium and potassium ions to flow against it. Sodium ions tend to pass to the inside of the cell and potassium ions tend to move out. This phenomenon perturbs the rest potential difference of the membrane. Therefore, ion pumps flow the ions to exchange 3 sodium ions with 2 potassium ions to keep the potential in a steady value[5].

Goldman equation expresses the contribution of each type of ion to the rest potential[6,7]:

$$V_m = \frac{RT}{F} ln \frac{P_K[K^+]_O + P_{Na}[Na^+]_O + P_{Cl}[Cl^-]_i}{P_K[K^+]_i + P_{Na}[Na^+]_i + P_{Cl}[Cl^-]_O} \qquad (2.1)$$

Here R is universal gas constant (~8.314 $kJ.mol^{-1}$), T is absolute temperature (in Kelvin), z is the valance of the ion, F is the Faraday constant and $[X]_o$ and $[X]_i$ are concentrations of the ion outside and inside the membrane. Permeability of each type of ion is considered as P. When the membrane is at rest, the highest permeability is for K^+ ions. For sodium and chloride ions: $P_{Na} = 0.04\, P_K$ and $P_{Cl} = 0.45\, P_K$. However, at the peak of the action potential, the most permeable ions are Na+ ions: $P_{Na} = 20 P_K$ and$P_{Cl} = 0.45\, P_K$. [8]

Some types of channels respond to the changes in the membrane potential by changing their permeability of the ion, these are called active channels. In our study, we consider passive channels that their permeability is almost independent of the membrane potential.

The equilibrium potential resulting from the permeability of a channel to a single ion is described by Nernst potential equation:

$$E_X = \frac{RT}{z_X F} ln \frac{[X]_i}{[X]_o} \qquad (2.2)$$

Where E_X is the equilibrium potential or Nernst potential and z is the ion valancy that is 2 for Ca^{2+} , 1 for k^+ and -1 for Na^+. The outward flux is considered in positive direction [9].

Concentration of ion X is not the same inside and outside of the cell, so the ions diffuse through the channels due to their concentration gradient $\frac{d[X]}{dx}$:

$$J_{X,diff} = -D_X \frac{d[X]}{dx} \qquad (2.3)$$

That D_X is the diffusion coefficient measured in $cm^2 s^{-1}$[10].On the other hand, the electric potential difference at both sides of the membrane results in the ionic flux down the neurite which is called drift flux:

$$J_{X,drift} = -\frac{D_X F}{RT} z_X [X] \frac{dV}{dx} \qquad (2.4)$$

Taking into account both diffusion flux and drift flux we can express the total electrodiffusion flux of ion X:

$$J_X = J_{X,diff} + J_{X,drift} \qquad (2.5)$$

This expression is named Nernst-Planck equation [9,11]. We will use this expression to explain the mathematics for function of TRPV1 channels.

Electrical circuits help explain neural functions

It is useful to consider the neurons as electrical circuit units. In this frame, conductors and resistors represent the ion channels, batteries represent the pumping of the charges, and Capacitors displays the ability of the membrane to store the charge.

Consider the neural membrane. Since, double lipid layer of the membrane is impermeable, the charges inside and outside of the membrane cannot move according to their electrical and chemical gradients. So the inside surface of the membrane is negatively charged and the outside surface of it is positively charged. This condition is similar to the capacitance with parallel plates. One of the plates is negatively charged and the other (outside surface) is positively charged. As we know, the separation of the positive and negative charges on both sides of the capacitor creates an electric field, and thus a potential difference between the plates is proportional to the charge excess between two plates:

$$V = \frac{q}{C} \qquad (2.6)$$

Here q is the charge excess between the surfaces and C is the capacitance measured in farads. The capacity of the parallel surfaces is proportional to the area of the plates ‘a’ and the distance between them ‘d’:

$$C = \frac{a}{\varepsilon d} \qquad (2.7)$$

Where ε is the permittivity of the insulator.

By differentiating the V=q/C formula it is found that current is proportional to the changes in the membrane potential and capacitance:

$$\frac{dV}{dt} = \frac{I}{C} = \frac{1}{C}\frac{dq}{dt} \qquad (2.8)$$

The electromotive force that causes the ions to gather in both side of the membrane is shown by a Battery in the equivalent circuit.

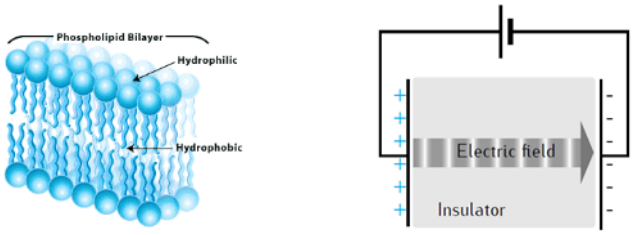

Figure 2.3 the collection of charges on both sides of dielectric membrane creates an electric field in the membrane that can be considered to function as a capacitor[8].

If potential of the inside of the cell is V_{in} and for outside is V_{out} then the membrane potential is determined as:

$$V_m = V_{in} - V_{out} \qquad (2.9)$$

The membrane potential is positive when the inside of the membrane is more positively charged than the outside. [5]

Ions flow in or out of the cell through the ion channels. Each channel can be considered as a resistor or conductor with a conductance of $\gamma\ (1/\Omega)$. If there was no electrochemical forces, the flow through the channel would be $i = \gamma \times V_m$. However, due to the effect of the electromotive force the ionic flow is determined by:

$$i = (\gamma \times V_m) - (\gamma \times \mathrm{E}) \qquad (2.10)$$

$$= \gamma \times (V_m - E)$$

Here $(V_m - E)$ is called electrochemical driving force.

For N number of a specific type of channel, the overall conductance is:

$$g = N \times \gamma \qquad (2.11)$$

In the equivalent circuit, each population of channels can be represented by a battery in series with a conductor (Fig 2.4)

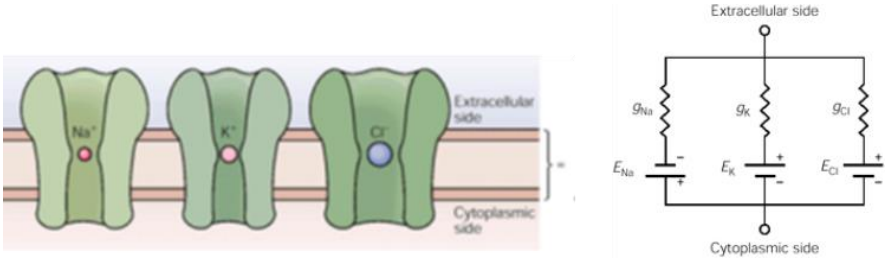

Fig 2.4 Each type of ionic channel is considered as a resistor and the electromotive force through the channels is illustrated as a battery that pushes the sodium ions inside the cell and the potassium and Chloride ions out of the cell[8].

As the ions flow through the selective ionic channels due to the electrochemical force, the pumps flow the ions back to keep the membrane potential at the steady state (for example Na^+-K^+ channels pump out three Na^+ for every two K^+ ions pumping inside the cell using an ATP molecule). This process can be represented as a current generator in the equivalent circuit.

The total membrane current is the sum of the capacitive current and the current passing through the channels[8].

Hodgkin and Huxley model for equivalent circuit of Na_V , K_V , Cl_V channels

The Hodgkin and Huxley (HH) model explains the effect of movement of ions through ionic pores on the membrane potential and generation of AP in voltage-gated channels. The current generated by the voltage-gated channels varies in time and voltage. Therefore, to model these channels, several methods were used to control the parameters. In 1940 Hodgkin and Huxley successfully used VClamp technique on squid giant axon to produce some experimental data for constructing their model [12-16].

Voltage clamp (VClamp) technique holds the voltage to a specific value to control the membrane potential and study the effects of stimuli on it. First, an electrode is injected to the membrane. It measures the membrane potential by an amplifier, then, to provide voltage difference between the measured and considered voltage, a proper current is generated by an amplifier and is injected to the membrane (Fig 2.5)

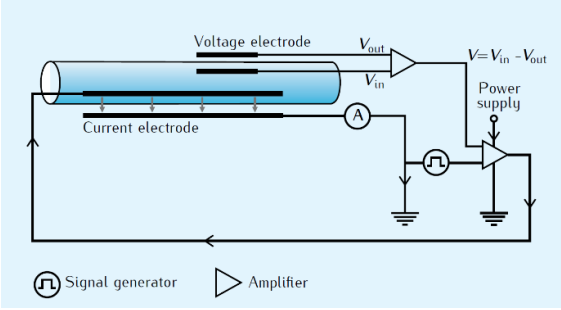

Fig 2.5 Voltage clamp technique used to keep the membrane potential unchanged. First the voltage difference(V) is measured for both sides of the membrane, then a current electrode injects current to provide the voltage difference(V) that was necessary to keep the membrane potential to a constant value [5].

To be sure that membrane potential is uniform in a large volume of the membrane, Hodgkin and Huxley used space clamp technique where the electrodes are long and thin

wires, so, the resistance of the cytoplasm and extracellular space can be assumed to be zero[17,18].

This technique is used in H-H model to analyze the function of each type of channels separately. The equivalent circuit of the H-H model is shown in Fig 2.6.

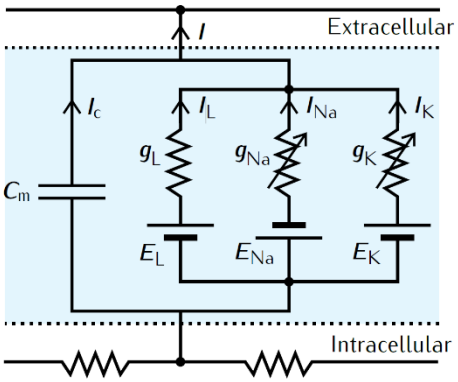

symbol	Correlated parameter
C_m	Membrane capacitance
I_C	Capacitive current
I	Total current
$\bar{g}_L$	Leakage conductance
g_{Na}	Sodium conductance
g_k	Potassium conductance
E_L	Leakage equilibrium potential
E_{Na}	Na^+ equilibrium potential
E_K	K^+ equilibrium potential
I_L	Leakage current
I_{Na}	Sodium current
I_k	Potassium current

Fig 2.6 HH circuit model [5] and the description of parameters used in the model

Figure 2.6 The equivalent circuit in HH model. The table shows the parameters used in the this model. The membrane lipid bilayer is shown as a capacitor, each channel is illustrated as a resistance and the electrochemical force through the channel is represented as a battery. The total current includes the sum of currents generated by each type of channel and the capacitive current.

The bar on the leakage conductance indicates that it is constant over potential and time.

Capacitance C_m represents the capacity of the membrane that creates a potential difference inside and outside of the cell. The capacitive current I_C occurs in a very short time at the beginning and the end of the pulse. The current passing to the outside of membrane is the sum of the capacitive current and the current passing through the channels:

$$I = I_C + I_i = C_m \frac{dV}{dt} + I_i \quad (2.12)$$

$$I_i = I_{Na} + I_k + I_L \quad (2.13)$$

The current passing from channel is calculated by multiplying the conductance of that type of channel and the electrochemical driving force.

$$(I_{channel} = g_{channel} \times (V - E_{channel})) \quad (2.14)$$

In voltage clamp technique $g_{channel}$ can be calculated this formula:

$$g_{channel} = \frac{I_{channel}}{V - E_{channel}} \qquad (2.15)$$

Action Potential

Action potential (AP) is an impulse phenomenon in which the membrane potential increases sharply to a positive value and then decreases to the rest value in a short period of time (Fig 2.7). The process and details of action potential was studied first by Hodgkin and Huxley. Their experiments show that the action potential can be described by the variation in the conductance of Na+ and k+ channels. Other type of channels has small contribution in action potential. They measured the rate, shape and other properties of the gated channels.

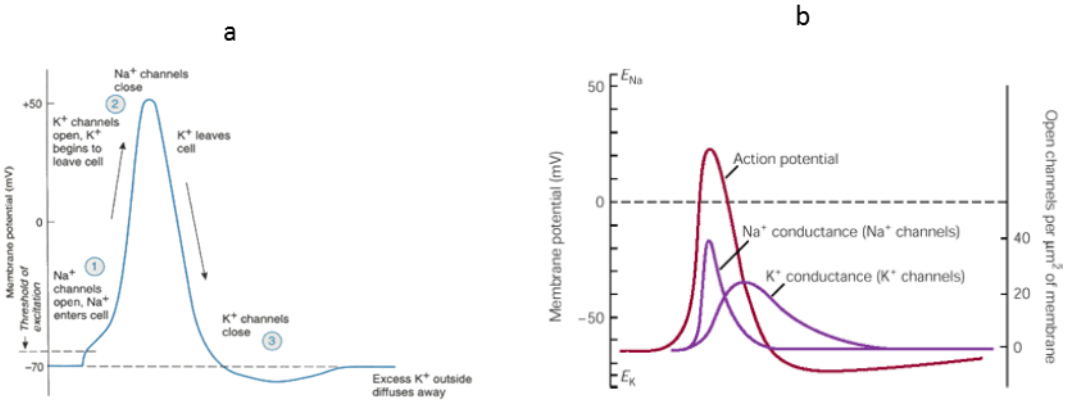

Fig 2.7 Action potential and the different stages that membrane passes to return to the rest value. The kinetics of sodium and potassium ions are illustrated at each state[8].

The first step to reach this model was discovering the increase in ion flow during the action potential.

For measuring the parameters contributed in action potential, 'Voltage Clamp' technique is used. This technique enables the experimenter to set the voltage of the membrane to the considered value. Hodgkin and Huxley used the ion substitution method to separate the inward and outward current. They prevented the inward current by decreasing the extracellular sodium concentration. The K^+ current was obtained by reducing I_{Na} ,I_L and I_C from the total current. Fig 6 illustrates the function of related channels in detail.

According to HH model for AP:

1- Increasing the membrane potential is called depolarization and decreasing the potential is named repolarization.

2- The depolarization of membrane leads the opening of Na^+ channels that results further membrane depolarization. So more Na_V channels are opened that causes increasing the inward current. After a very short period time, Kv channels are opened and K^+ current begin flowing outward. The outflow of potassium ions prevents the voltage inside the cell to increase, so the membrane potential reaches to a peak value. This process continues to decrease the potential of cell to the rest value.
3- When the membrane potential reaches the rest value, some of the potassium channels are still open and flow the positive ions outside the cell. This process leads decreasing the membrane potential to a value a little smaller than the rest value (hyperpolarization) After a short time all the stimulated K_V channels close and the membrane potential increases to the rest value.

HH model suggests all –or- none behavior for the action signals. It means that for a voltage more than threshold value, the amount of signal does not affect the amplitude of the action potential.

In the HH model, the first order chemical reaction model is used to express the 'open' or 'close' state of the individual gates.

$$C \underset{\beta_n}{\overset{\alpha_n}{\rightleftharpoons}} O \qquad (2.16)$$

that α_n is the number of times per second that a close-gate opens and β_n is the number of times per second that a gate closes. These two factors are called 'rate constants' and depend on the membrane potential.

In HH model, the probability of an individual gate to be in open state is P_n ranging between 0 and 1. For a large number of a specific type of channel, P_n and $(1 - P_n)$ can be expressed as the fraction of gates in the open state and close state respectively. The rate of transition between open and close state is:

$$\frac{dP_i}{dt} = \alpha_i(V)(1 - P_i) - \beta_i(V)P_i \qquad (2.17)$$

If the membrane potential is clamped to a fixed value, the fraction of gates in open state reaches a steady-state value ($dP_i/dt = 0 \; as \; t \to \infty$)

$$P_{i,\infty}(V) = \frac{\alpha_i(V)}{\alpha_i(V) + \beta_i(V)} \qquad (2.18)$$

And the time needed to reach the steady state is called time constant $\tau_i(V)$ given by:

$$\tau_i(V) = \frac{1}{\alpha_i(V) + \beta_i(V)} \qquad (2.19)$$

The general form of the answer for equation 2.17 is:

$$P(t) = P_{\infty}(V) - [P_{\infty}(V) - P_0] \exp\left(\frac{-t}{\tau_i(V)}\right) \qquad (2.20)$$

Or

$$\tau_i(V)\frac{dP_i}{dt} = P_{i,\infty}(V) - P(t) \qquad (2.21)$$

Here P_0 is the initial value of P at the beginning of the step. Equation (2.20) describes that $P(t)$ reaches to the steady value at time $\tau_i(V)$.

The value of $P_{i,\infty}(V)$,$\tau_i(V)$, $\alpha_i(V)$ and $\beta_i(V)$ is determined(as a function of voltage) from experiment. However, to give a physical description for $\alpha_i(V)$ and $\beta_i(V)$, the thermodynamic arguments are useful. The rate of function of $\alpha_i(V)$ and $\beta_i(V)$ is controlled by barriers requiring thermal energy. The function of rate constants is effective when an effective charge (denoted by qB_α) passes the membrane (with potential V), so the thermal energy barriers depend on the membrane potential [19].

In the AP process, Boltzmann factor is used to express the probability that the thermal energy transitions provide enough energy to come over the energy barrier: $\exp(-qB_\alpha/KT)$. The expression for $\alpha_i(V)$ can be determined based on this factor:

$$\alpha_i(V) = A_\alpha \exp(-qB_\alpha/KT) = A_\alpha \exp(-B_\alpha V/V_T) \qquad (2.22)$$

In this equation A_α and B_α are determined from experimental data. The closing rate $\beta_i(V)$ is expressed similarly with different constants.

If we consider $\bar{g}_i$ as the maximum possible conductance in the condition that all the channels are open for a specific type of ion, the total conductance for that type of channel will be [19]:

$$g_i = \bar{g}_i \prod_i P_i \qquad (2.23)$$

Potassium current

To determine the K_V channel conductance, from the Hodgkin and Huxley experiment, the time course of the potassium conductance shows that the steady-state potassium conductance ($g_{k\infty}$)increases with increasing the voltage. The graph also shows that $g_{k\infty}$ reaches a maximum value (denoted$\bar{g}_K$). At higher voltages, the speed at which the conductance reaches the maximum value becomes faster (Fig 2.8).

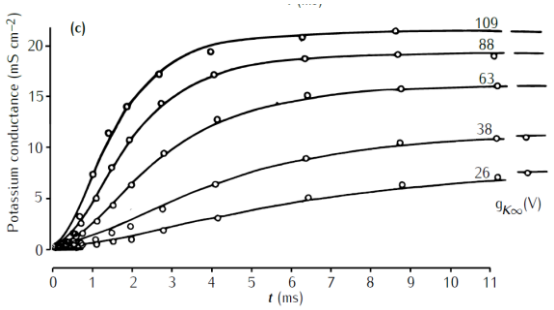

Fig 2.8 Potassium conductance changing with time in VCLAMP technique. Conductance of potassium increases faster in higher membrane voltages to its maximum value[5,16].

To describe this process, Hodgkin and Huxley represent that the expected fraction of K_V channels in open state($\prod_i P_i$) is n^x, so from equation(2.23) the potassium conductance is:

$$g_K = \bar{g}_K n^x \qquad (2.24)$$

Hodgkin and Huxley fit the calculated date with the experimental data by assuming x=4. Therefore, the conductance of K_V channels is (Fig 2.9):

$$g_K = \bar{g}_K n^4 \qquad (2.25)$$

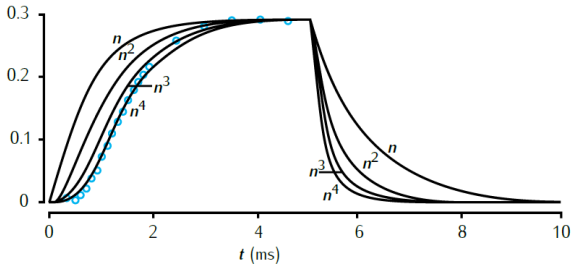

Fig 2.9 The time evolution of potassium conductance with different values for power of n. The data fit well with n^4.[5,16]

According to Equation (2.17) the time evolution of a first order kinetic process is:

$$\frac{dn}{dt} = \alpha_n(1-n) - \beta_n n \qquad (2.26)$$

According to Equation (2.20) the general form for n(t) is:

$$n(t) = n_\infty(V) - [n_\infty(V) - n_0]\exp\left(\frac{-t}{\tau_n(V)}\right) \qquad (2.27)$$

Where n_0 is the value of n at the beginning of the step.

From Equation (2.18) and (2.19) the values for $n_\infty(V)$ and $\tau_n(V)$ can be calculated:

$$n_\infty(V) = \frac{\alpha_n(V)}{\alpha_n(V) + \beta_n(V)} \qquad (2.28)$$

$$\tau_n(V) = \frac{1}{\alpha_n(V) + \beta_n(V)} \qquad (2.29)$$

To simplify Equation (2.26) we consider that the increment of the open-gates(α_n) is linear with voltage(Fig 2.9).

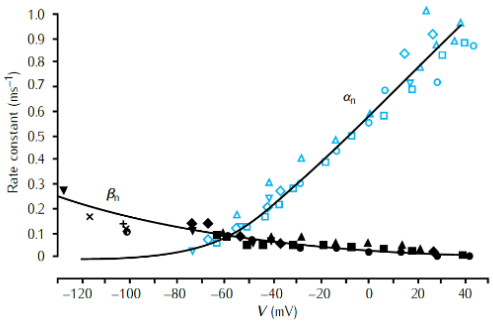

Fig 2.10 Rate constants of potassium conductance as a function of voltage can be considered linear[5,16].

Therefore the amount of changes from n to dn during dt is the same as the changes from n to n_∞ during time τ_n:

$$\frac{dn}{dt} = \frac{n_\infty - n}{\tau_n} \qquad (2.30)$$

And:

$$\alpha_n = \frac{n_\infty}{\tau_n} \qquad (2.31)$$

$$\beta_n = \frac{1 - n_\infty}{\tau_n} \qquad (2.32)$$

Using Equation (2.25) we can find the value for n_∞:

$$n_\infty(V) = \left(\frac{g_{K\infty}(V)}{\bar{g}_K}\right)^{\frac{1}{4}} \qquad (2.33)$$

Finally, the summary of the calculations for the potassium ionic current through the membrane is:

$$I_k = \bar{g}_K n^4 (V - E_K) \qquad (2.34)$$

$$\frac{dn}{dt} = \alpha_n(1 - n) - \beta_n n \qquad (2.35)$$

$$\alpha_n = 0.01 \frac{V + 55}{1 - \exp(-(V + 55)/10)} \qquad (2.36)$$

$$\beta_n = 0.125\exp(-(V+65)/80) \qquad (2.37)$$

Sodium current

Hodgkin and Huxley isolated the sodium current using the substitution method and measured the conductance of Na^+ current in voltage clamp condition.

As we see in the Fig (2.11) Na^+current increases and reaches a peak value, then, decreases to the rest condition (inactivation). In potassium channels, the conductance reaches a maximum value and remains constant. However, for the sodium channels, the gates spend very short period at the maximum conductance state. To explain the difference in the conductance of sodium channels with potassium gates, Hodgkin and Huxley suggested activation and inactivation gate for sodium channels.

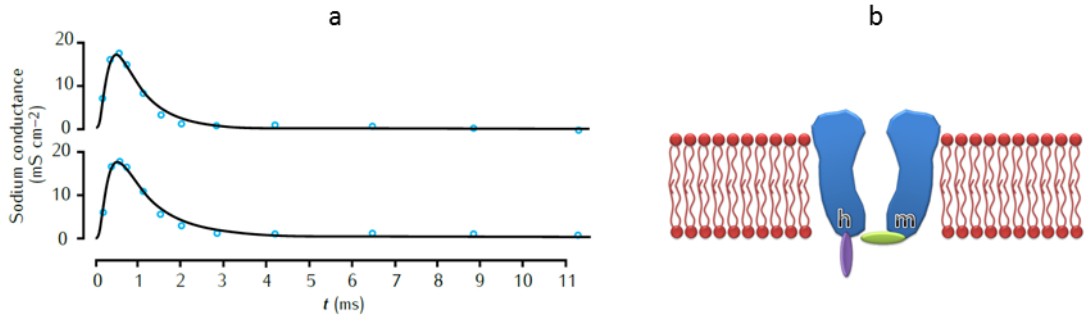

Fig 2.11 The conductance of sodium channel over time. The conductance reaches a peak value and then decreases by time. Two gates (activation and inactivation gates) are considered to explain these channels conductance [5,8,16].

The variable ‘h’ represents the level of inactivation and ‘m’ for activation level.

The rate of transition between two open-close states for ‘h’ gating particle is:

$$\frac{dh}{dt} = \alpha_h(1-h) - \beta_h h \qquad (2.38)$$

And for ‘m’ gating particle is:

$$\frac{dm}{dt} = \alpha_m(1-m) - \beta_m m \qquad (2.39)$$

Using the above formulas, the inflected activation curve for sodium conductance is explained by:

$$g_{Na} = \bar{g}_{Na} m^3 h \qquad (2.40)$$

That fit well with the experimental recordings. So the model of sodium current is:

$$I_{Na} = \bar{g}_{Na} m^3 h (V - E_{Na}) \qquad (2.41)$$

With the same method for potassium channels, Hodgkin and Huxley find the model for sodium conductance:

$$\alpha_m = 0.1\frac{V+40}{1-\exp(-(V+40)/10)} \qquad (2.42)$$

$$\beta_m = 4\exp(-(V+65)/18) \qquad (2.43)$$

$$\alpha_h = 0.07\exp(-(V+65)/20) \qquad (2.44)$$

$$\beta_h = \frac{1}{1+\exp(-(V+35)/10)} \qquad (2.45)$$

These expressions for rate constants of sodium channels are used to find the number of activated and inactivated sodium channels in HH model.

Leak current

When there is no sodium current and potassium flux is the major current, the diving force of K+ ions is zero (V-$E_K = 0$) and no potassium current flows. At this level of potential, Hodgkin and Huxley found some non-sodium current. They suggested that this current is the mixture of ions (mostly chloride ions) that does not depend on voltage and named it leakage current 'I_L'. Using aquasi-ohmic current–voltage relationship they derived[15]:

$$I_L = \bar{g}_L \times (V - E_L) \qquad (2.46)$$

Summary of HH model:

HH current model is the sum of the contributed ionic current models[12-16]:

$$C_m\frac{dV}{dt} = -\bar{g}_L(V - E_L) - \bar{g}_{Na}m^3h(V - E_{Na}) - \bar{g}_K n^4(V - E_K) + I \qquad (2.47)$$

That I is the circuit current. Fig 2.12 shows the contribution of sodium and potassium conductance in action potential.

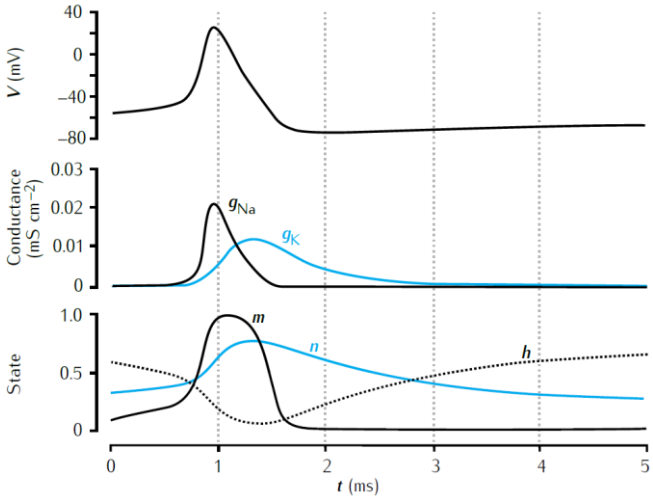

Fig 2.12 time evolution of membrane potential during the action potential phenomenon. The second graph compares the conductance of Na+ and k+ channels over the action potential period and the last graph illustrates the related gating variables[12-16].

From Fig 2.12 it is clear that the conductance of sodium channels starts increasing earlier than that for potassium channels, so we can conclude that sodium current is the beginner of action potential. The outflow of potassium channels and inactivation of sodium channels lead the voltage stop increasing and go back to the rest value. However, since a proportion of potassium channels are still activated, the membrane voltage continues to decrease under the rest potential value.

A number of numerical methods attempt to solve the HH model, such as: forward Euler, modified Euler, backward Euler, Runge-Kutta, Adams-Bashforth-Moulton predictor-corrector, and Matlab's ODE45 function[19].

Effect of temperature

Temperature highly affects the constant rates. To involve its effect a temperature coefficient is used. Temperature coefficient Q_{10} is a measurement of increasing in the rate coefficient due to 10^oC temperature alteration:

$$Q_{10} = \frac{rate\ at\ T + 10^oC}{rate\ at\ T} \qquad (2.48)$$

We can find the rate constants by using this factor:

$$\alpha(V, T_2) = \alpha(V, T_1) Q_{10}^{\frac{T_2 - T_1}{10}} \qquad (2.49)$$

And

$$\beta(V, T_2) = \beta(V, T_1) Q_{10}^{\frac{T_2 - T_1}{10}} \qquad (2.50)$$

And for maximum conductance:

$$\bar{g}_X(T_2) = \bar{g}_X(T_1)Q_{10}^{\frac{T_2-T_1}{10}} \qquad (2.51)$$

This expression can be explained also by Arrhenius equation. This equation is a formula for temperature dependent reaction rates in equilibrium condition. According to this equation for a mole of particles, the rate constant k is:

$$k = Ae^{-\frac{E_a}{KT}} \qquad (2.52)$$

That E_a is the activation energy, R is the Boltzmann constant and T is the absolute temperature.

The rate coefficient at temperature T_1 and T_2 is $k(T_1)$ and $k(T_2)$:

$$log\left(\frac{k(T_2)}{k(T_1)}\right) = \frac{E_a}{R}\left(\frac{1}{T_1} - \frac{1}{T_2}\right) \qquad (2.53)$$

We consider $T_2 = T_1 + 10$. [12,20,21]

So:

$$log(Q_{10}) = \frac{E_a}{R}\left(\frac{10}{T_1(T_1+10)}\right) \qquad (2.54)$$

Voltage gated Calcium currents

Voltage-gated Calcium channels initiate and moderate many physiological events. Ca_V channels are effective in mechanisms such as cardiac and smooth muscle cells[22,23],Skeletal muscles[24,25] and in neurons, they initiate synaptic transmission[24,26,27,28].

Concentration of calcium inside the cell is very low, so a model named GHK is used to study the behavior of voltage-gated calcium channels. Goldman (1943) and Hodgkin and Katz (1949) devised the theory of membrane current flow and derived GHK formula based on this theory that describes the currents and voltages through permeable membranes[6,29,30]. The net current I_X (in cm^{-2}) of ion X through a unit area of membrane is:

$$I_X = P_X z_X F \frac{z_X FV}{RT}\left(\frac{[X]_{in} - [X]_{out}e^{-z_X FV/RT}}{1 - e^{-z_X FV/RT}}\right) \qquad (2.55)$$

That z_X and P_X in (cms^{-1}) are the valency and permeability of ion X respectively:

$$P_X = -\frac{J_X}{[X]_{in} - [X]_{out}} \qquad (2.56)$$

P_X is proportional to the diffusion coefficient (D_X) described by Fick's low. It is assumed that the membrane includes a homogenous distribution of the activated calcium ion channels. However, to consider the direct relationship of the number of opened channels with the amount of ionic current, diffusion coefficient D_X is interpreted as variable:

$$J_{X,diff} = -D_X \frac{d[X]}{dx} \qquad (2.57)$$

Here $J_{X,diff}$ is the molar flux of ion X that is diffused due to concentration gradient $\frac{d[X]}{dx}$.

The current is not proportional to the voltage, so the I-V curve does not abbey the Ohm's law. In the GHK equation, it is assumed that ions flow independently. According to Nernst–Plank equation, the gradient of ion internal concentration and electric field control the movement of the ions through the membrane.

This expression can also be used to obtain more accurate I-V relationship for sodium and potassium voltage gates[20] .

Transition State Theory

Transition State theory is based on Arrhenius (1889) concept and describes the energy E_a required for an ion to pass through the voltage gated channels [31]. The reaction rate k_μ is given by

$$k_\mu \propto exp\left(-\frac{E_a}{RT}\right) \qquad (2.58)$$

That R is the universal molar gas constant and T is temperature in Kelvin.

To find an expression for the reaction rate between the opening and closing states, Gibbs free energy is introduced as the required energy to activate the channels:

$$k_\mu = \frac{k_B T}{h} \exp\left(-\frac{\Delta G_\mu}{RT}\right) \qquad (2.59)$$

Where k_B is the Boltzmann constant and h is the planck's constant. The difference in the Gibbs energy is described by:

$$\Delta G_\mu = \Delta H_\mu - T\Delta S_\mu \qquad (2.60)$$

Here ΔH_μ and ΔS_μ are the differences in enthalpy and entropy between the two states [31-33].

TRP channels

Our nerve system is capable of detecting the changes in the environment temperature. Thermal detection occurs in the dorsal root and trigeminal ganglia through the primary afferent sensory neurons [34,35].TRP superfamily is mainly responsible for temperature sensation[36,37].Different types of temperature sensitive channels exist that each can be activated in a specific temperature range. The basic principle for temperature sensing of these channels belong to the Transient Receptor Potential (TRP) family [36-40]. There are four types of heat sensitive channels. Increasing the temperature first excites TRPV4 channels which are activated for the temperature ranges higher than 25^oC, when the temperature reaches 31^oC TRPV3 channels produce signal[41-45],ranges higher than 43^0C results in generation of action potentials by TRPV1 channels[46,47] and the TRPV2 channels begin to produce signals for temperatures greater than 52^oC [48]. Indeed, TRPM8 and TRPA1 are cold sensitive TRP channels [49-51]. TRPs are also sensitive to pain, touch, taste and other stimulations [52]. Although several studies evaluated the mechanism of these channels [55-59], the fundamental knowledge of the gating mechanism of TRP channels is still unsolved.

In this study, since TRPV1 channels are activated in the temperature range that magnetic stimulations are applied, this channel type is studied in more details.

Effect of Magnetic field

Some physical explanations are developed to provide a new insight for utilizing the magnetic stimulation technique. Magnetic stimulation of the tissue induces electric field that causes AP or inhibition in the nerve cell. The connection between time varying electric and magnetic fields can be described by Maxwell equations.

In Transcranial Stimulation of the brain, magnetic field penetrates through the skull with ignorable interaction. Therefore, this technique is the most interesting method to stimulate the nervous system[60,61].

Basic principles

Several Experiments have done to study TMS mechanism. In an experiment that successfully described the mechanism of signaling, a time-varying electromagnetic field is applied externally which results in excitation in nerve cells. In this method, a coil is

placed on the surface of the skin or over the tissue. Pulses with current I(t) passes through the coil and magnetic field B is produced according to Biot-Savart law:

$$B(r,t) = \frac{\mu_0}{4\pi} I(t) \oint_C \frac{dl(r') \times (r - r')}{|r - r'|^3} \qquad (2.61)$$

Where l is the length of the coil and μ_0 is the permeability of free space measured in H/m. in practice, first, a large capacitor is charged a passing current to a high voltage, then it discharges by a thyristor switch through the coil.

According to Faraday's law, magnetic waves then induce an electric field E in the tissue:

$$\nabla \times E = -\frac{\partial B}{\partial t} \qquad (2.62)$$

Fig 2.13 shows the process of inducing magnetic field and the neural response[62] . This magnetic field induction method is called TMS or Transcranial Magnetic Stimulation. The induced magnetic field has a sinusoidal wave form that lasts about 300 μs 16.

The required threshold voltage for generation of AP is described by cable equation [63,64].

The required energy to excite the nerve cells in tissue is proportional to the square of magnetic field: $W \propto B^2$, that B is the magnetic flux density

According to Faraday's law, the magnetic field is proportional to the product of the electric field and the pulse duration:$B^2 \propto E^2 t^2$ [65,66].

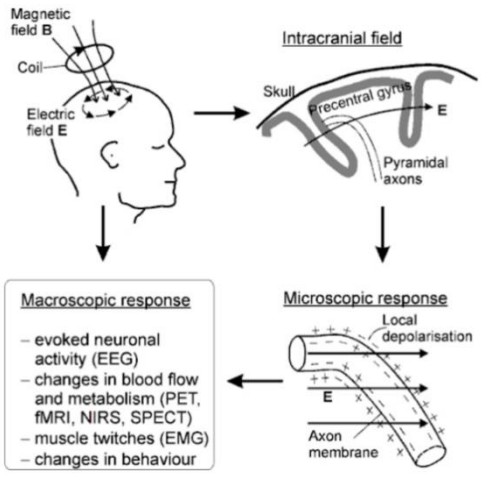

Fig 2.13 TMS technique, magnetic field B induces electric field E by a coil placed over the patient' head. Induced electric field then excites the Pyramidal nerves. The activation of nerves can be detected by some tools such as EEG, PET, fMRi, NIRS and Spect, with behavioral or surface EMG changes. [62]

In an experiment, Rotem and Moses located a closed loop over a disk of 1-D cell culture and generated magnetic field induced an electric field in the culture. They present a mathematical expression for generation of AP due to MF induction[67].We consider a coil of radios R placed in x-y plane at z=0. We can calculate the induced electric field E along the closed loop L. According to Faraday's law, the changes of magnetic flux (ϕ(t)) with time through the surface s enclosed by L is equal to the induced electric field along the loop with radios r:

$$\int_{\mathrm{L}} \vec{\mathrm{E}}(\mathrm{t}).\, \mathrm{d}\vec{l} = \frac{\partial}{\partial \mathrm{t}} \phi(\mathrm{t}) = \frac{\partial}{\partial \mathrm{t}} \int_{\mathrm{s}} \vec{\mathrm{B}}(\mathrm{t}).\, \mathrm{d}\vec{s} \qquad (2.63)$$

Magnetic field near and inside the coil is almost uniform and perpendicular to the coil plane:

$$\int_{\mathrm{s}} \vec{\mathrm{B}}(\mathrm{t}).\, \mathrm{d}\vec{s} = B(t) \int_{\mathrm{s}} \mathrm{ds} = B(t) \times \pi r^2 \qquad (2.64)$$

Therefore, magnetic flux through L is

$$\phi(\mathrm{t}) = B(t) \times \pi r^2 \qquad (2.65)$$

and

$$\frac{\partial}{\partial \mathrm{t}} \phi(\mathrm{t}) = \pi r^2 \times \frac{\partial}{\partial \mathrm{t}} B(t) \qquad (2.66)$$

In this experiment, all boundaries of the vessel and neurites are concentric with the coil, thus, the amount of the electric field in any radius is uniform.

$$\int_{\mathrm{L}} \vec{\mathrm{E}}(\mathrm{t}).\, \mathrm{d}\vec{l} = 2\pi \mathrm{r} \times \mathrm{E}(\mathrm{t}) \qquad (2.67)$$

So, the equation is simplified to

$$\mathrm{E}(\mathrm{t}) = \frac{r}{2} \frac{\partial}{\partial \mathrm{t}} B(t) \qquad (2.68)$$

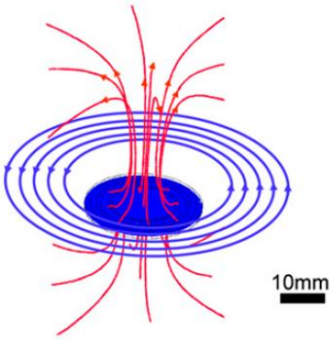

Fig 2.14 Magnetic stimulation of a culture in the form of a ring . A 1-d neuronal ring culture is placed 5 mm under the circumference of a coil. We use Faraday's law to calculate the electric field induced at rings concentric and parallel to the plane of the coil[67].

We consider that the neurite lie along the x direction and its passive length and passive time constants are λ and τ

$$\lambda^2 \frac{\partial^2 \varphi_m}{\partial x^2} - \tau \frac{\partial \varphi_m}{\partial t} - \varphi_m = \lambda^2 \frac{\partial E_x}{\partial x} \qquad (2.69)$$

That φ_m is the deviation of the membrane potential from the resting value. To solve the passive cable equation, it is necessary to use Green's function:

$$G(x, y; t) = \frac{e^{-\frac{t}{\tau}}}{L} + \frac{2}{L} \sum_{n=1}^{\infty} (cos \frac{n\pi x}{L} cos \frac{n\pi y}{L} e^{-\alpha_n \frac{1}{\tau}}) \quad t \geq 0 \qquad (2.70)$$

And

$$\alpha_n = 1 + (\frac{n\pi\lambda}{L})^2 \qquad (2.71)$$

The magnetic sinusoidal pulse induce an electric field parallel to the x direction, consisting a sinusoidal cycle with a constant time cycle of $240\ \mu s$ that depends on the amplitude of the magnetic field

$$E_{\hat{x}}(x, t) = \left(\overrightarrow{E_0} . \hat{x}\right) \cos \omega t \qquad \omega = \frac{2\pi}{240 \mu s} \approx 25\ KHz \qquad (2.72)$$

Here E_0 is the maximum amplitude of the electric field. It depends on the strength of the magnetic pulse and the geometry of the experiment. In Table 2.1 the geometrical and electrophysiological parameters of neurons are given.

PARAMETERS	**DENDRITE**	**AXON**
DIAMETER	$5\ \mu m$	$1\ \mu m$
LENGTH CONSTANT λ	$865\ \mu m$	$384\ \mu m$
PHYSICAL LENGTH L	$\leq 200 \mu m$	$\geq 1000 \mu m$
TIME CONSTANT τ	$\approx 5\ ms$	$\approx 300\ ms$
$\mathbf{E_T}$	$\geq 458\ V/m$	$\approx 280\ V/m$

Table 2.1 the model parameters of axons and dendrites [64,68-71] The data is collected by Rotem et al.[67]

$$E_x(x, t) = E_0 \cos \omega t \qquad \omega t \in [0, 2\pi] \qquad (2.73)$$

To determine the boundary condition we assume that φ_T is the voltage threshold of the membrane and induces a threshold electric fieldE_T.

Boundary conditions:

Uniform external field induces currents in the membrane at the two ends (0, L) of the neurite.

$$F(x,t) = \lambda^2 \frac{\partial}{\partial x}\left(\overrightarrow{E_0}.\hat{x}\right)\cos\omega t = \lambda^2 E_0[\delta(x) - \delta(x-L)]\cos\omega t \qquad (2.74)$$

Combination of this formula with Green function yields[72]:

$$\varphi_m(x,t) = \int_0^L G(x,y;t)\,\varphi_m(y,0)dy + \int_0^L \int_0^L G(x,y;t-s)\,F(y,s)dsdy \qquad (2.75)$$

To solve the integral, it is important to note that the ends of the neurite is considered to be fixed:

$$\frac{\partial \varphi_m(0,t)}{\partial x} = \frac{\partial \varphi_m(L,t)}{\partial x} = 0 \qquad (2.76)$$

Membrane resting potential is assumed to be zero before the excitation:

$$\varphi_m(x,0) = 0 \qquad (2.77)$$

Therefore

$$\int_0^L G(x,y;t)\,\varphi_m(y,0)dy = 0 \qquad (2.78)$$

SO

$$\varphi_m(x,t) = 0 + \lambda^2 E_0 \int_0^L \int_0^t \left[\frac{e^{-\frac{t}{\tau}}}{L} + \frac{2}{L}\sum_{n=1}^{\bowtie}(cos\frac{n\pi x}{L}cos\frac{n\pi y}{L}e^{-\alpha_n\frac{t-s}{\tau}}cos\omega s\right][\delta(y) - \delta(y-L)]dsdy \qquad (2.79)$$

The existence of two delta functions gives two discrete values for y (y=0 and y=L) .Thus

$$\int_0^t \left[\frac{e^{-\frac{t}{\tau}}}{L} + \frac{2}{L}\sum_{n=1}^{\bowtie}(cos\frac{n\pi x}{L}cos\frac{n\pi y}{L}e^{-\alpha_n\frac{t-s}{\tau}}cos\omega s\right][\delta(y) - \delta(y-L)]dy$$

$$= 0 + \frac{2}{L}\sum_{n=1}^{\bowtie}(cos\frac{n\pi x}{L})(1-\cos n\pi)e^{-\alpha_n\frac{t-s}{\tau}}cos\omega s \qquad (2.80)$$

So for n= 2,4,.. the above equation is zero[$(1-\cos n\pi) = 0\ for\ n = 2,4,\dots$]. The solution for $\varphi_m(x,t)$ will be

$$\varphi_m(x,t) = \frac{2\lambda^2 E_0}{L}\sum_{n=1}^{\bowtie}\left[(cos\frac{n\pi x}{L})(1-\cos n\pi)\int_0^t e^{-\alpha_n\frac{t-s}{\tau}}cos\omega s dy\right]$$

$$= \frac{4\lambda^2 E_0}{L}\sum_{n=1}^{\bowtie}\left[cos\frac{n\pi x}{L}\times\frac{\alpha_n cos\omega t + \omega\tau sin\omega t - \alpha_n e^{-\alpha_n\frac{t}{\tau}}}{{\alpha_n}^2+(\omega\tau)^2}\right]$$

$$= \frac{4\lambda^2 E_0}{L}\times\left\{\sum_{n=1}^{\bowtie}cos\frac{n\pi x}{L}\left[\frac{\sin(\omega t+\phi_n)}{\sqrt{{\alpha_n}^2+(\omega\tau)^2}}+\frac{\alpha_n e^{-\alpha_n\frac{t}{\tau}}}{{\alpha_n}^2+(\omega\tau)^2}\right]\right\} \quad (2.81)$$

The answers for α_n and ϕ_n is:

$$\alpha_n = 1+(\frac{n\pi\lambda}{L})^2 \qquad \phi_n = tan^{-1}\left(\frac{\alpha_n}{\sqrt{{\alpha_n}^2+(\omega\tau)^2}}\right) \quad (2.82)$$

For numerical solutions:

The passive cable can be solved numerically using PDE toolbox in MATLAB. The boundary conditions are ($\frac{\partial\varphi_m(0,t)}{\partial x}=\frac{\partial\varphi_m(L,t)}{\partial x}=0$), initial value ($\varphi_m(x,0)=0$). The biological values for l, L and t are substitute. We assume that the cell start to be activated when the membrane reaches the threshold value.

Considering the boundary conditions ($\frac{\partial\varphi_m(0,t)}{\partial x}=\frac{\partial\varphi_m(L,t)}{\partial x}=0$), initial value ($\varphi_m(x,0)=0$), and an external force, we can solve passive cable numerically using PDE toolbox in MATLAB (The Math Works, Natick, MA).

The values for l, L and t are chosen according to biological data. When membrane voltage reaches a threshold value (Here is considered φ_T =30 mV), AP happens. The correlated threshold electric field E_T is:

$$E_T = \left(min\{E_0\}\middle|max_{x,t}\{\varphi_m(x,t)\}\geq\varphi_T\right) \quad (2.83)$$

Where E0 is the minimum electric field amplitude matches with the requirements. So the value of φ_m in the boundaries (0, L) is maximum. For x=0

$$max_x\{\varphi_m(x,t)\} = \varphi_m(0,t) \quad (2.84)$$

$$= \frac{4\lambda^2 E_0}{L}\sum_{n=1}^{\bowtie}\left[\frac{\sin(\omega t+\phi_n)}{\sqrt{{\alpha_n}^2+(\omega\tau)^2}}+\frac{\alpha_n e^{-\alpha_n\frac{t}{\tau}}}{{\alpha_n}^2+(\omega\tau)^2}\right] \quad (2.85)$$

For a typical dendrite, we use the approximation ($\lambda/L \gg \omega\tau \gg 1$:

$$\varphi_{max} = max_{x,t}\{\varphi_m(x,t)\} \quad (2.86)$$

$$\approx max_t \left\{ \frac{4E_0 L}{\pi^2} \cos(wt) \sum_{n=1,3,..}^{\infty} \frac{1}{n^2} \right\} = \frac{E_0 L}{2} \qquad (2.87)$$

$$\lambda > 0.8\, mm \quad L < 0.1\ mm \quad \tau < 10\, ms$$

If the length L increases or I decreases, axon condition will be $\lambda/L < \omega\tau$. The maximum value for φ_m is the sum that can be solved numerically using PDE:

$$\varphi_{max} \approx \frac{E_o \lambda}{\sqrt{\omega\tau}} \qquad (2.88)$$

$$\lambda < 0.5\, mm \quad L > 1\ mm \quad \tau > 0.1\, ms$$

Reduction of τ to to <0.1 ms results in saturation of φ_m at the highest value ($\varphi_{max} = E_o \lambda$). Therefore, reducing τ does not result in maximum value of φ_m.

Likewise, we can not increase L , λ to reach the maximum value. So, we conclude that φ_{max} has a limited range[67]

$$max_\tau\{\varphi_{max}\} \leq min\left\{\lambda, \frac{L}{2}\right\} \times E \qquad (2.89)$$

NEURON software

NEURON is a simulation environment that present neural models. This program is designed with a flexible environment that includes a high range of simulation scales from (or a part of) a single neuron to complex nerve models. It allows inserting the properties of nerve sections and connecting them together to form complex morphologies. In Neuron software, simulation of models are specified with GUI tools or with the HOC language. The NMODL language allows for development and improvement of neural models by adding new components to a model [73]. These advantages allowed the researches in Human Brain Project (HBP) for modeling several neural instructions by this software [74,75].

NEURON is an object-oriented interpreter based on creating cable sections which include the physical properties of the section and can be connected together to form an arbitrary branched cable[76].

Creating a simple compartment

To create a compartment in NEURON using Hodgkin and Huxley model, the simplest possible model is neuron's body simulation. In this model, neuron's axon and dendrites are removed: According to HH model, the simplest form of the membrane circuit consists of a membrane capacitance C_m, a membrane resistance R_m, a leakage reversal potential E_L and a current source I_e (Fig 2.14).

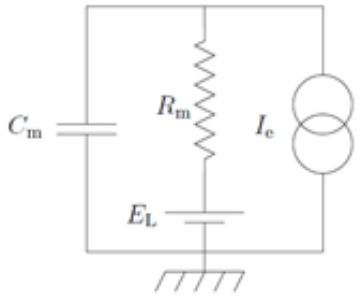

Fig 2.15 The simplest compartment in HH model considered in modeling by NEURON, consisting of a capacitanceC_m that represents the voltage difference between two sides of membrane lipid bilayer, a resistor and battery representing the conductance and passing force of the channel and a current source [78]

To create this circuit first we create a section. Each section contains several segments that have the same membrane potential. We create soma:

create soma

A new section with default properties (Table 2.2) is created.

To refer to this section in the object oriented environment of NEURON we type:

access soma

To print the properties of the section type:

soma psection()

The printed properties, their default values and units are shown in Table.

VARIABLE	MEANING	VALUE	UNITS
NSEG	Number of segments in section	1	
L	Length of section l	100	μm
RA (PASSIVE)	Specific axial resistance R_a	35.4	Ω cm
DIAM	Diameter d	500	μm
CM (PASSIVE)	Specific membrane capacitance C_m	1	$\mu F/cm^2$

Table 2.2 Default properties of a section[78]

The section has nseg segments with L/nseg length.

The default values of the parameters can be changed. For example, we change the diameter to 400 μm, soma length to 120 μm and $\mathrm{R_a}$ to 70 Ω cm:

soma.diam = 400

soma.L = 120

soma.Ra = 70

or we can type the name of the parameter in front of the statement without using dot:

soma diam = 400

soma L = 120

soma Ra = 70

or :

```
soma {
    diam =  400
    L = 120
    Ra = 70
}
```

The third way to change the values is :

access soma

diam = 400

L = 120

Ra = 70

The access statement should not be used for more than one otherwise, we will get confused what section we are referring to.

Inserting the properties of the membrane

To create channels on the model, NEURON includes two mechanisms: passive channels(pas) and Hodgkin and Huxley channels(hh).

According to Fig 2.14 we need to create the properties for the leakage channel that are the *leakage reversal potential* 'E_L' and its related *specific leakage conductance* '$\bar{g}_L$'. To introduce the membrane conductance and reversal potential to the leakage and other types of channels we use **pas** channel[78]:

soma insert pas

This command adds more two properties to soma section that are listed in Table 2.4. The resistance of the channel is the reverse of the conductance, so $r_m = \frac{1}{0.001} = 1000\ \Omega\ cm^2$

VARIABLE	MEANING	VALUE	UNITS
G_PAS	Specific leakage conductance $\bar{g}_L$	0.001	S/cm^2
E_ PAS	leakage reversal potential E_L	-70	mV

Table 2.3 Default properties of the pas channel.

Injection of current:

To complete the model of Fig 2.14, we have to insert a current source I_e that represents the passive current injected to the section. The current will be injected in a point on soma, so it will work on a specific area of the section. It is proper to express the injected parameter in absolute value (in this example, we express the current in terms of nA instead of nA/cm^2). The related commands are:

objref stim or *objectvar stim*
soma stim = new IClamp(0.5)

The object is named stim, objref creates a new reference to stim. In the second command, we created an object variable named stim. In the second line the property of the new object (stim) is determined that is the injection of current (current clamp: IClamp). The new created object is associated to soma section. The location of the point process is justified in the parenthesis.

Three properties of IClamp are:

- del: The delay until the onset of the stimulus (in ms)
- dur: The duration of the stimulus (in ms)
- amp: The amplitude of the stimulus (in nA)

In our model, we set the properties of the IClamp as follows:

stim.amp = 1
stim.del = 100

The current pulse has 1 nA amplitude, starts after 100 ms and lasts for 90 ms.

For point process objects we have to use ‘dot’ notation.

The point processes are expressed in absolute terms(ex: nA) whereas the parameters that are attributed to the entire section are usually expressed in terms of per unit area(ex: nA/cm^2).

In addition to IClamp, there are VClamp, ExpSyn poin processes.Each of them have their own properties that should be set.The program for our model is [77,78]:

create soma

access soma

soma diam = 400
soma L = 120
soma Ra = 70

objectvar stim
stim = new IClamp(0.5)

stim.amp = 0.1
stim.del = 100
stim.dur = 90

How to run the simulation?

A simple command to run the program is.

run()

To compare the changes in membrane potential, we use ‘print’ command before and after running the program:

soma print v

The default duration for running the program is 5 ms. However, we can change the duration time by the command bellow [77]:

tstop = 300

run()

Modeling by graphical interface

From the main menu (Fig 2.16.up) click Tools/RunControl. A window will be open that allows us to specify the related parameters for the simulations (Fig 2.16.down). There are several buttons; each is used to determine the value of a specific property on the membrane. A general initial default values are set in front of each icon. We can change the values by typing the numbers or using the ‘up& down’ button. When a new value is set, a check mark appears beside the value. Clicking on it returns the parameter to the initial default value.

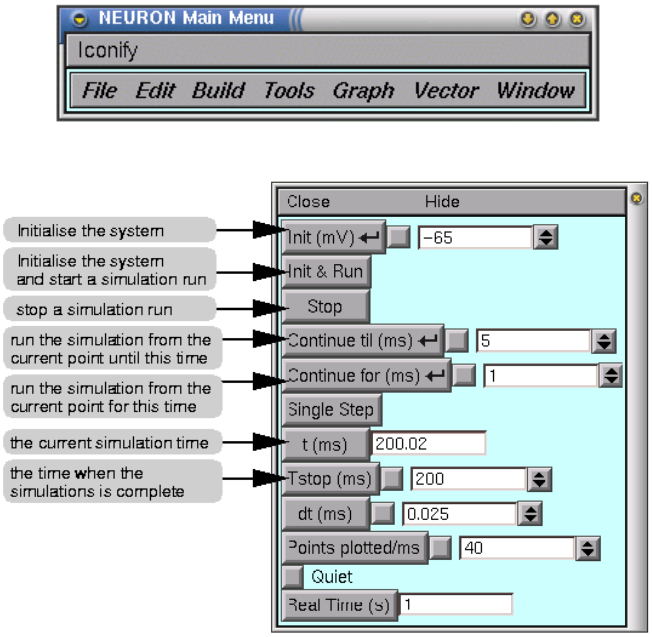

Fig 2.16 up) the NEURON main menu, down) RunControl window is designed to determine the related values of properties of the model and see the graphical plot of the changes of the membrane parameters[77].

After specification of the parameter values, we apply them on the model by pressing Enter key or clicking or Init&Run button.

To see the plot for the time evolution of the membrane voltage, we click the Voltage axis button from the Graph window of the NEURON main menu. A window will open that shows the time course (horizontal axis) of the voltage (vertical axis).

The initial value for membrane potential is -70 mV. This amount of voltage is related to the voltage difference in the capacitance, leakage reversal potential and resistance. Application of current with 1 nA amplitude, and 5 mS duration (is plotted as a sloping line) increases the membrane voltage to -40 mV.

There is a square mark at the top-left corner of the window. We can study the figure with more details by clicking on it or just right-click on the plot and choosing the submenus[77].

Kirchhoff's law:

From the Kirchhoff's first law, we drive the equation which relates the time corse of voltage with other related parameters:

$$C\frac{dV}{dt} = -\frac{V - E_L}{R_{in}} + I_e \quad (2.90)$$

Here R_{in} is the inject current needed to increase the membrane potential by a desired amount and I_e is the current injected.

The answers of equation above is:

When the current is began to inject at t=0, the time evolution of the membrane is:

$$V = E_L + R_{in} \quad (2.91)$$

When there is no injected current, membrane potential changes according to the equation below:

$$V = E_L + V_0 e^{-\frac{t}{\tau}} \quad (2.92)$$

That V_0 is membrane voltage at the beginning t=0 and τ is the time constant that is the time it takes for the membrane potential to get the limited value.

$$\tau = r_m c_m \quad (2.93)$$

To defineR_{in} , we use Ohm law that is the ratio of the small changes in membrane potential over the injected current:

$$R_{in} = \frac{\Delta V}{\Delta I_e} \quad (2.94)$$

The input resistance depends on the specific membrane resistance and the area of the membrane:

$$R_{in} = \frac{r_m}{A} \quad (2.95)$$

The area of the membrane 'A' is defined by:

$$A = \pi . diameter . L \quad (2.96)$$

In our model:

$$A = \pi . 50 \times 10^{-4} . 120 \times 10^{-4}$$

$$= 1.88 \times 10^{-4}\ cm^2 \quad (2.97)$$

According to table 2.3, the specific membrane resistance is:

$$r_m = \frac{1}{specific\ leakage\ constant} = \frac{1}{g\_pas} = \frac{1}{0.001} = 1\ k\,\Omega\,cm^2 \quad (2.98)$$

Therefore R_{in} is:

$$R_{in} = \frac{r_m}{A} = \frac{1000\ \Omega cm^2}{1.88 \times 10^{-4}\ cm^2} = 5.3 \times 10^6 \Omega = 5.3\ \mathrm{M}\Omega \quad (2.99)$$

We compare the result for R_{in} with the result calculated with the other formula:

$$R_{in} = \frac{\Delta V}{\Delta I_e} = \frac{V_0 - E_L}{I_e - 0} = \frac{(-59.69 - (-65)) \times 10^{-3}}{1 \times 10^{-9}} = 5.3 \times 10^6 \Omega = 5.3\ \mathrm{M}\Omega \quad (2.100)$$

Immediately after the current injection, membrane potential is -59.69 mV and its value before the injection (initial value determined for the model) is -65 mV. The amplitude of the injected current is 1 nA and there is no initial current. The results show that the value of R_{in} calculated using the two methods match each other[77].

Saving the program

To edit the commands and reuse them, it is more practical to enter the commands in notepad for windows users and save them. We can reopen the program by double click on it.

Neuronal Network

In the next step, we connect the dendrites to the soma and then design a network of neurons.

In object oriented programs, for each section of the model, specific characters and functions are defined, then, these independent elements are programmed to be a component of a larger functional environment. The same concept is applied for neurons when we consider each component of the membrane as a combination of circuit elements. These chain components connect together as shown in Fig 2.17 and are called cables.

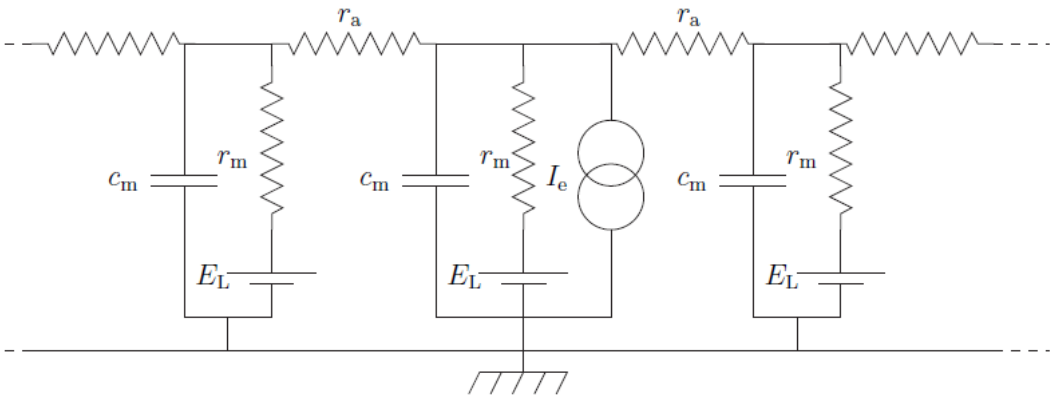

Fig 2.17 consideration of the neuron as a cable that is a chain of components connected each other[78].

In NEURON the cable is considered as several components connected each other (Fig 2.17). The soma is considered as a sphere and the dendrites are assumed cylinders.

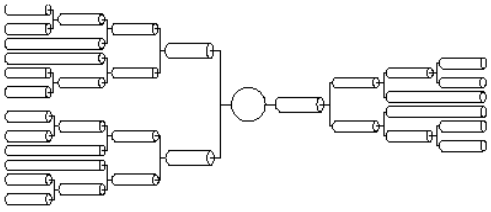

Fig 2.18 Construction of a complex network of neural compartments by connecting independent sections [80]

Before we start programing, it is useful to note the importance of the segments: The point possesses are poison processes that are defined in an small area that depends on the dimension of the segment. The point process acts on the middle of the segment. If section is considered as a segment, the point process will end up at the middle of the section. If the section consists of several segments, the point process is defined to act in the middle of one of the segments and not necessarily on the middle of the segment.

Therefore, division of the section into segments increases the spatial resolution of the simulation.

In this report, our approach is to add two dendrites to the soma. A simple model of connection is illustrated in Fig 2.19.

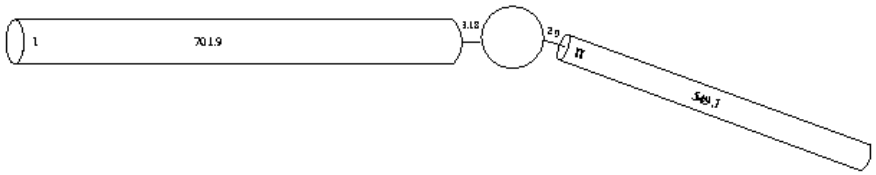

Fig 2.19 Three independent segments are connected each other. Dendrites are shown in cylindrical shape are connected to a soma (with spherical shape).

To create the components, we type create command with the name of the sections that are two dendrites and a soma:

```
ndend = 2
create soma, dend[ndend]
access soma
```

The second step is defining the characteristics of each of the sections. For soma:

```
soma {
    nseg = 1
    diam = 18.8
    L = 18.8
    Ra = 123.0
    insert hh
}
```

Then, we determine the properties for each dendrite:

```
dend[0] {
    nseg = 5
    diam = 3.18
    L = 701.9
    Ra = 123
```

```
    insert pas
}

dend[1] {
    nseg = 5
    diam = 2.0
    L = 549.1
    Ra = 123
    insert pas
}
```

To connect the components, we use *connect* command in the form below:

```
connect dend[0](0), soma(0)
connect dend[1](0), soma(1)
```

After introducing the components, we can apply different processes on the sections. For example, we inject a current pulse in the soma:

```
objectvar stim
stim = new IClamp(0.5)

stim.del = 100
stim.dur = 100
stim.amp = 0.1
tstop = 300
```

It is important to note that the initial potential of the membrane is similar but not necessarily the same in all the components. Voltage variation on the membrane depends on time, so , to reach a stable state, it is better to let the simulation run for a while before applying a stimulation (in our program the delay is 100 ms before applying IClamp)[79,80].

Figures generation

To plot the voltage graph of the three section, we right click on the voltage graph window and choose "*plot what?"* A window will open with the list of the sections and their properties.

The variables are calculated at different times. For example, voltage is calculated at the beginning of the time step, whereas current is calculated at the middle of the time step[80].

Chapter 3

Effect of temperature on voltage-gated sodium, potassium and calcium channels

Regarding the influence of temperature on chemical and enzymatic processes involved in channels function, as well as its effect on membrane lipids associated with channels [81], effect of temperature on channel responses is an important issue. Influence of temperature on ion channels of unmammalian neurons have been studied in several researches [82-85], nevertheless its effect on mammalian neural channels have become a hot topic recently.

In this section, we analyze the response of the voltage gated sodium Na_V and potassium K_V channels to the changes in temperature with NEURON software. We apply Hodgkin and Huxley equations for Na, K, leak currents in mammalian nerve cells (HH2). Using ICLAMP technique, we injected a current with specific amplitude (0.1 nA) and duration (5 ms) and simulate the behavior of voltage gated ionic channels at temperatures 30 (activation range of TRPV4 channels), 36, 40, 43 (TRPV1 is activated at this temperature [46]), 45, 52 (activation temperature of TRPV2 channels) and 55^oC. Finally, we use VCLAMP technique and find the changes in time constant and gating parameters versus temperature and voltage.

Methods and Settings

In this simulation, a typical soma with $20\mu m$ length and $20\mu m$ diameter is considered, then we express Na_V and K_V channels by inserting hh2 model and adding leakage current:

create soma

soma diam = 20

soma L = 20

insert hh2

insert pas

The amplitude of the leakage current is set to $0.0001\ \ (S/cm^2)$. The values of $\overline{g_{Na}}$ and $\overline{g_k}$ equals to $0.003\ (mho/cm^2)$ and $0.005\ (mho/cm^2)$ respectively according to the hh2 model conditions. After initial settings , we fix the temperature to $25^{O}C$ and form ' NEURON Main Menue' we choose 'Tools' and select 'RunControl' to control the initial potential , simulation duration and other parameters. Then from 'Tools' , 'Point Processes' we select ' Managers' then ' Electrode'. 'I/V Clamp Electrode' window will open. We choose ICLAMP and set the delay period to 5 ms, current injection period to 5 ms and the current amplitude to 0.1 nA. In Fig 3.1 the considered settings are illustrated.

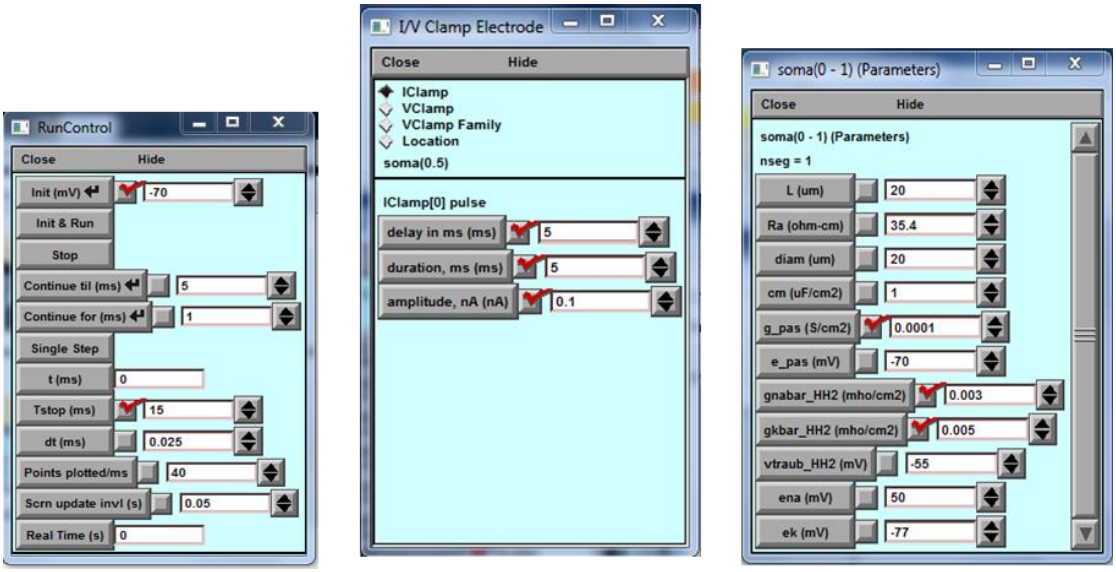

Fig 3. 1 Initial settings for our simulations with ICLAMP technique.

After setting the parameters, we run the program for several considered temperatures. To see the simulation results, Neuron has graph options that is explained in Ch2. We illustrated V-t, gating numbers-t and time constant $\tau - t$ graphs in the following sections.

Result 1: Membrane voltage versus time

Membrane potential remains at rest value until the time the current is injected (t = 5ms to 10 ms). From t = 5ms, the potential starts to rise and when it passes the threshold potential, AP happens. According to Fig 3.2.a, the amplitude and duration of the spikes decrease with temperature significantly.

For more precised evaluation, we divide the AP process to 3 stages as shown in Fig 3.2.b. The first stage is from the time that the current is turned on to the threshold voltage which is about -40 mV (from Voff to Vinit), the second stage is the time that the potential

jumps from the threshold value (-40 mV) to the maximum peak of the spike(Vmax) and the last stage is the time interval that the membrane potential drops from Vmax to its threshold value named Vend.

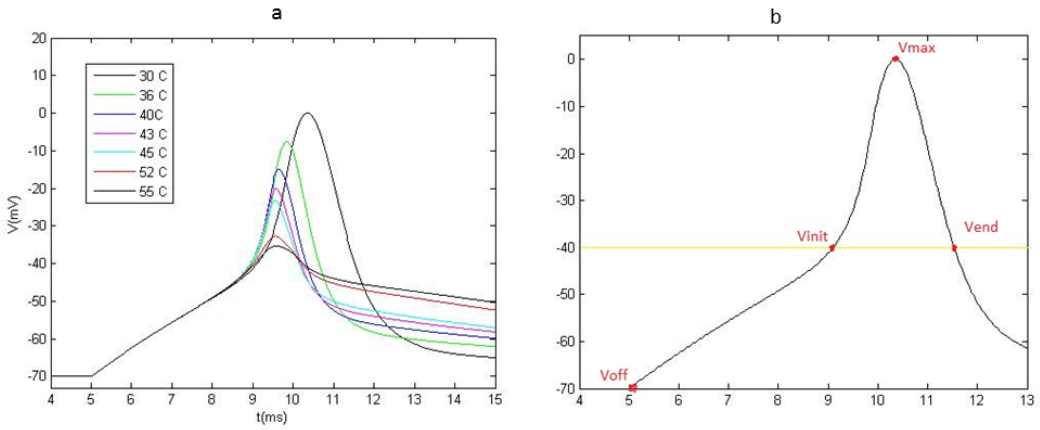

Fig 3. 2 a) Reaction of soma to the injection of current with 0.1 nA amplitude and 5ms duration at 30, 36, 40, 43, 45, 52, and $55^{o}C$. The dynamic rate of channels increases with temperature. b) AP at 30 C◦ that is pointed by four voltage values to divide the AP process to several stages for more precise evaluation.

Fig 3.3 shows the changes in potential versus time. As it is clear form Fig 3.3.a, membrane potential at lower temperatures rises more than the case it does at higher temperatures. The pattern of membrane voltage is similar from Voff to Vinit in all temperatures as shown in Fig 3.3.b.But the differences are significant from Vinit to maximum peak (Fig 3.3.c) and it is almost equal for the pattern from Vmax to Vend but with inverse trend.

Fig 3.3.e, f and g show the duration of APs in various temperatures. In these figures, the duration of the ionic flux from Voff to Vmax have an exponential trend. At low temperatures, the spike duration is high. However, alteration of the temperature results in decreasing the duration of the ionic fluxes except in Fig 3.3.f that the duration of the ion flux from Voff to Vinit is highest at $30\ ^{0}C$, then it decreases by temperature and hits a minimum peak at $45\ ^{0}C$ and then rises again. Although, the changes of the period from Voff to Vinit is very small in this graph, it has a small effect on the total figure of APs.

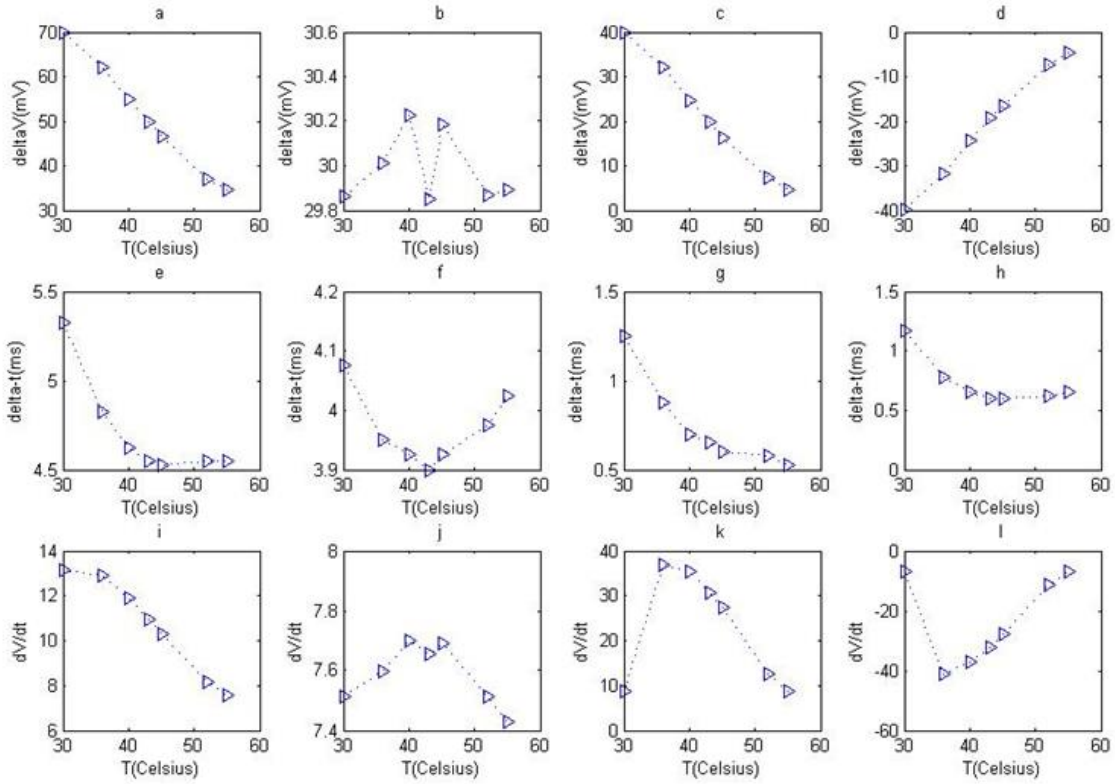

Fig 3. 3 Voltage difference, rate and duration of spikes at different temperatures. The ion fluxes is described in four phases: The first column of figures from left side (a, e and i) show the changes from Voff to Vmax. The second and third column illustrates the changes from Voff to Vinit and from Vinit to Vmax respectively. The last column is about the changes from Vmax to Vend.

The last four plots (Fig 3.3 i, j, k and l) show the changes of voltage over time (i.e voltage rate) versus temperature. In Fig 3.3.i, the voltage rate decreases slowly but steadily at lower temperatures. However, it falls more steeply as the temperature alters. Enhancement of the temperature results in a small fluctuation in Fig 3.3.j that is from Voff to Vinit. An unusual figure is shown in Fig 3.3.k. The slope of V over t is low at $30\ ^{0}C$, it plunges and hits a maximum peak at $36\ ^{0}C$ and then falls again. The opposite pattern is resulted in Fig 3.3.l from the simulations.Total width of the spike (duration of AP) is illustrated in Fig 3.4. It decrease exponentially with rising the temperature.

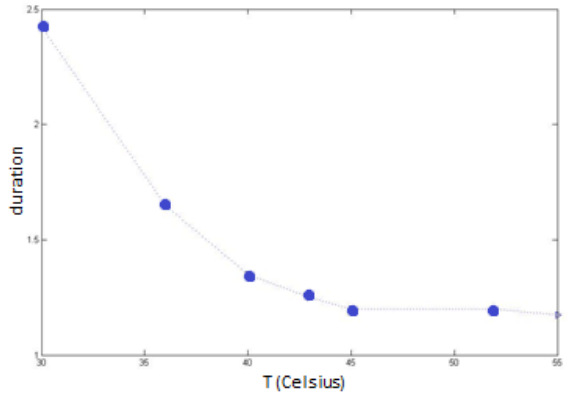

Fig 3. 4 Changes of the spike durations (spike width) with temperature. As the temperature alters, the duration decreases exponentially.

Result 2: Gating parameters

We also study the contribution of m and h gates for sodium channels and n gates of potassium channels. The time course of these gate activations is illustrated in Fig 3.5.

In Fig 3.5a, as the temperature increases, the percentage of the activated m gates and its duration decreases. The apposite pattern is shown for h gates (Fig 3.5.b). For Potassium channels only one type of gate is defined (n gates). In Fig 3.5.c, the enhancement of temperature results in decreasing the width and amplitude of the n-t graphs. The plot for n gates at 43^oC follows an unusual trend. It is important to note that at this temperature range TRPV1 channels are activated. We can conclude that K_V channels may moderates the TRPV1-caused spikes.

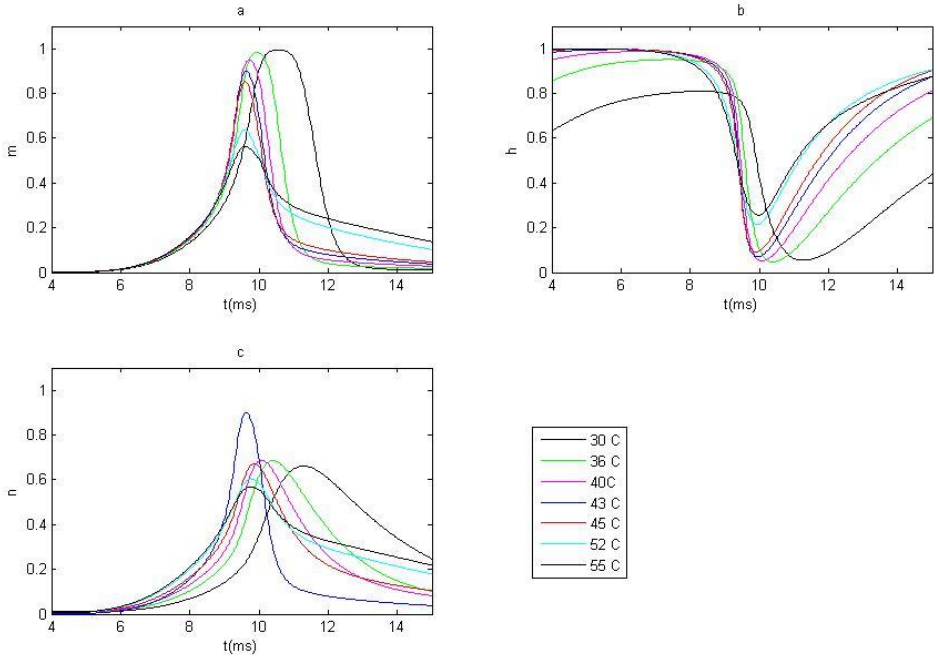

Fig 3. 5 The percentage of the activated gating number of a)Na-m, b)Na-h and c) k-n gates over time and at various temperatures. In all plots, as the temperature rises, the proportion of reacted gates decreases except the n gates at 43^oC that show a different pattern in plot c

Fig 3.6 shows the maximum number of activated *m*, *h* and *n* gates and the related time.

Considering that *m* gates of the sodium channels start action potential, and HH model considers all or none role, response is possible only when high proportion of m gates are activated. Since only around 60% of the channels get activated, we can indicate from Fig 3.6.a that the membrane perturbations at 53 and $55\ ^0C$ are not defined as an AP.

It is important to note that in Fig 3.6.c, mechanism of n gating at $43\ ^{0}C$ does not follow similar pattern of gating at other temperatures.

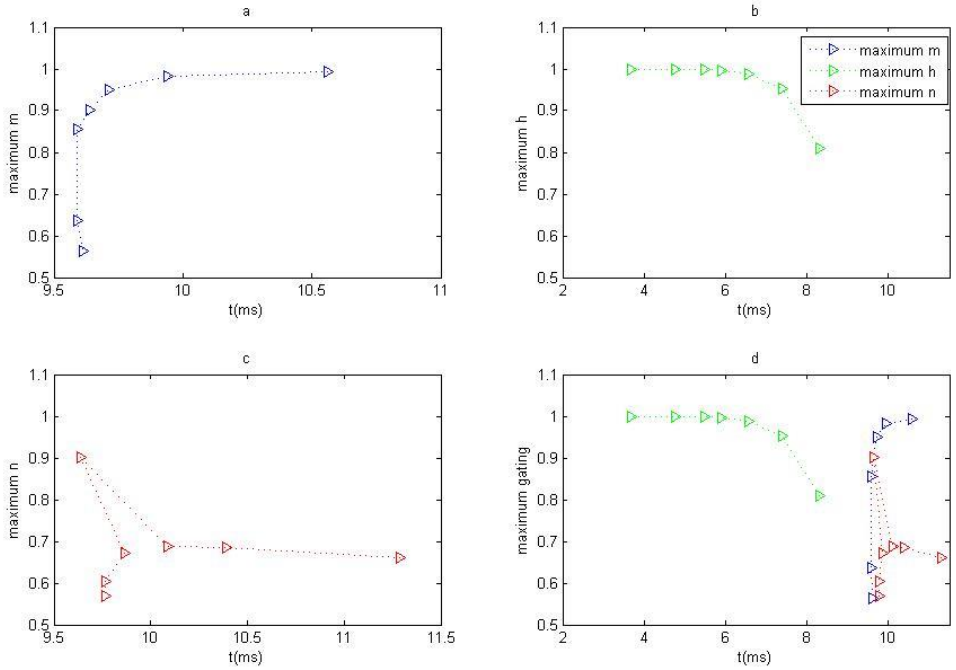

Fig 3. 6 the maximum percentage of gating of a) m gates for sodium channels, b) h gates for sodium channels, c) n gates for potassium channels and d) comparison of the three plots. The time and maximum gating numbers decrease with temperature. However, maximum n at 43o C shows a different trend.

From Fig 3.6.d it is clear that *h* gates reach their maximum activation percentage earlier than the *m* and *n* gates. Comparing the plots for *m* and *n* gates for sodium and potassium channels, the time and percentage of maximum gating for both gates and the related time period is similar at high temperatures($55, 52, 45, 43\ ^{0}C$) but at low temperatures the plot for *m* gates is far higher than *n* gates. Indeed, although the numbers of activated gates change very small by temperature, the *m* gates activation percentage is increasing but for *n* gates it is decreasing.

Fig 3.7 compares the activation percentage of *m*, *h* and *n* gates as a function of voltage for different temperatures. As it is clear from Fig 3.7a, none of the *m* gates are in activated condition at rest potential. Injection of current leads to the activation of gates that is continued until it reaches a maximum value, which is proportional reversely to the temperature. Then it goes back to the initial value. Fig 3.6.b shows the activation percentage of *h* gates. For the membrane temperature of $30\ ^{0}C$, the activation process happens in vast wide of voltages, however as we set the membrane to higher temperatures, the width and the percentage of the *h* gates become smaller. For the *n*

gates of potassium channels, in low temperatures ($30, 36, 40, 45\ ^0C$), the maximum number of activated gates have similar value around 60% of the total number of gates. In this plot also, we see the activation trend of *n* gates at $43\ ^0C$ behave differently with others. The maximum percentage and the voltage interval of the activation at 52 and $55\ ^0C$ is much smaller than those for low temperatures.

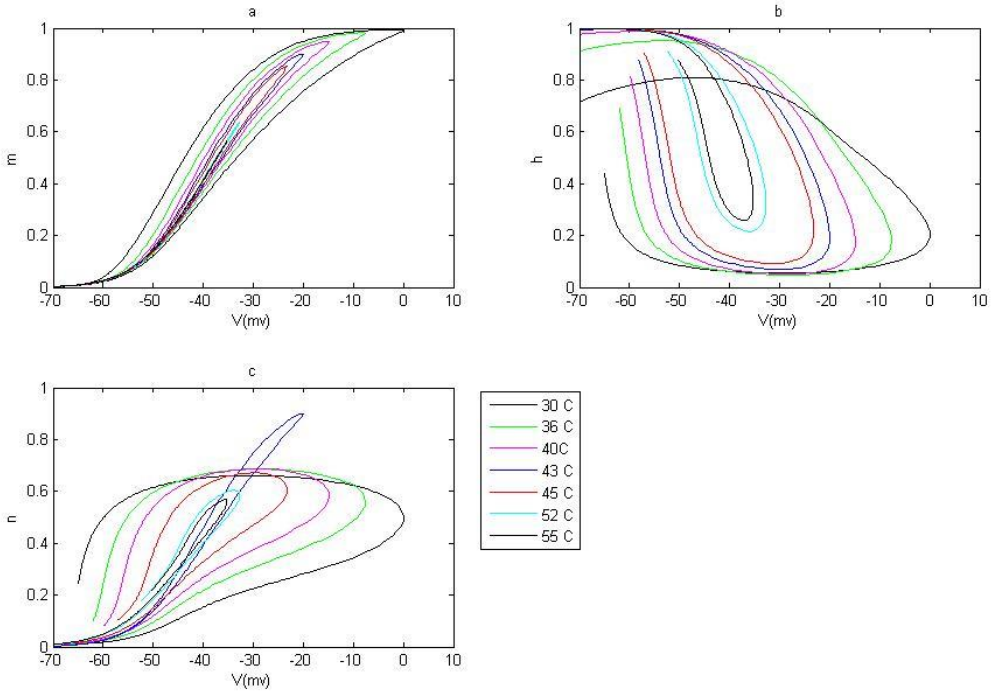

Fig 3.7 Activation percentage versus membrane voltage for a)m gates and b)h gates of voltage gated sodium channels and c)n gates of potassium channels at different temperatures. As the temperature decreases the rating process happens in smaller range of voltage.

Effect of thermal and electrical stimulation in VClamp condition

Vclamp technique is the other method that is used in HH model. In this case, the voltage remains constant during the experiment. To study the effect of temperature on the kinetics of ionic fluxes, we use the formulas in the HH2 model. We set the voltage to change from -75 to 45 mV and the temperature from 25 to $65\ ^0C$ with 1^oC steps. The results are shown in Fig 3.8.

Result 1 : Effect of temperature on time constant

Before analyzing the results, it is useful to note that changes in temperature affects the time constant (τ) directly:

$$\tau = \frac{1}{(a + b)tadj} \qquad (3.1)$$

That

$$tadj = 3^{\frac{T(^0C)-36}{10}} \qquad (3.2)$$

The temperature factor (tadj) is appeared only in time constant parameter in HH model in NEURON [73].

In this simulation, we changed the temperature from 25^oC to 65^oC with 1^oC steps to find the relation of time constants with temperature.

Fig 3.8 compares the changes in the time constant of m, h and n gates with temperature. The m gates, which are beginners of AP, are affected very small from changing the temperature, but the time constant for h gates of sodium channels decrease exponentially. Effect of temperature on time constant for n gates of potassium channels is higher than for those of sodium channels but the trend of changes is similar with the h gates.

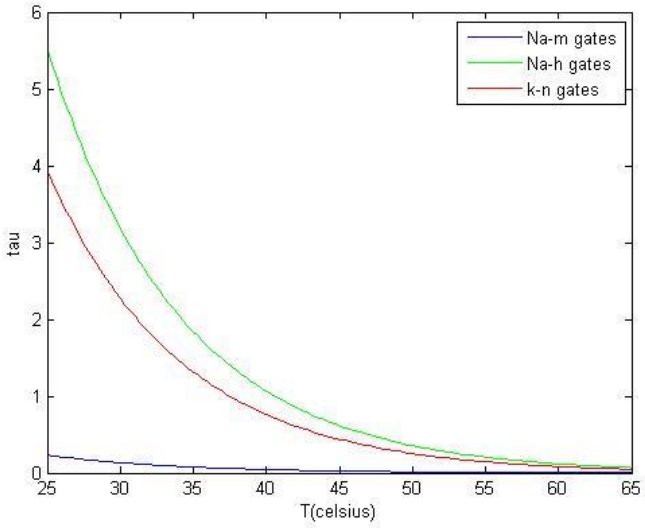

Fig 3. 8 Changes of the time constant for m, h gates of the sodium channels and n gates of the potassium channels. Temperature increases from 25° C to 65° C with 1° C steps.

Result 2: Gate number versus temperature and voltage

Fig 3.9 illustrates the kinetics of Na_V and k_V channels as a result of thermal and electrical stimulation of soma. In the first plot, the fraction of activated gates is shown (in 20 temperature values) as a function of voltage. The graphs at different temperatures almost coincide each other. As it is clear from the plots, the number of activation of m and n

gates increases by thermal and electrical stimulations, but the number of activated h gates decreases from 100% to zero. At first glance, we see that the patterns of the gating is the same in both types of stimulation. However, it is important to note that the voltage stimulation is in [-80(mV):1 mV: 60(mV)] interval but the thermal stimulation is between 25 to $65\ ^{0}C$ with $1^{o}C$ step.

For better comparison between the effect of thermal and electrical stimulation, the 3 dimensional plot is illustrated for changes in fraction of activated gates with temperature (Fig 3.9.a) and also with voltage (Fig 3.9.b).

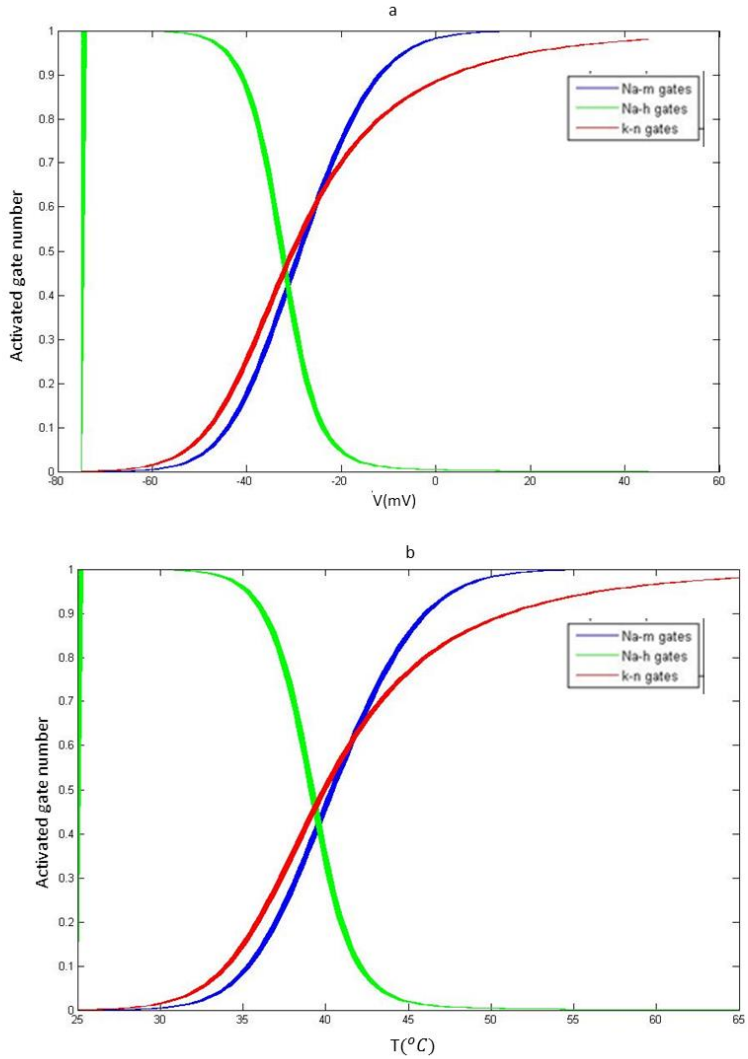

Fig 3. 9 Fraction of m gates(blue), h gates(green) and n gates(red) that are activated due to change in a) voltage from -80 to -60 mV. Each gating number trend is simulated at temperatures 25,26,… , 65^{o} C . b) Fraction of m gates (blue), h gates(green) and n gates(red) that are activated due to change in temperature at constant voltage of -80,-79,…,60 mV.

As it is clear from Fig 3.9.a, the GateNumber-V graph for each gate is almost the same at all temperatures.(The lines include the overlapped plots of the Gate Number-V graph at considered temperatures). Similar figure is recorded for Gate Number-T at considered voltages). Changes in Gate number with temperature and voltage looks similar. The only

notable difference is the range of variations in voltage(-80 to 60 mV) and temperature(25 to $65^{o}C$). For better comparison, we illustrate the 3-D plot for the Gate Number-V-T in Fig 3.10.

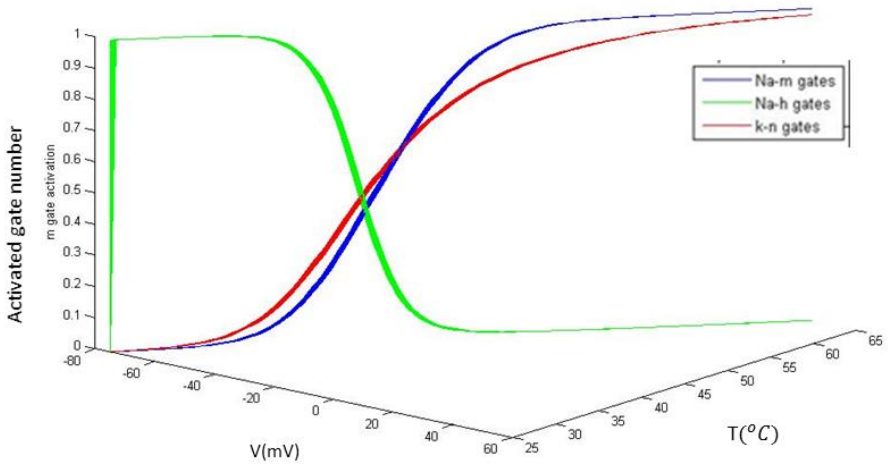

Fig 3.10 changes in the fraction of activated gate number as a result of thermal (25:1: 65^{o} C) and electrical (-80:1:60 mV) stimulations.

Chapter 4

A code for TRPV1

Mechanism of TRPV1 channels is still obscured. However, some experimental attempts involve the contribution of electrical stimulation on TRPV1 channels [4]. To construct an appropriate numerical model for gating mechanism of TRPV1 channels, we first use these experimental results to study the mathematics for involvement of voltage changes on TRPV1 gating. These expressions help us to provide an algorithm for electrical stimulation of TRPV1 channels at different temperatures. After bulding a computational model, we design several simulations similar to the experimented data recorded by Voets et al. [4] and discuss the cases that the results agree or disagree with experimental records. We also simulate and discus the effect of voltage on Na_V, k_V, Ca_V and TRPV1 channels.

Experiments on dependence of TRPV1 on membrane voltage

Heat-sensitive TRPV1 channels are also sensitive to the changes in membrane voltage. It seems that voltage and temperature dependency are linked together.

In an experiment, Voets et .al used whole-patch clamp technique on human embryonic kidney (HEK) 293 cells to study the kinetics of ion flux through TRPV1 gates[4]. The time course of current is described with a two state model for voltage gated channel.

$$\text{Closed} \underset{\beta(V,T)}{\overset{\alpha(V,T)}{\rightleftarrows}} \text{Open} \qquad (4.1)$$

They fitted the results to a mathematical model and derived a formula for opening and closing rate of the TRPV1 channels that determines the contribution of voltage on them:

$$\alpha = Ae^{-\frac{E_{a,open}}{RT}} e^{\frac{\delta zFV}{RT}} \qquad (4.2)$$

$$\beta = Be^{-\frac{E_{a,close}}{RT}} e^{-\frac{(1-\delta)zFV}{RT}} \qquad (4.3)$$

That $E_{a,open}$ and $E_{a,close}$ are activation energies for opening and closing the gates, R is the gas constant(8.31 J.$mol^{-1}.K^{-1}$), T is absolute temperature, z is effective charge associated with voltage dependent gating , δ is the fraction of z moved outward, F is Faraday constant(9.65× 10^4 $Celsius.mol^{-1}$) and A and B are preexponential factors.

According to Eyring rate theory, the activation energy is calculated by[20,87]:

$$E_a = \Delta H + RT \qquad (4.4)$$

And $$A = k_0 e^{\Delta S/R} \qquad (4.5)$$

Where k_0 is the frequency factor. The gating rates are related to channel opening probability by:

$$\alpha = P_{open}/\tau \qquad (4.6)$$

And

$$\beta = (1 - P_{open})/\tau \qquad (4.7)$$

The following parameters are obtained for TRPV1 channels in -100 and +100 mV :

A =1.61 × 10^{37} S^{-1} , $E_{a,open}$ = 208 kJ. mol^{-1} (4.8)

B = 9.67 × 10^{5} S^{-1}, $E_{a,close}$ = 23.2 kJ. mol^{-1} (4.9)

δ= 0.5

z = 0.71

We used the above information to build our model for voltage sensitivity of TRPV1 channels in NEURON. In this model, we can fix membrane temperature at different temperatures and inject arbitrary amount of current. The same as K_V channels, only one type of gating is considered for TRPV1s. The following sections explains the results of simulations we did with our model that matches well with the experimental records.

Results of simulations for voltage dependency of TRPV1

We provided a model that is the computational construction of the set of equations explained above. To check if the computational model match with the experimental records, we designed some simulations:

We create a soma with 20 μm length and 20 μm diameter and then insert TRPV1 model. After that, we use VCLAMP technique to keep the membrane voltage at a constant value. The value for g_pas is set to 0.0001 (S/cm^2).

Create soma

Soma diam = 20

Soma L = 20

insert pas

insert TRPV1

The primary membrane voltage is set to -70 mV with 100 ms duration and the simulation voltage amplitude is set to 100 mV with duration of 100 ms. Fig 4.1 shows the VCLAMP settings.

Voets et al. calculated the opening probability and activation and inactivation rates for 25, 30, 35, $42^{O}C$ temperature (Fig 4.2) [4]. We do the same measurements to test if the simulation results match with the experimented records. We plot n_{∞}(i.e P_{open}) and τ_n for 25, 30, 35, $42^{O}C$ temperature as a function of time for each temperature and find α , β and P_{open} and compare them with the correlated experimental result.

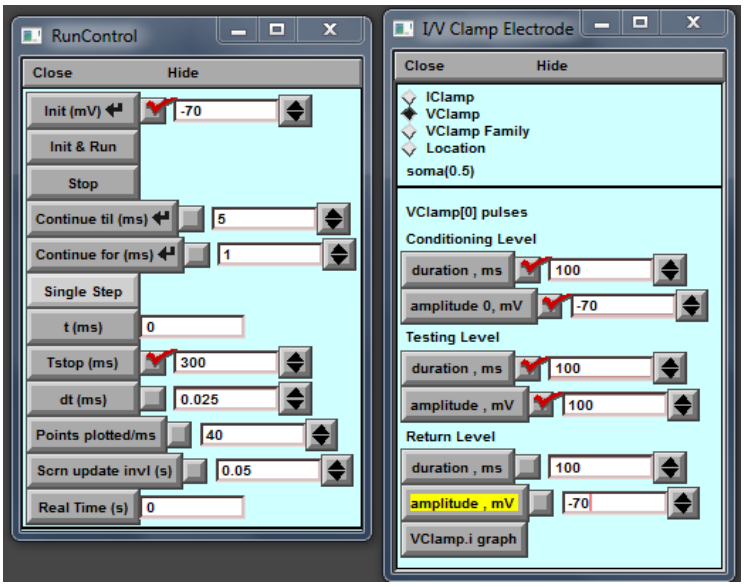

Fig 4.1 initial settings for simulation of the activation current and opening probability of TRPV1

a

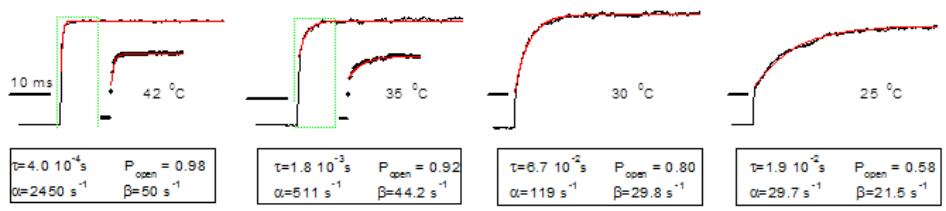

b

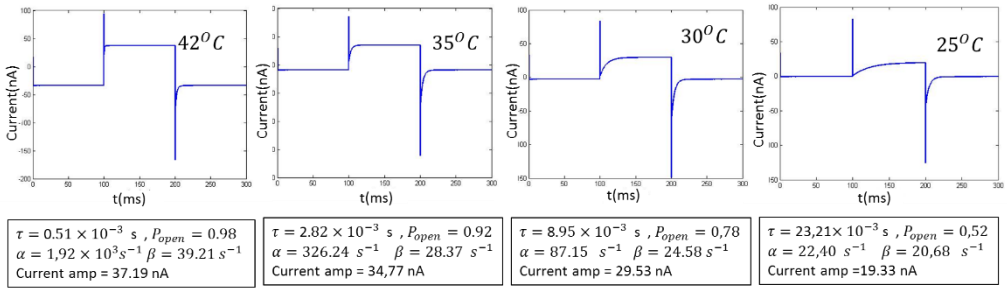

Fig 4.2 a) Current(nA) related to the activation of TRPV1 channels at 25, 30, 35, 42^O Cduring depolarization of the membrane from 0 to 0100 mV. Opening probability and the time constant is indicated under each graph and the constant rates is calculated from the measurements [4]. The fitted currents is shown in red and scale bars indicate 10 ms duration. b) Similar trend is used to simulate the related parameters in NEURON with TRPV1 code and non-passive current condition.

Fig 4.2.a illustrates the experimental measurements of current, opening probability (P_{open}) ,the time constant (τ) and the activation and deactivation rate constants at 25,30,35 and 42^{O}C.

Changing the membrane voltage results in a rising trend of current through TRPV1 channels. As the result of electrical stimulation, the low-level current increases in all four temperatures albeit to varying the flux rates and then remains stable. It can be concluded that temperature alteration leads to decrease in time constant and increase in P_{open} , and the constant rates.

Simulation of this experiment in NEURON with TRPV1code is illustrated in Fig 2.b It shows that the stimulation of TRPV1 channels results in dramatic increasing of the ionic current. At $42^{O}C$ the current increases from about -34 nA to 36 nA. As the temperatures falls, the primer current increases to about -9, -3 and -1 nA, and the maximum current amplitude also decreases. As temperature declines, the value for P_{open} decreases and the time constant rises which result in smaller flux rates.

Overall, it can be concluded that the quantity for the parameters simulated using TRPV1 code does not show a considerable difference with the experimental records.

In the next simulation, we evaluated the changes in current amplitude at various injected voltage (-120, -100 , -80, … , 100, 120 mV) with similar condition with the experiment done by Voet et al. which is illustrated in Fig 4.3.a below. In this experiment, the primary voltage is set to 0 mV for 12 ms and the final voltage is set to +60 mV with 38 ms duration. The injected voltages range from -120 mV to +160 mV with 20 mV steps and the duration is 100 ms (Fig 3c and Fig 2.c Voet et al). In our simulations the function of TRPV1 channels are simulated by TRPV1 code(Fig 4.3.b). In Fig 2 the related settings is illustrated.

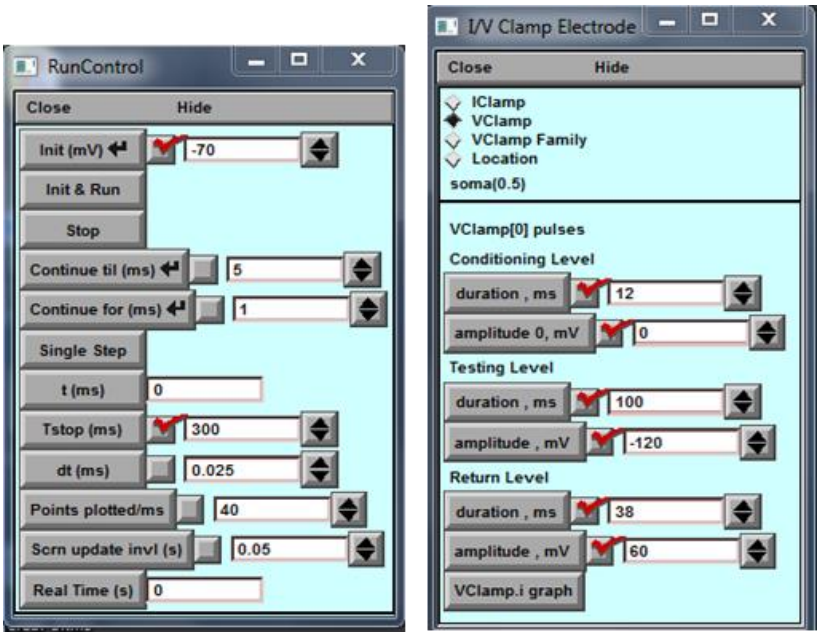

Fig 4.3 Simulation settings related to measurement of effect of voltage changes on TRPV1 in different temperatures (The result of simulations is shown in Fig 4.3)

The experimental records[4] in Fig 4.3.a show that changes in voltage does not affect the mechanism of TRPV1 channels significantly at low temperatures, but as the temperature increases, increasing voltage cause a larger alteration of ionic current through the TRPV1 gates. Indeed, stimulation of the TRPV1 gates with positive voltages leads large ionic fluxes.

a

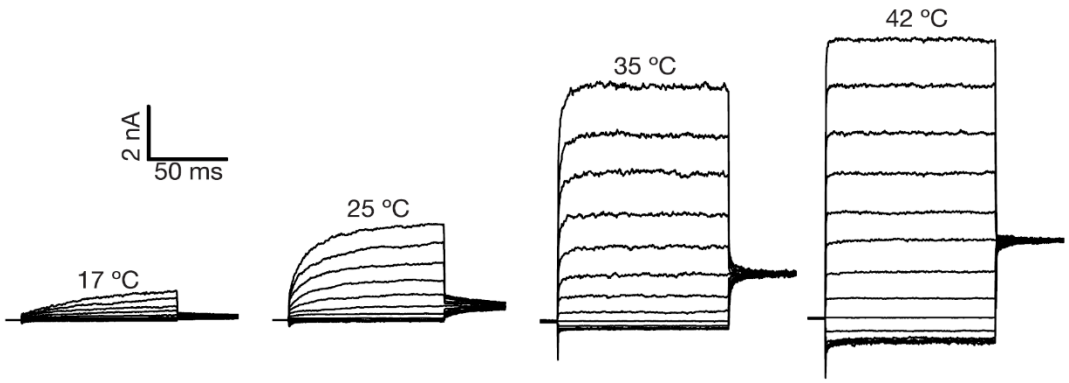

b

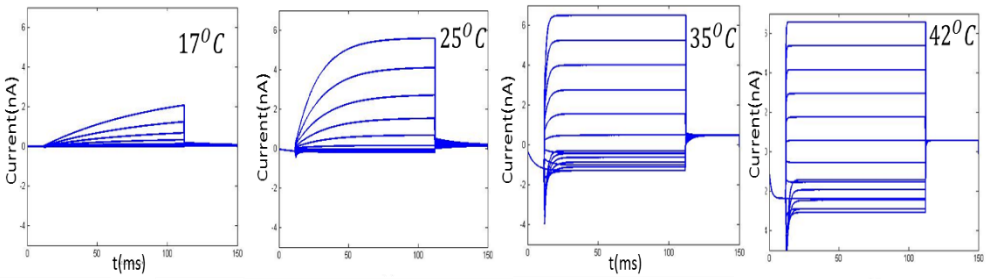

Fig 4.4 Effect of changing in the amplitude of injected voltage to dynamics of TRPV1 channels at 17, 25, 35 and 42° C. A) the experimental results recorded by Voet et al [4] b) result of simulations by TRPV1 code

It is also clear from the graphs that stimulation of membrane with negative voltages does not affect the gates considerably, however as the voltage increases (voltage steps are equal, 20 mV), the current steps become larger. At $42^{O}C$,the difference between the current flowed in +160 mV and in -120 mV is about 11 nA in the records of Voet et . al. However, the current amplitude difference in our simulations with TRPV1 code is about 8 nA.

The last simulation is set to check the opening probability of the TRPV1 gates in different voltages and temperatures. Fig 4.5 shows the related settings.

Voet et .al studied the probability of gating of the TRPV1 channels (P_open)at various temperatures(Fig 4.6.a). They set the temperature to a specific value and injected -120 mV voltage and recorded P_{open}, they measured P_{open} each time they increased the voltage to +20 mv higher amplitude.

Fig 4.6 b show that the opening probability obtained from simulations by TRPV1 code is similar with the experimental records.

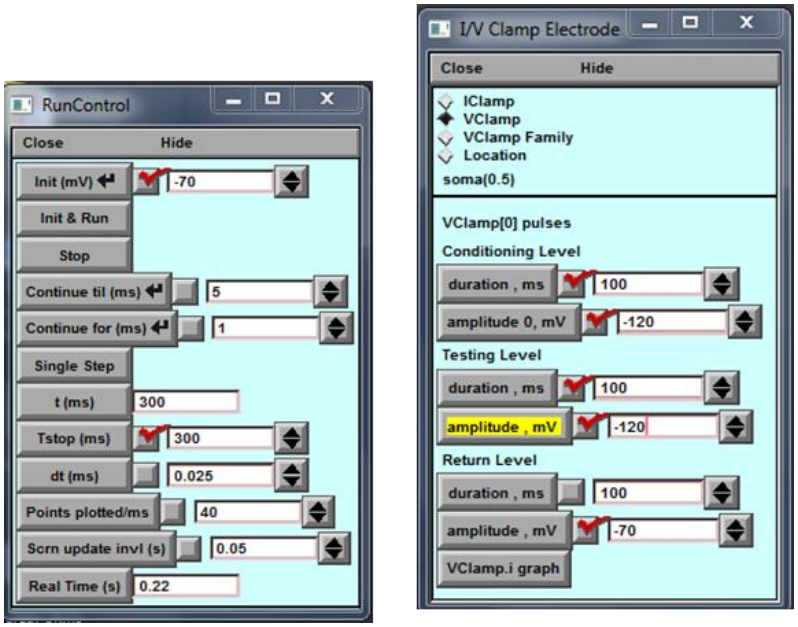

Fig 4.5 Settings related to simulation of opening probability at different voltages and temperatures

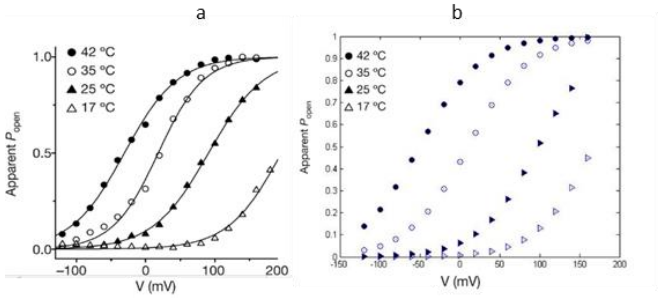

Fig 4.6 The opening probability versus voltage at different temperatures. A) experimental records by voet et .al [4] b) Results of simulation by TRPV1 code

Chapter 5

Simulation: Role pf TRPV1 channels in membrane stimulations

We aim to investigate some properties of TRPV1 channels function and compare it with Voltage gated sodium, potassium and calcium channels for mammalian. We compare the voltage and its rate of change, duration of spike and related gating numbers when thermal or electrical stimulation is applied in the cases with and without TRPV1 channels. In the next step, we compare the threshold current required to generate AP with contribution of all the considered channels. Finally, the firing rate and the spike widths at different simulation condition is studied.

Simulation settings

To construct the model of our simulations, first, we create soma with $20\mu m$ diameter and $20\mu m$ length. Second, we insert passive current, HH2 and Ca_t_thal. Finally, we insert TRPV1 model to the previous simulation instruction and compare the kinetics of ionic fluxes through Ca_V Na_V and k_V and TRPV1 gates.

create soma

access soma

L = 20

diam=20

insert pas

insert hh2

insert Ca_t_thal

**insert TRPV1*

We set the passive conductance to 0.0005 $S/cm^2$and $\bar{g}_{TRPV1}$ to 1.7 × 10^{-4}mho/cm^2. Fig 5.1 shows the primer settings for the simulations. We simulate the stimulation of soma at 30, 36, 40, 43, 45, 52, $55^O C$. At each temperature, we inject 0.1 nA current with 5 ms duration.

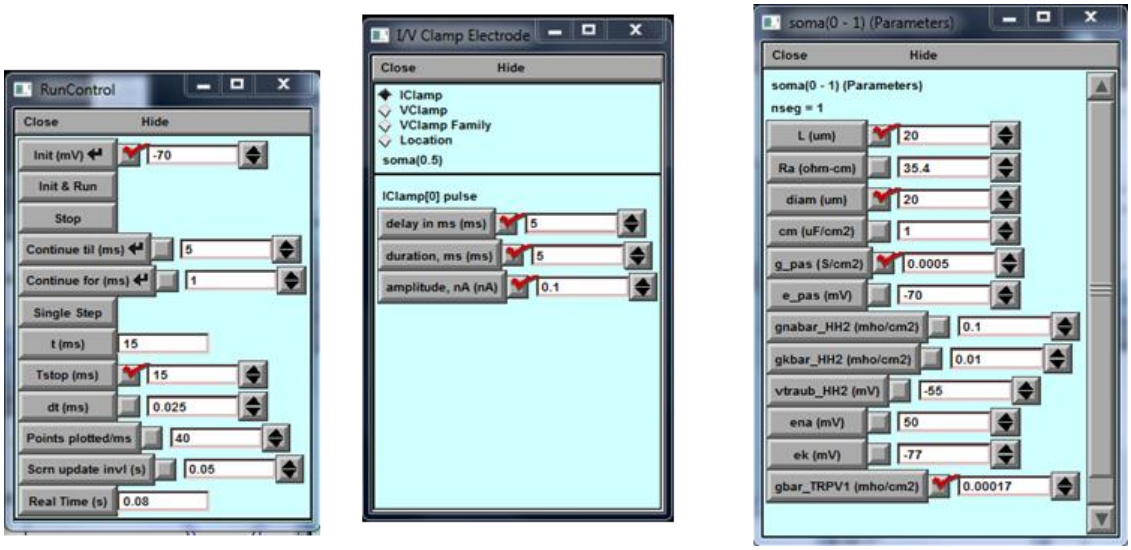

Fig 5. 1 Settings for simulating the stimulation of a soma using ICLAMP technique .

Result 1: Simulation of Pulses caused by alteration of temperature

Using TRPV1 model, it is possible to study the effect of fixed temperatures on TRPV1 channels and the spikes produced by these temperature sensitive channels. We set the amplitude of the current to zero and increase the temperature to evaluate the mechanism of voltage gated and TRPV1 channels in the condition that no current is injected.

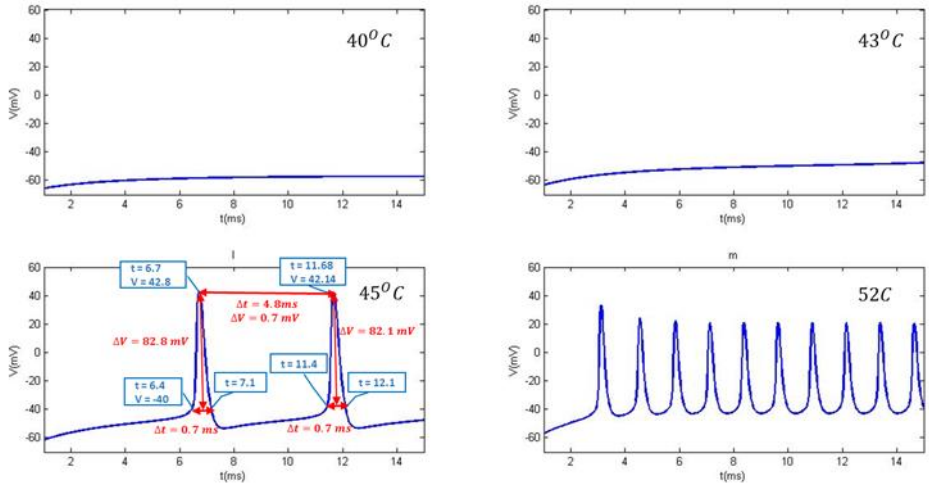

Fig 5. 2 changes in membrane voltage due to the change in temperature in the condition with 0 nA current amplitude

Fig 5.2 shows that at low temperatures, TRPV1 channels are not activated to produce AP, therefore at $43^{O}C$ and lower temperatures, AP does not happen. However, in higher temperatures, ionic fluxes through TRPV1 gates are high enough to generate AP. This figure is illustrated for simulation of TRPV1 gates together with the $Ca_V\ Na_V\ and\ k_V$ channels. Two spikes can be observed at $45^{O}C$, one of them is occurred

during the current application, the second spike is after stimulation period. The width of the AP is the same for both spikes (0.7 ms) but the height of the spike for the first AP is slightly higher than the second spike. At T= $52^{O}C$, although we see several APs in the V-t graph, since the membrane voltage after each spike does not pass to hyperpolarization stage, these spikes are do not occur in reality and perhaps another temperature sensitive TRP channel is activated to moderate the condition.

Result 2: Membrane potential perturbations

We can study the effect of temperature on AP at different temperatures. The graphs for spikes at various temperature are illustrated in Fig5.3 .We use MATLAB in our evaluations.

Fig 5.3.a shows the voltage perturbations resulted due to the ionic flux through $Ca_V\ Na_V\ and\ k_V$ channels. The same stimulation is applied for only $Na_V\ and\ k_V$ channels. As it is clear from the figures, injection of current from 5 ms to 10 ms results in small increase in the potential that its magnitude is the same in all considered temperatures. Comparing the two figures, function of calcium channels do not cause any significant difference in the pattern of voltage changes.

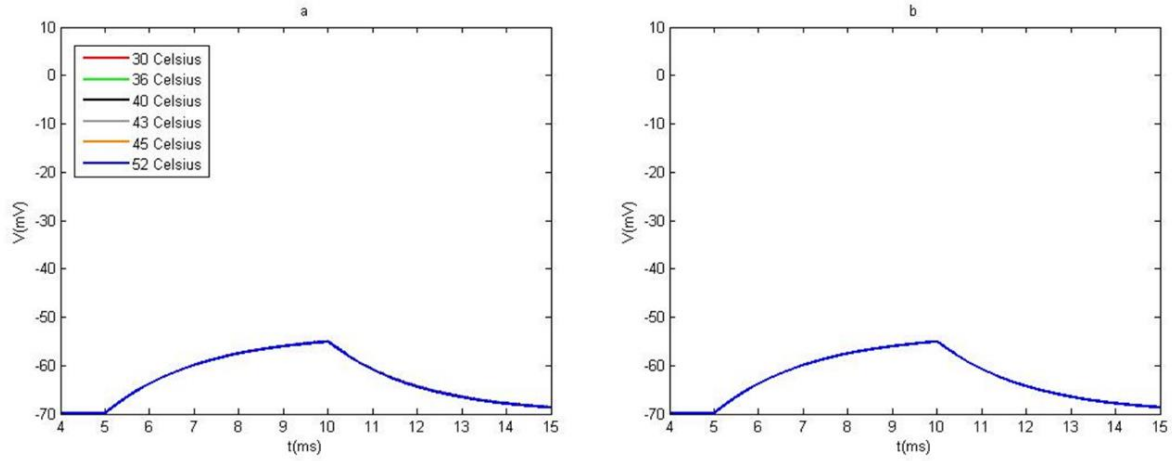

Fig 5. 3 perturbation in membrane potential caused by ionic flux through a) $Na_V\ and\ k_V$ channels and b)$Ca_V, Na_V\ and\ k_V$ channels under the stimulation of the soma with 0.1 nA current with 5 ms duration.

However, when TRPV1 model is inserted in the simulation instruction, notably several spikes are observed.

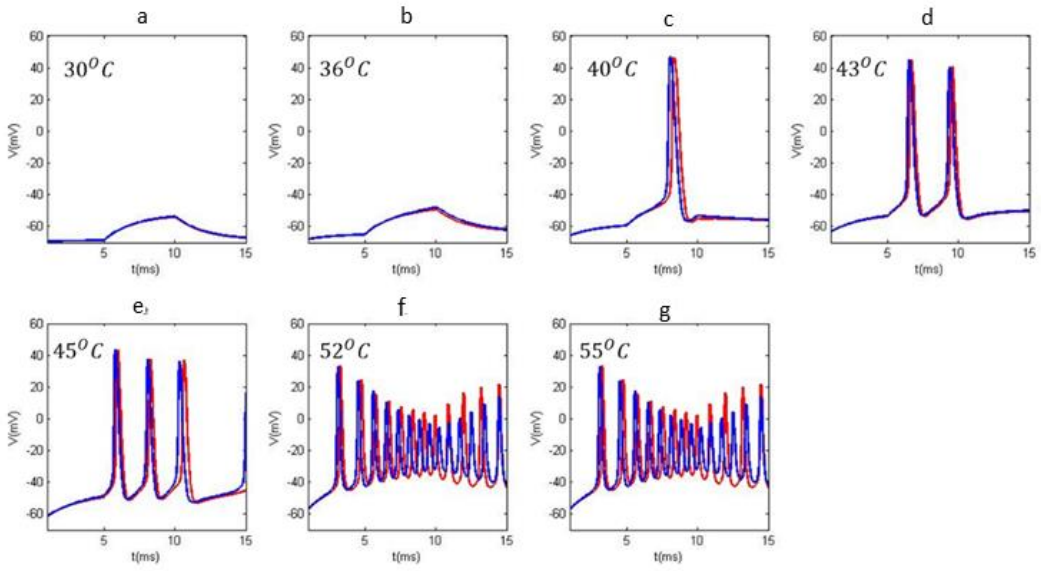

Fig 5. 4 perturbation in membrane potential due to injection of 0.1 nA current with 5 ms duration at different temperatures. Red graphs represent the ionic fluxes through) $Na_V, k_V \; and \; TRPV1$ channels, and the blue graphs show the flux through) Ca_V , Na_V, k_V and TRPV1 channels.

Now we analyze the APs illustrated in Fig 5.4. These spikes are generated by voltage gated sodium, potassium, calcium and temperature sensitive TRPV1 channels. At low temperatures of 30^OC and $36^O C$ the voltage rose gradually to about -55 mV, so no spike is occurred. Nevertheless, at $40^O C$ an AP with 1ms duration is happened due to the alteration of temperature and injection of current. Fig 5.5 shows the details of the spike. Application of current at t=5 ms cause the membrane voltage increase slowly, then after 2.7 ms an AP starts at 7.7 ms, the membrane voltage is soared from -40 mV to 47 mV, then it plummeted to again -40 mV at 8.7 ms. Then it dips during the hyperpolarization. After this injection period that ends at 10 ms, the membrane potential decreases steadily. Comparing Fig 5.4.c with Fig 5.3.a, it can be concluded that despite the fact that temperature has a large effect on production of AP at $40^O C$, the main reason for its generation is injection of 0.1 nA current to the membrane that include TRPV1 channel distribution.

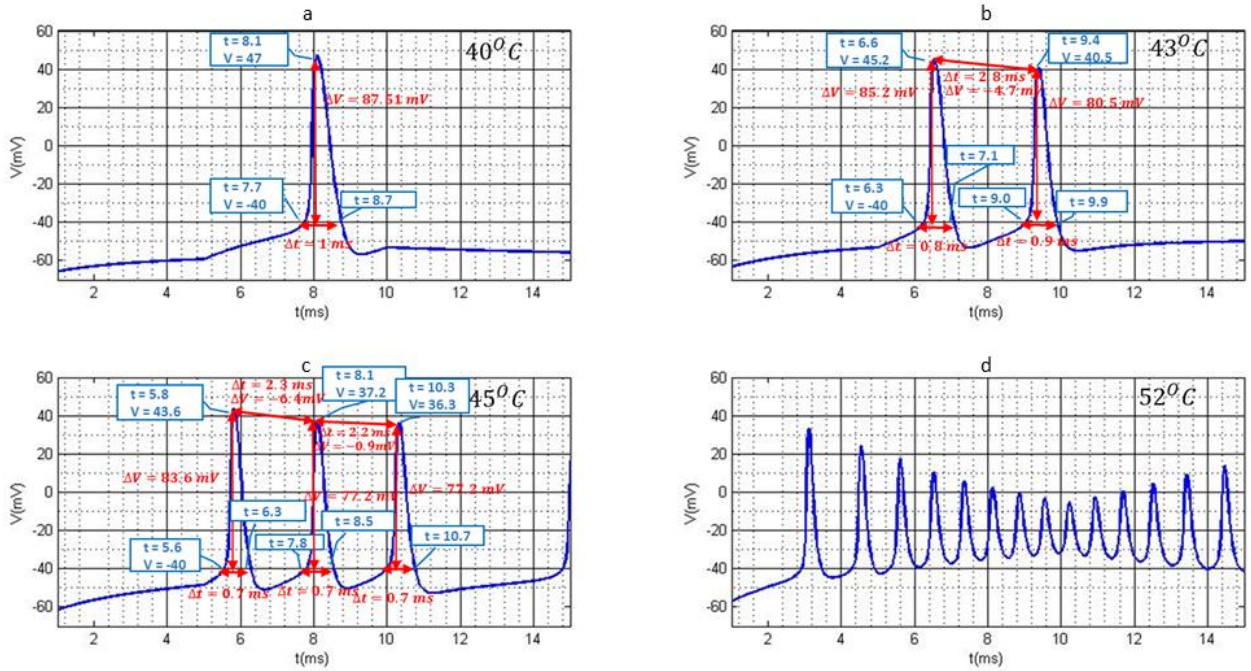

Fig 5. 5 Detail of V-t graphs for the spikes happened at different temperatures and 0.1 nA current application with 5 ms duration in ICLAMP technique.

At higher temperature of 43^OC two APs are recorded that both are generated during the stimulation period. AP durations are almost the same, but the peak value of the second spike is slightly smaller than the first spike. Also, at 45^OC two APs are produced. In addition to these spikes, we can see a third AP that happens after the stimulation period. The width of all three spikes are the same with 0.7 ms duration. The magnitude of peak voltage is highest in the first spike, decreases about 6.4 mV in the second peak, and stays almost the same in the third AP.

Comparing the V- t graphs at considered temperatures, we conclude that with an insignificant difference, the height and the duration of the spikes decreases as the temperature alters. It is interesting to note that the width of the AP does not change in a specific temperature. In addition, the spike at 40^OC begins at t=7.7 ms with 1 ms duration. At 43^OC, generation of spike starts earlear at t=6.3 ms with lower duration(0.7 ms) than that for the AP at 40^OC. The time of AP generation is even smaller at 45^OC (t=5.6 ms) and the duration of the AP is also smaller (0.7 ms) . Therefore, increasing the temperature alters firing rate when soma is exposed to electrical stimulation.

Fig 5.2.c shows that at higher temperatures even without current injection, the membrane can have an AP. At 45^OC two spikes are recorded that the first spike occurs during the stimulation. It is produced at 6.4 ms with 0.7 ms duration and the maximum voltage in 42.8 mV. Injection of 0.1 nA current (Fig 5.5) causes generation of AP 0.6ms earlier and alteration in firing rate. However, the width of the spike is the same in both conditions.

The graphs related to T= $52^{O}C$ and higher temperatures show that since the membrane does not pass to hyperpolarization stage, the temperature sensitive TRPV1 channels and voltage gated channels do not generate action potential at this temperature (Fig 5.2 and 5.4).

Result 3: Contribution of Ca_V, Na_V, K_V channels in membrane potential variations

We aim to find out which channel is the main responsible for beginning of AP at $36, 40, 43\ and\ 45^{O}C$. The candidates are m, nTRPV1 and mCa channels. First, we compare m_∞ and $nTRPV1_\infty$ versus time. We plot the kinetics of ionic flux through the channels in Fig 5.6.

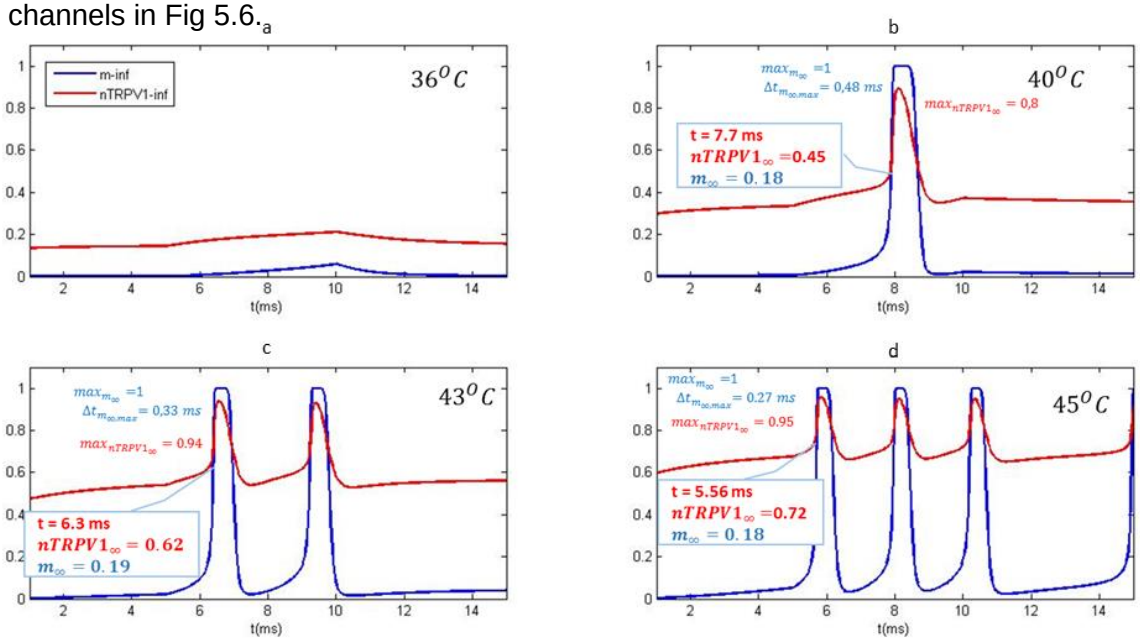

Fig 5. 6 proportion of activated m_∞ for Na_V channels (blue) and $nTRPV1_\infty$ (red) at different temperatures

According to Fig 5.6.a, at $36^{O}C$ the proportion of both m_∞ and $nTRPV1_\infty$ parameters does not increase significantly when current is applied at 5 ms. For this reason, AP does not happen at this temperature. Fig 5.6.b shows the proportion of the considered parameters at $40^{O}C$. At t=7.7 ms that the membrane voltage reaches -40 mV (beginning of AP) 45% of $nTRPV1_\infty$ is activated but only 18% of m_∞ is opened. The value of $nTRPV1_\infty$ is much higher than m_∞ at high temperatures. Therefore, nTRPV1 channels are mainly responsible for beginning of AP and contribution of sodium channels is small. In addition, it seems that temperature does not affect the gating of m channels at -40mV, because at this voltage, the percentage of m_∞ is the same (18%) in all temperatures. On the other hand, although the width of spikes is the same for m_∞ and $nTRPV1_\infty$, the maximum value and the related duration is larger for nTRPV1 channels. During the spike,

the maximum value that m_∞ of sodium channels reaches is 100% and remains in this stage for a short period. This period is less than 1 ms and decreases by temperature, nevertheless, the maximum percentage of $nTRPV1_\infty$ is not constant and increases as the temperature alters, but unlike the m gates, the duration of this condition is about a microsecond.

In Fig 5.7 all these parameters and the correlated time constants are compared at a 36^OC and 40^OC.

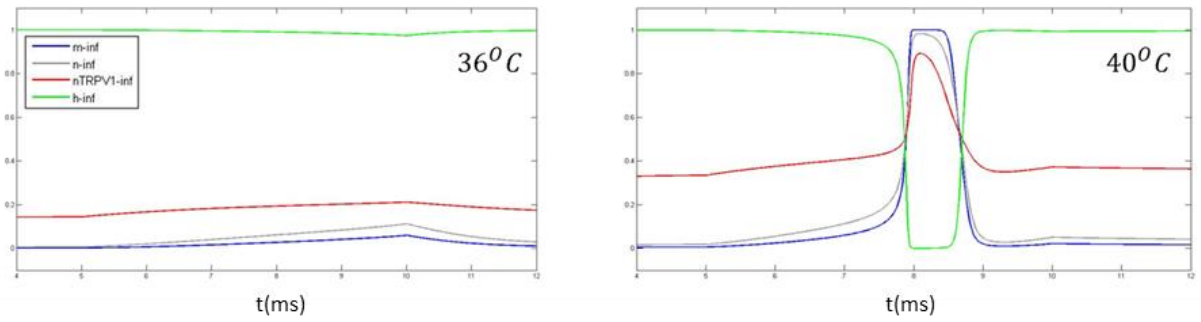

Fig 5. 7 changes of $m_\infty, h_\infty, n_\infty \; and \; nTRPV1_\infty$ when 0.1 nA current with 5 ms duration is injected at left) 36^OC right) 40^OC

As it is clear in Fig 5.7, although at 36^OC the current is induced, the proportion of the parameters do not change significantly. However, when we increase the temperature and apply the current the gates become activated and after a while, they approach their maximum possible percentages. This pattern is the same at higher temperatures of 43^OC and 45^OC illustrated in Fig 5.8.

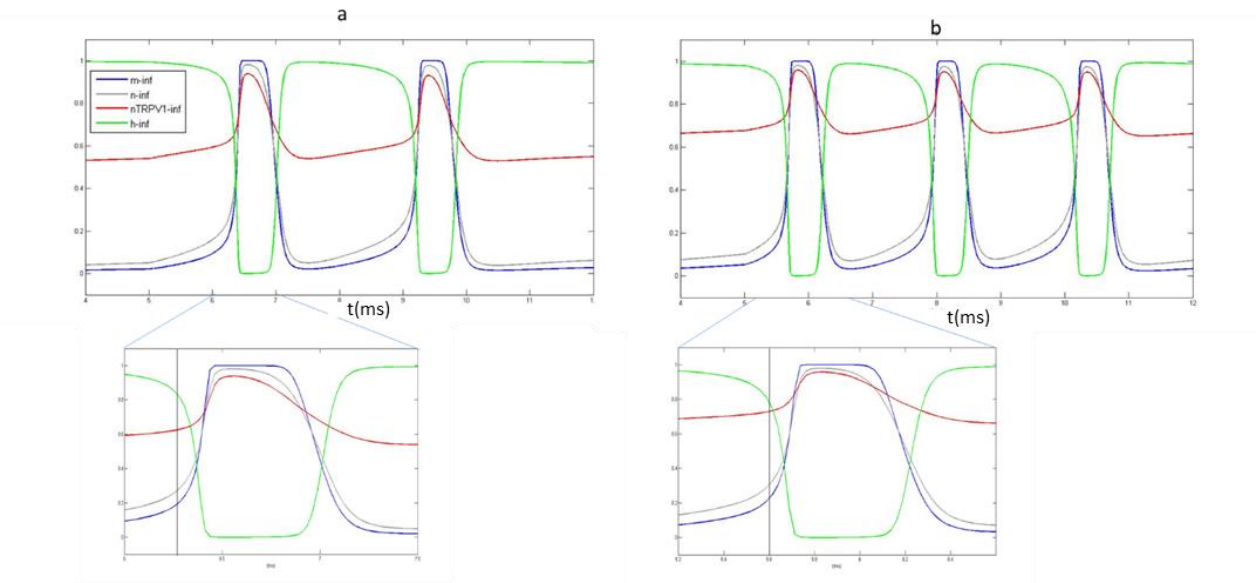

Fig 5. 8 Changes of $m_\infty, h_\infty, n_\infty \; and \; nTRPV1_\infty$ when 0.1 nA current with 5 ms duration is injected at a) 43^OC b) 45^OC . The period of first spike is zoomed below each graph. The black line shows the time that the AP is began.

According to Fig 5.8, the percentage of $m_{\infty,max}$ and also the rate of activation of sodium gates is the largest during action potential at all temperatures. The two graphs are plot

in a larger scale to focus on the stage that AP starts. The vertical black line shows the time that AP started (-40 mV). As it is clear from the figures, although the rate and the maximum value of m_∞ of sodium channels is much higher than those for $nTRPV1_\infty$, the TRPV1 gates begin the spike due to their high concentration. Interestingly, since the initial proportion of nTRPV1 gates depend strongly on temperature, so the time that AP starts also depends on the temperature of the membrane.

For better analyzation of the changes in $gate - number_\infty$, in Fig 5.9 we plot it versus membrane voltage from t=0 to the time that the considered value reaches its maximum. In all the cases that AP occurs, although the initial proportion of $nTRPV1_\infty$ is much higher than that for voltage gated channels, the rate of alteration of m_∞ is the highest, and when the voltage reaches 0 mv, its proportion gets the higher value than n_∞ and even $nTRPV1_\infty$. In addition, during the period that m_∞ is 100%, the other parameters had reached their maximum value and start to return back to their initial values.

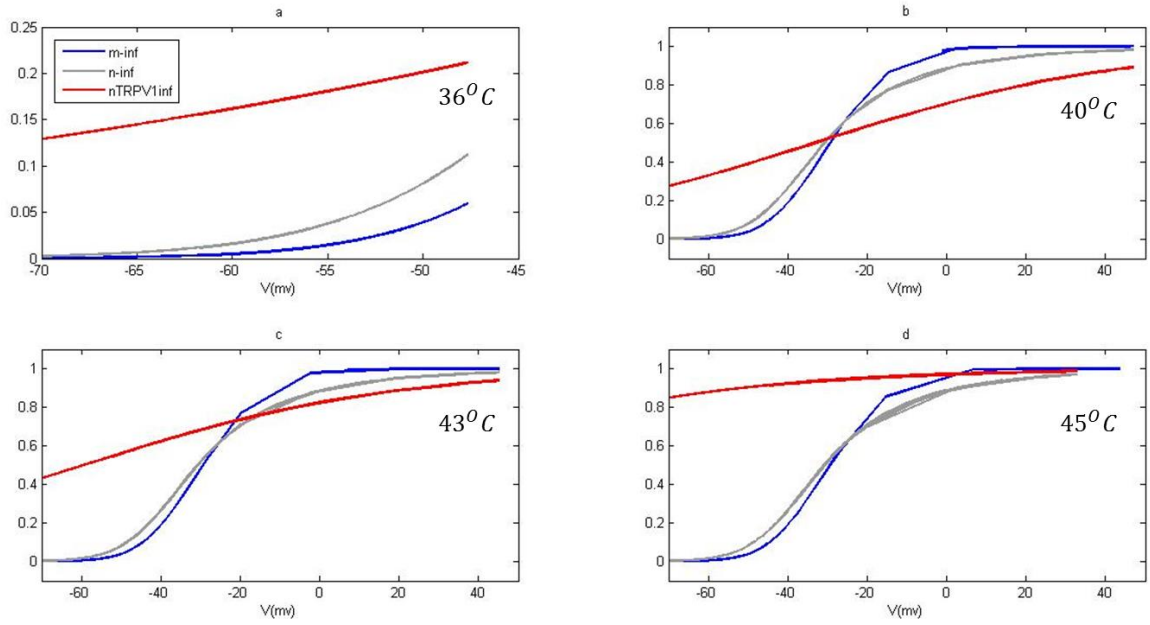

Fig 5. 9 the percentage of $gate - number_\infty$ when reaches its maximum value, during the first AP that is plot for T=36, 40, 43, $45^O C$. At $36^O C$ AP does not happen, so the scales of the graph for this temperature is different from the other graphs.

In the next step, we study the effect of stimulations on the time constant of each gating parameter. According to Fig 5.10, The initial value of τ_{nTRPV1} is maximal, but the rate of alteration of τ_n is particularly noticeable overtaking the figure for τ_{nTRPV1} . The inititial value and the rate of rising of τ_m is minimal throughout the period.

Since at $36^0 C$ AP does not occur, application of current from t= 5ms to 10 ms results in increasing the time constant for all gates. After the current injection, the time constants fall and then level off. Fig 5.10.b shows that after peaking, when Ap begin τ_h plunge to their minimum value ,but jump to create the second maximum peak. And they fell quickly

and then slightly recover. This trend is repeated whenever an AP happens throughout the period in all temperatures albeit to widely varying degrees. The time constant for h gates of sodium channels see a dramatic changing trend and the figure of τ_m remained the smallest over the simulation period. Despite a minimum peak in the figure for τ_{nTRPV1}, the graph does not show a significant rising trend for this parameter. τ_n show similar trend but with a noticeable gap with τ_{nTRPV1} figure.

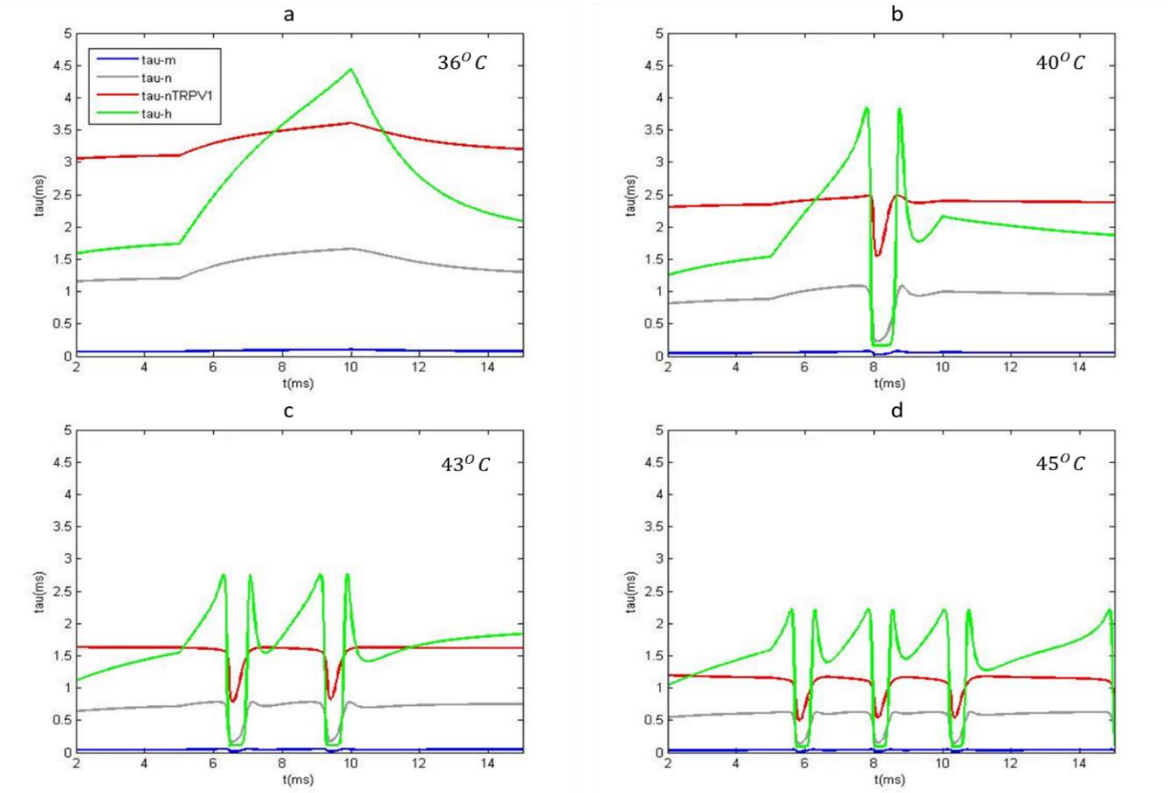

Fig 5. 10 the time constant for m, h,n and nTRPV1 gates in different temperature.

The last parameter we evaluate is the gating number m,h for Na_V, n for k_V, mCa and hCa for Ca_V and nTRPV1 for TRPV1 channels. Fig 5.11 shows that m gates of sodium channels have the maximum percentage and duration among other gates. Graph for activation of mCa gates is almost similar with m gats. However, it takes longer time for mCa gates to inactivate. The rate and proportion of activation of gates is smaller for n gates, but the ending tail is much longer than the other voltage gated channels. Finally, the proportion and the rate of TRPV1 gates is the lowest among the other channels. In the right side, the graphs for h and hCa gates is illustrated. Although the proportion of hCa is minimal in all considered time, the rate of function of h gates is much higher.

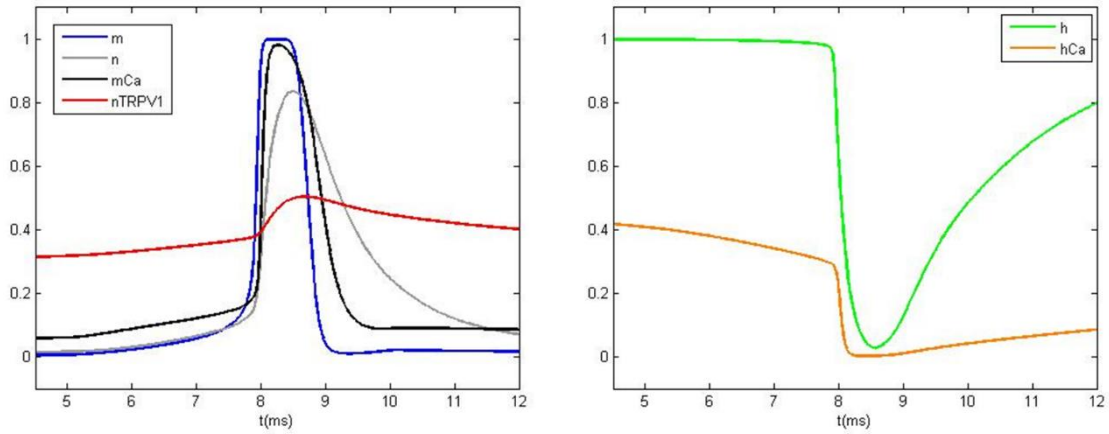

Fig 5. 11 the proportion of m and h gates of Na_V , n gates of k_V , mCa and hCa gates of Ca_V and nTRPV1 gates at 40^OC during the stimulation of the soma.

Result 4: Threshold values

In this section, we study the effect of TRPV1 channels on the minimum current required to produce AP. Fig 5.12 shows that in the condition we insert only voltage gated channel models in our simulation, when we inject 0.7 nA current with 5 ms duration, no spike is produced. However, this amount of current can produce an AP when we insert TRPV1 model to the program construction. In addition, for temperatures higher than 55^OC the graph show an irregular v-t trend when only Na_V, K_V *and* Ca_V channels are distributed on soma. We will discuss the role of TRPV1 channels on V-t graphs at this temperature range in this section.

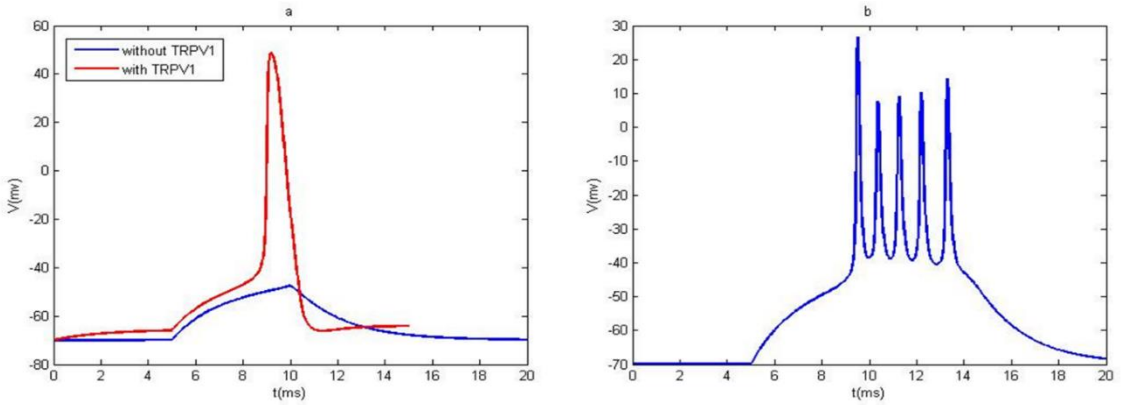

Fig 5. 12a) Voltage-time graph for the condition that only voltage gated Na, K and Ca channels are considered (in blue) and the condition that TRPV1 model is added to the simulation program(in red). B) Voltage –time graph at 55^OC for the case that TRPV1 channels are not considered.

measurements. As it is clear from the figure, at room temperatures, TRPV1 channels do not show reaction to electrical stimulations, However as the temperature increases, the role of TRPV1 gates become more notable(Fig 5.13.a). For the temperatures higher than 43^OC, alteration of temperature is more effective than

the injection of current in producing spikes and further for T>45^{O}C contribution of temperature is dominated and application of current does not affect significantly in the process of generation of first AP.

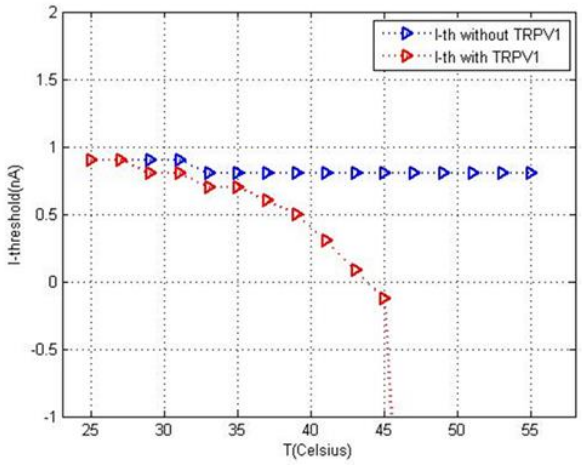

Fig 5. 13 the amplitude of threshold current at different temperatures for blue)Na_V , K_V and Ca_V, red) Na_V , K_V and Ca_V and TRPV1 gatings.

Since the role of temperature at T>43^{O}C is more important than in low temperatures, we focus on the behavior of considered channels at this range. At low temperatures, only one or two spikes appear during and after the application of current. However, when the temperature reaches $43^{O}C$ or higher values, series of APs happen that the time and type of spikes depend on the current amplitude. In these conditions, application of negative currents also generates APs. Nevertheless, this process continues until the temperature reaches $51^{O}C$. At larger temperatures, spikes are not be produced any more. In Fig 5.12.a , the plot of V-t graph at $55^{O}C$ is shown as an example.

Result 5: Series of APs

We measure the time, type and voltage of APs produced from $43^{O}C$ to $51^{O}C$ in the condition that current with -2, -1.5, -1, 0, 0.5 and 1 nA amplitude and 5 ms duration is injected and study the results from t=0 to t=30 ms. The initial setting is the same with our previous simulation that is illustrated in Fig 5.1.

Fig 5.14 shows the changes of the membrane voltage with time when currents with negative, zero and positive amplitude of -1.5, 0 and 0.5 nA is injected. The figure includes the simulations at $44, 48 \text{ and } 51^{O}C$. We analyze compare the results in three stages: from t= 0 to 5 ms that the current is not injected yet, the period that the current is applied, i .e from 5 to 10 ms and the period after the stimulation from t=10 to 30ms. Although the

peaks are continued to be recorded after this time, they do not happen in the real soma because the related changes are effective maximum for 20 ms after the stimulation.

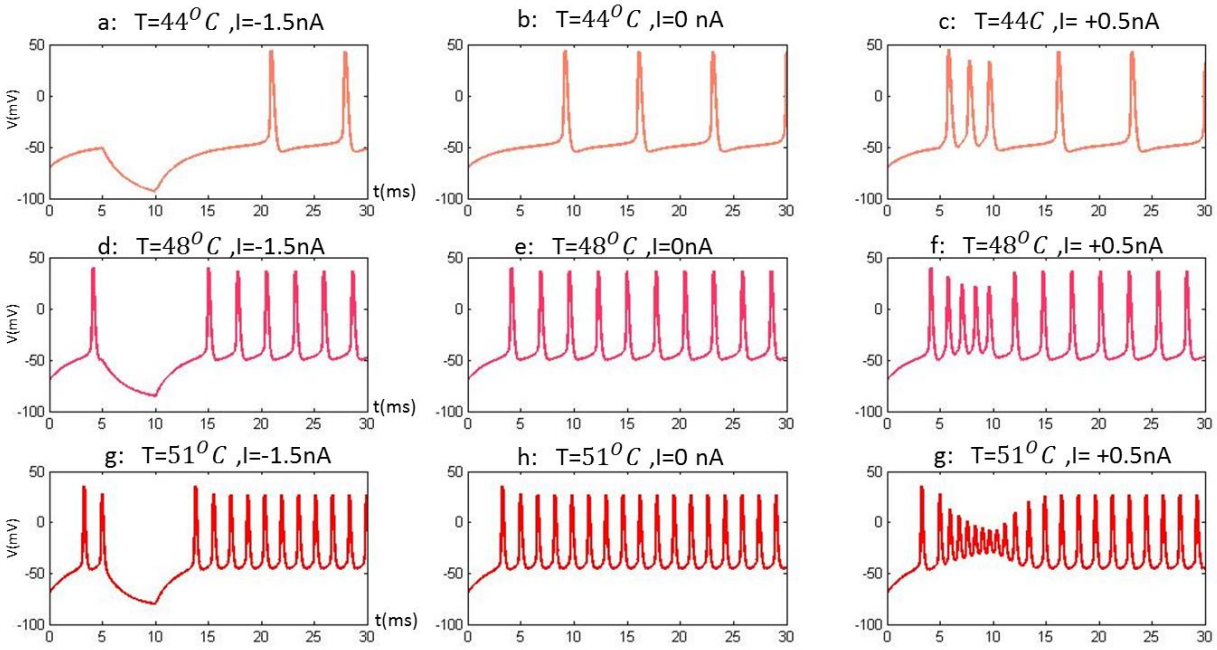

Fig 5. 14 membrane voltage versus time at T= $44, 48, 51^{O}C$ when current with I= -1.5, 0 and 0.5 nA amplitude is applied from t= 5 to 10 ms.

From t = 0 to 5 ms we do not see any spike from 43 to $46^{O}C$ even when the amount of current is increased. However, due to alteration of temperature, one spike is produced from T= 47 to 50^{O}C. Until this temperature, the AP happens few seconds earlier as we increase the temperature, but it does not change by current. At 51^{O}C , the number of spikes increase to two. In fact the spikes that happen in this time interval are survived from the current applied to the membrane at 5 ms. In the case that we do not inject any current to the membrane (I= 0 nA) spikes with the same delay and rate happens. Fig 514.b,e and h show the condition that the spikes are produced as the result of high membrane temperature. As it is clear from the graphs, the height and the frequency of APs at each temperature remains constant and interestingly increases by temperature. In the next section, we will compare the firing rates at different temperatures.

Induction of current cause perturbations in the trend of spikes. When negative current is applied to the membrane(Fig 5.14.a, d, g) the membrane potential starts to decrease until the end of the stimulation at 10 ms. Since the voltage decreases, no AP happens in this condition. In the case we inject positive current, at low temperatures, the firing rate increases, thus there is not enough time for complete outflow of the positive ions from cell. Therefore, the next spike starts in the condition that there is a small amount of

unflawed ion inside the cell(voltage is higher than the rest potential) , additionally, the difference between the peak value and the voltage before the event gets smaller. The vertical axis shows the changes of the voltage on the membrane, therefore the height of the events decreases by time.

After the stimulation, from t= 10 ms to 30 ms, the membrane recovers and the trend of spike becomes normal. Although the firing rate in this condition is the same with no-current condition, the time of APs change insignificantly.

Firing rate (spike/total time) versus temperature is illustrated in Fig 5.15. Total time in this case is 30 ms and no current is injected. According to this graph, as the temperature rises, the frequency of AP generation increases. It is important to note that either positive or negative current is applied; the firing rate is the same. In other words, firing rate depends on temperature and is independent of injected current.

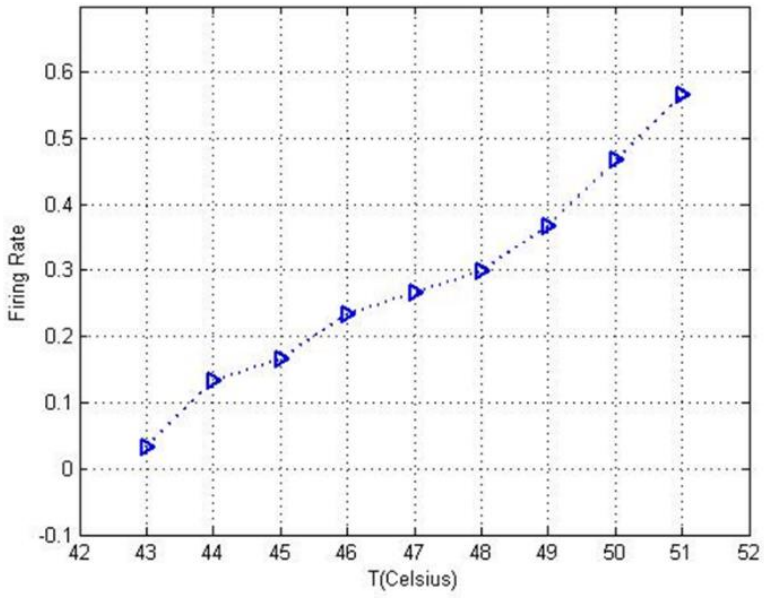

Fig 5. 15 firing rate of APs versus temperature. The total time of simulation is 30 ms

Chapter 6

A mathematical model for ionic channels

One of the recent challenges in neuroscience is to find out how nervous system discriminate different stimulations. A number of quantitive models have been proposed for mechanism of voltage gated channels which are also exhibit high temperature sensitivity. However, the mechanism underlying the temperature sensory of Transient Receptor potential (TRP) channels is still unknown. We expanded the Hodgkin and Huxley model by entering an additional term for mechanism of TRPV1 channels. In this model, we investigate transition state theory for a two state process for both voltage gated and temperature gated channels. This study offers a physical point of view for the evaluations with chemistry and biology perspectives. We suggest that using the basic roles of thermodynamics we can present a unified expression for voltage and temperature sensitivity of considered channels. This expression therefore can solve the problems related to the explanations for temperature sensitivity (Q_{10}) for voltage gated channels. However, experimental measurements are required to determine the precise value of the parameters used in the model.

Theory and Facts

This paper suggests considering the process of channel gating with physical and thermodynamical framework.

The gate opens when a selective ion provides a specific amount of energy rate range. Several thermodynamical facts are considered to build up the model:

1. Each type of channel requires specific amount of energy in a specific time interval (specific energy rate) for gating.
2. If ion provide the required amount of energy rate, it can open the barrier.
3. Physical stimulation input is considered as a specific amount of energy given to the system in a specific period.
4. Since all the stimulation methods result in changing the membrane potential, we relate all the physical inputs to voltage. This is possible by Gibbs energy equation, because Voltage and other types of stimulations transfer the required energy by changing the entropy and enthalpy of the channel system.

New Model

For the two sate model and in constant pressure and acidity the parameters related to gating of voltage gated channels and TRPV1 is:

$$I = \sum I_{channel} \quad (6.1)$$

$$I_{channel} = P_X z_X F.\nu.\frac{[X]_{in} - [X]_{out}e^{-\nu}}{1 - e^{-\nu}} \quad , \quad \nu = \frac{\Delta C_P(T - T_0)}{RT} + \frac{z_X FV}{RT} - \frac{\Delta C_P}{R}\ln\left(\frac{T}{T_0}\right) \quad (6.2)$$

For a simple two state model ($open \underset{\beta(V,T)}{\overset{\alpha(V,T)}{\Longleftrightarrow}} close$) the activation and deactivation rates are:

$$\alpha = k_0 \exp\left(-\frac{\Delta C_P(T - T_0)}{RT} - \frac{\delta zFV}{RT} + \frac{\Delta C_P}{R}\ln\left(\frac{T}{T_0}\right)\right) \quad (6.3)$$

$$\beta = k_0 \exp\left(\frac{\Delta C_P(T - T_0)}{RT} + \frac{(1-\delta)zFV}{RT} - \frac{\Delta C_P}{R}\ln\left(\frac{T}{T_0}\right)\right) \quad (6.4)$$

$$k_0 = \exp(-\frac{\Delta H_0}{RT} + \frac{\Delta S_0}{R})$$

That k_0 is the frequency factor, ΔH_0 and ΔS_0 are the initial enthalpy and entropy and δ is the fraction of ions that pass through the channel. The time constant is

$$\tau = \frac{P_{open}}{\alpha} \quad (6.5)$$

And

$$P_{open} = \frac{1}{1 + \exp(-1 \times \left(\frac{\Delta H}{RT} - \frac{\Delta S}{R}\right))} \quad (6.6)$$

$$= \frac{1}{1 + \exp\left[\left(-\frac{\Delta H_0}{RT} - \frac{\Delta C_P(T - T_0)}{RT} - \frac{zFV}{RT} + \frac{\Delta S_0}{R} + \frac{\Delta C_P}{R}\ln\left(\frac{T}{T_0}\right)\right)\right]} \quad (6.7)$$

$I_{channel}$:current of ion X through channel

P_X : permeability of ion X

z_X : valency of ion X

F : Faraday constant

$[X]_{out}$: concentration of the ion outside

$[X]_{in}$: concentration of the ion inside

C_P : heat capacity of the channel at constant pressure

T : absolute temperature

T_0 : an arbitrary reference temperature

R :universal gas constant

H : enthalpy of system

S : entropy of the system

ΔH_0 : enthalpy at T_0

ΔS_0 : entropy at T_0

δ : fraction of z moves outward direction

Calculations

Transition state theory is one of the methods that can be applied to express the reaction of ionic channels to voltage and temperature [18]. It describes the required work to activate/inactivate a channel. It describes the activation energy of the channel as Gibbs energy. Gibbs energy is sum of changes in enthalpy(H) and entropy(S) terms of a system. ($\Delta G(P,T) = \Delta H - T\Delta S$).

Considering transition state theory in combination with the first and second thermodynamic roles, each channel can be considered as an energy barrier. The correlation of the activation probability and the required gating energy is described by Van't Hoff equation [87-89].

$$P_{gating} = \frac{K}{1+K} \qquad (6.8)$$

$$lnK = \frac{\Delta G}{-RT} \qquad (6.9)$$

Here k is the equilibrium constant, P_{gating} is the gating probability ΔG is the Gibbs energy R is the universal gas constant (8.31 J.$mole^{-1}K^{-1}$) and T is absolute temperature (Kelvin).

Changes in enthalpy and entropy of the system depends on temperature [90-92]. Considering a molar heat capacity for a channel, contribution of temperature on K can be determined by [53]:

$$\ln K = -\frac{\Delta H_0 + \Delta C_P(T - T_0)}{RT} + \frac{\Delta S_0 + \Delta C_P \times \ln\left(\frac{T}{T_0}\right)}{R} \quad (6.10)$$

Where ΔH_0 is enthalpy at a reference temperature (T_0), ΔS_0 is entropy at T_0 and ΔC_P is the temperature-independent heat capacity of the barrier at fixed pressure [93].

On the other hand, Voets et. al offer an expression for involvement of voltage in activation of TRPV1 channels [4]

$$lnP_{open} = -\frac{E_{a,open}}{RT} + \frac{\Delta S}{R} + \frac{\delta zFV}{RT} \quad (6.11)$$

That z is the effective charge associated with voltage dependent gating, δ is the fraction of z moves outward direction, V is the membrane potential and $E_{a,open}$ is the activation energy [20,87]. The effect of temperature is involved in $E_{a,open}$. Eq (6.11) separates the effect of voltage from other parameters in channel activation. So, we conclude that using the term ($\frac{\delta zFV}{RT}$) will help us to get V-independent expression for temperature contribution. Therefore, if we use Eq(6.10) to explain the effect of T on $E_{a,open}$,the heat capacity ΔC_P will be voltage-independent.

Using Eq 6.10 to describe the contribution of temperature parameter in Eq 6.11 we have:

$$lnP_{open} = -\frac{\Delta H_0}{RT} - \frac{\Delta C_P(T - T_0)}{RT} - \frac{z\delta FV}{RT} + \frac{\Delta S_0}{R} + \frac{\Delta C_P}{R}\ln\left(\frac{T}{T_0}\right) \quad (6.12)$$

We can write Eq 6.12 in the form of:

$$\ln k/k_0 = -\frac{\Delta G_0}{RT} - \frac{\Delta C_P(T - T_0)}{RT} - \frac{zFV}{RT} + \frac{\Delta C_P}{R}\ln\left(\frac{T}{T_0}\right) \quad (6.13)$$

for simplicity in our calculations;

$$\nu = \frac{\Delta C_P(T - T_0)}{RT} + \frac{zFV}{RT} - \frac{\Delta C_P}{R}\ln\left(\frac{T}{T_0}\right) \qquad (6.14)$$

This expression is used to extend the GHK equation. We consider that the concentration of ion X at any binding site is large, therefore, its movement is independent. The electrical distance of the barrier is denoted by λ.

We assume that channel includes n barriers with electrical distance of λ.The flux across the jth barrier is proportional to c_{j-1}. So the flux over the jth barrier is assumed to be:

$$J_j = \lambda\left(\, k_{j-1}c_{j-1} - k_{-j}c_j\right) \qquad (6.15)$$

The total flux is the sum of fluxes across all the barriers:

$$J = \frac{\lambda k_0\left(c_0 - c_n\dfrac{k_{-1}\dots k_{-n}}{k_0\dots k_{n-1}}\right)}{1 + \dfrac{k_{-1}}{k_1} + \dfrac{k_{-1}k_{-2}}{k_1k_2} + \dots + \dfrac{k_{-1}\dots k_{-(n-1)}}{k_1\dots k_{n-1}}} \qquad (6.15)$$

We consider $n \to \infty$ and there is no barrier height difference through the membrane:

$$J = \frac{D_X}{L}.\nu.\frac{c_0 - c_n e^{-\nu}}{1 - e^{-\nu}} \qquad (6.16)$$

Here D_X is the diffusion coefficient ($D_X = k_{0(V=0,T=T_0)}\lambda^2$) over the membrane in the absence of electric or thermal induction and L is the width of the membrane.

In conclusion, for voltage sensitive and some channel types of TRP family, the flux of ion X can be explained by:

$$J = P_X.\nu.\frac{[X]_{in} - [X]_{out}e^{-\nu}}{1 - e^{-\nu}} \qquad (6.17)$$

That is very similar with the GHK equation explained by Goldman-Hodgkin-Katz, but the value of ν is determined by taking account the effect of temperature on the enthalpy and entropy of the system.

Therefore the current is:

$$I = P_X z_X F.\nu.\frac{[X]_{in} - [X]_{out}e^{-\nu}}{1 - e^{-\nu}} \quad , \quad \nu = \frac{\Delta C_P(T - T_0)}{RT} + \frac{zFV}{RT} - \frac{\Delta C_P}{R}\ln\left(\frac{T}{T_0}\right) \qquad (6.18)$$

With time constant:

$$\tau = \frac{P_{open}}{\alpha} \qquad (6.19)$$

And activation and deactivation rates[20,87]:

$$\alpha = \exp\left(-\frac{\Delta H_0}{RT} - \frac{\Delta C_P(T - T_0)}{RT} - \frac{\delta zFV}{RT} + \frac{\Delta S_0}{R} + \frac{\Delta C_P}{R} ln\left(\frac{T}{T_0}\right)\right) \qquad (6.20)$$

$$\beta = \exp\left(\frac{\Delta H_0}{RT} + \frac{\Delta C_P(T - T_0)}{RT} + \frac{(1-\delta)zFV}{RT} + \frac{\Delta S_0}{R} - \frac{\Delta C_P}{R} \ln\left(\frac{T}{T_0}\right)\right) \qquad (6.21)$$

That k_0 is the frequency factor, ΔH_0 and ΔS_0 are the initial enthalpy and entropy and δ is the fraction of ions that pass through the channel.

Eq (6.11) is similar to the relation used to describe the dependence of the voltage gated channels. In V-gated channels, changing the membrane potential leads the movement of channel protein and changing the state of the channel. Here, we focus on the work that electric energy consumes to activate the voltage gated channels:

$$lnP_{open} = -\frac{zF\left(V - V_{\frac{1}{2}}\right)}{RT} \qquad (6.22)$$

Where $V_{\frac{1}{2}}$ is the half activate voltage ($V_{\frac{1}{2}} = \frac{\Delta G_{V=0}}{zF}$) [3,4] that includes the contribution of temperature dependency of voltage gated channels. Using Transition state theory and Eyring equation we can correlate the temperature changes to thermodynamic of the system [33,35]. Nevertheless, it does not describe the dependence of transition state theory to membrane voltage. A number of researches have done to produce an explanation for the contribution of voltage on the enthalpy and entropy of the system [33,94,95]. Using transition state theory parameters, the voltage dependence of Na_V channels[96-99], Ca_V channels[96,100-103], k_V channels [94,97,102,104-109] and other types of voltage gated channels is described.

Since we consider the channel as an energy barrier, we can use Eq 6.10 to express the contribution of temperature on gating probability. Therefore, Eq 6.12 can be used also for voltage gated channels.

Conditions

This model uses basic physics roles. The concept is simple: How much energy does an ion need to open the barrier. Since we can consider all types of the channels as gating barrier(s), it is possible to use this model for mathematical explanation of any channel dynamics. Each physical stimuli such as changing the pressure or PH or exposure of radiation, changes the enthalpy and entropy of the system. Since, the opening probability of the channel is related to the Gibbs energy, it is possible to calculate theoretically the effect of each physical input on the opening probability of a channel.

In channels that sensations happen by phase transition of lipid membrane or conformational transition of the channel protein structures, these phenomenon change the enthalpy and entropy of the system. Therefore, these gating processes also can be studied by our model by calculating the energy required for an ion to provide the conformation or transition energy to open the barrier.

Presentation of the model for TRPV1 and voltage gated sodium and potassium channels is only an example for application of this model. In our calculations for TRPV1, we only considered the variation of two inputs: voltage and temperature. However, it is possible to measure the effect of other stimulus.

Some types of channels such as TRPV1, are multiple gating channels. This model can offer expression for two conditions. First, the simplest expression is to present an overall estimation in energy, enthalpy and entropy of all barriers in a single channel. In this case two state of open-close system is considered. The second case is finding the changes in Gibbs energy over each barrier in a single channel. Since first and second roles of thermodynamic is universal, the explanations for both cases is correct theoretically.

Model for TRPV1 and voltage gated sodium and potassium channels

TRPV1 is a type of TRP channels, which play important role in mammalian senses. TRPV1 channels are mainly expressed in small-diameter primary afferent neurons. They respond to many unpleased or harmful stimuli such as heat changing (t≥ $43^{o}C$)[47], low PH(<6) and also are activated by capsaicin[34,36,46,58,110]. The duration of AP caused by TRPV1 channels is about 100 times larger than the wide AP generated by voltage gated sodium channels. In ischemia and inflammation acidification increases, it is suggested that in this conditions, the temperature-threshold activation of TRPV1

decreases and AP occurs [111,112]. TRPV1s are permeable toNa^+ ,Mg^+ and mainly to Ca^{2+} ions ($\frac{P_{Ca}}{P_{Na}} = 10\ and \frac{P_{Mg}}{P_{Na}} = 5$) [36, 58]

TRPV1 is also sensitive to changes in membrane potential [20,113,114].Having similar topology with voltage gated channels, including (S1-S6)segments and reentrant pore loop between S5 and S6, TRPs are less sensitive to voltage because of the lack of a charged S4 segment[115].

The temperature sensitivity of the TRPV1 channels is a thermodynamic process and does not associated with the temperature –dependent phase transition of the channel protein structure [4]. Therefore, to explore the mechanism of this process, it is desirable to consider some basic thermodynamic roles [116]. Although experiments on gating mechanism of a single TRPV1 channel recorded multiple open and closed sates[89] for simplicity, we consider two state model for a voltage gated channel with correlated opening and closing rates $\alpha\ and\ \beta$ respectively [20,87].

On the other hand, voltage dependency of the voltage gated channels can be expressed by thermodynamic roles. According to these explanations, the voltage course of considered functions has exponential forms. The temperature dependence of the considered functions is described by Q_{10} parameter, which is a nominal function. However, experimental results showed that using this parameter, some unignorabl errors happen in describing the processes. Controlling the temperature dependence by thermodynamical expressions links the activation energy andQ_{10}.

Since fitting the processes to the most principled functions is likely to minimize errors, it is desirable to base the form of voltage gated and temperature gated functions as much as possible on the thermodynamic theories [94].

We plot the changes in the opening probability due to changes of T or V for TRPs ad voltage gated Na_V and K_V channels and compare the effect of considered parameters on them.

For Na_V and K_V channels $Q_{10} \approx 3$ [5] and for TRP channels $Q_{10} \approx 20$ [53].we set T_0 to $273 + 25^oC = 298\ K$, rest potential to -70 mV.

We can estimate the heat capacity for Na_V and K_V channels using eq (6.13). We ignore the voltage dependent term ($-\frac{zF\mathrm{V}}{RT}$) and use the approximation for the logarithmic term ($\ln\left(\frac{T}{T_0}\right) \approx 1 - \frac{T_0}{T} + (\frac{T_0}{T})^2$) we have:

$$lnP_{open} = lnP_{i,open} - \frac{\Delta C_P}{R}(1 - \frac{T_0}{T}) + \frac{\Delta C_P}{R}(1 - \frac{T_0}{T} + \left(\frac{T_0}{T}\right)^2) \quad (6.23)$$

lnk_0 is the sum of initial entropy and enthalpy terms.

$$\ln(\frac{P_{open}}{P_{i,open}}) = \frac{\Delta C_P}{R}(\frac{T_0}{T})^2 \quad (6.24)$$

Q_{10} is the ratio $(\frac{P_{open}}{P_{i,open}})$. Therefore it is possible to calculate ΔC_P from Q_{10} :

$$\text{Ln}\ (Q_{10}) = \frac{\Delta C_P}{R}(\frac{T_0}{T_0+10})^2 \quad (6.25)$$

A typical value for this ratio for Na_V and K_V is 3.8 [5] but Hodgkin et al. (1952) recorded the value to be 3.and T=$T_0 + 10$. According to Rosen [117], the value for Q_{10} is different for sodium channels in 23-28^oC and in 29-37^oC. For the membrane voltage of -70 mV and in the temperature interval of 29-37^oC the value for Q_{10} equals to about 3.8.

So for voltage gated sodium and potassium channels at $T_0 = 25^0C$ the heat capacity is $\Delta C_P \approx 250\ \left(\frac{cal}{mol.K}\right) * 4.184 \times 10^6(\frac{mJ}{cal})$ that is about 1/8 of TRP heat capacitance. The effective charge of sodium channels is about 6[118,119].

Eq (6.13) enables us to compare the reaction of voltage gated and TRP channels to thermal and electrical stimulation. To study the effect of temperature, we first consider that stimulation occurs only by changing the membrane temperature and not the voltage. Fig 6.1 compares the kinetics of Na_V , K_V and TRP channels under thermal stimulation. It can be seen that the activation probability in all cases increased, but activation probability for TRPV1 remained at higher rate throughout the stimulation period.
Contribution of temperature in activation probability of Na_V , K_V is similar because their heat capacities are considered to have ignorable difference. At the room temperature, the activation probability of voltage gated channels is not considerable, but it increases continuously as the temperature reaches higher values. Although according to Eq (6.13), the rates for TRP and voltage gated channels follow similar pattern, the probability of activation increased quite sharply from about 8 at T=273 K to about 35 at 393 K. This is because the heat capacity of TRPs are assumed to be 8 times larger than voltage gated channels. Thus, they are more sensitive to the changes in the temperature of the membrane.

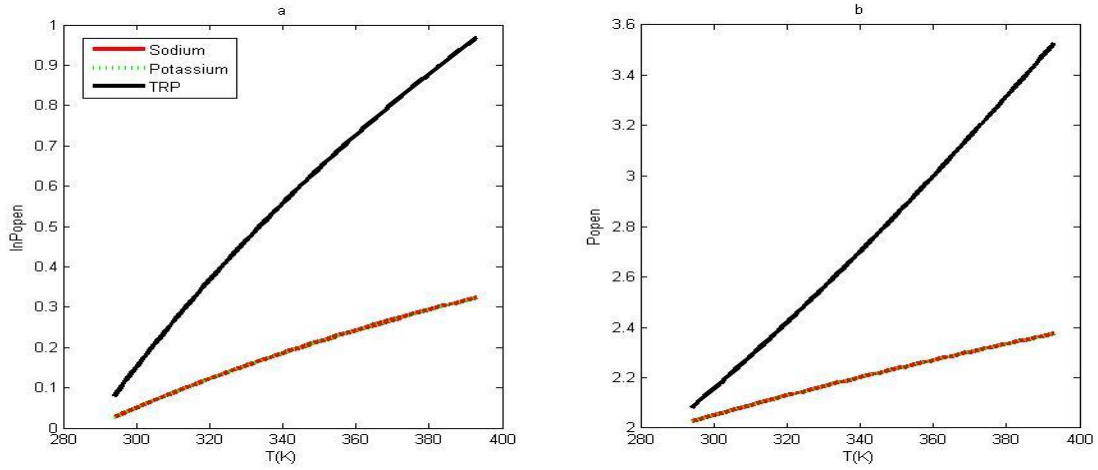

Fig 6. 1 contribution of temperature (in Kelvin) in the changes in activation probability of temperature sensitive TRP and voltage gated Na_V and K_V channels.

Voltage is the other parameter that is considered to affect the kinetics of voltage gated and TRP channels. Fig 6.2 compares the activation probability of Na_V , K_V and TRP channels at constant temperature. It can be seen that the value of activation probability in all three cases is currently declining as the membrane voltage is increasing. Overall, the activation probability of sodium channels is far higher than that for the remaining channels (Fig 6.2.b) so the correlated graphs coincide each other. This is because the effective charge of the sodium channels is assumed to be around 6, which is 3 and 12 times higher than that for potassium and TRPs respectively.

When we increase the temperature, in fact, we provide a fraction of energy required to come over the barrier energy, the rest of the energy will be provided by electric energy. As the temperature increases, less amount of voltage is needed for ion to pass through a channel. Since each channel requires smaller amount of energy to activate in higher temperatures, the injected electric energy is consumed to activate larger number of channels. This is the reason that the rate of activation is larger in higher temperatures.

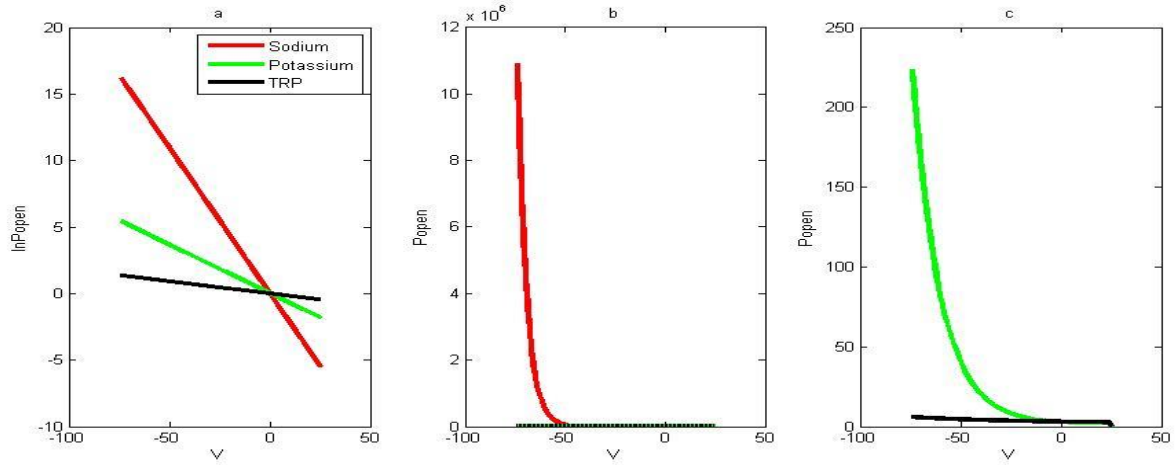

Fig 6. 2 The activation probability of Na_V , K_V and TRP channels are compared. A) the logarithmic graph lines for the activation probability of the considered channels. B) The activation probability of sodium channels is much higher in the negative membrane potentials. C) comparison between the activation probability of K_V and TRP channels

Chapter 7

Conclusions & Discussion

The purpose of this research is to develop methods for measuring the parameters contribute to generate signals when nano-labeled neuron is heated under exposition of magnetic field. We provide mathematical and computational analyses to measure the contribution of voltage gated and TRPV1 channels in the generation of AP.

Conclusions

In this study, we evaluated the involvement of temperature on dynamics of voltage gated and Temperature Resistor Potential, member V, number1 (TRPV1) channels. To approach this goal, we used NEURON software that is one of the important programing environments for simulations of nervous system behavior. This software is used in several important neuroscience studies such as Human Brain Project (HBP).

In our simulations, first, voltage gated potassium and sodium channels are distributed on a single soma by inserting Hodgkin and Huxley (hh2) model for mammalian. Behavior of these channels under electrical stimulations (using IClamp and VClamp stimulation techniques) is studied at various membrane temperatures. Results show that alteration of temperature increases the rate of channels dynamic. Notably the pattern of changes in potassium gate number at $43^{o}C$ (the temperature that TRPV1 channels produce AP) is significantly different from the patterns generated in other temperatures.

Secondly, we used the expression suggested by Voets et .al explaining the effect of voltage on temperature sensitive TRPV1 channels [4] to construct a computational model for voltage sensitivity of TRPV1s in NEURON environment. We simulated the APs produced at different temperatures by Na_V , k_V ,Ca_V and TRPV1 channels and compare with simulations when only voltage gated channels are inserted. Results show that existence of TRPV1 channels leads generation of a spike that does not occur in the case that only voltage gated channels are inserted. According to these results, firing rate increases with temperature, but the spikes width does not change significantly. In addition, only in the range of temperature between 43 to $52^{o}C$, high temperature causes spike(s), even without electrical stimulation.

Since magnetic stimulation of neurons is effective only when it is converted to thermal energy by magnetic nano particles, the most important issue in this type of stimulation is

the involvement of temperature on behavior of membrane channels. Therefore, the information of these simulations can be used to define the magnetic stimulation protocol, by providing insights. For example, it is possible to measure the effect of temperature(and thus the effect of magnetic field) on duration, current threshold, gating numbers etc. by our analyses.

Finally, this thesis proposed a mathematical model to express the effect of arbitrary inputs on gating of ionic channels. We used basic thermodynamic rules to express channel behavior. According to the transition state theory, the channel is considered as a single or a number of barriers. In the case that a selective ion provides the required energy, the channel activates and ion passes through the gate. The amount of this energy- that is described as Gibbs energy- is specific for each type of ionic channel and is dependent on environment condition. It includes the contribution of enthalpy and entropy on the system of the channel and its environment. As the physical stimulations change the entropy and/or enthalpy of the system, it is possible to calculate their effect on gating dynamics by this expression.

This model suggests a single expression for effect of different inputs on different types of channels. We applied this model on TRPV1 and voltage gated channels to compare the effect of temperature and voltage on them. Results show that in voltage-gated channels, the dependence of Gibbs energy on voltage is larger than the temperature. Thus, they are affected highly by electrical stimulations. However, in TRPV1 channels, the barrier energy depends strongly on the temperature than the voltage; therefore, thermal energy is more effective on their behavior.

Investigation of this model will enable the scientists to study and discover the effect of changes in environment on nervous system.

Discussion

The goal of this study is to evaluate the neuronal processes occur in the magnetic stimulation of the nano—labeled neurons. Since for effective stimulation, magnetic energy is converted to thermal energy by the labeled nanoparticles, the most important parameter contributed in this type of stimulation is temperature.

Experimental records show that magnetic stimulation results in an action potential at temperature range of 40-43^oC that is the range that TRPV1 channels are activated. To find the contribution of TRPV1 channels in gating processes, we provided a programming model using NEURON environment. With this model, it is possible for the scientists to measure the contribution of TRPV1 channels in different signaling processes.

The neural modeling approach proposed evaluates the function of TRPV1 channels under electrical stimulations at different membrane temperatures. This model is the first construction used to simulate the ionic flux through TRPV1 channels. Using this new model, it is possible to design several simulations to study the effect of temperature on the function of TRPV1 channels under electrical stimulation. However, other channels may also involve in signaling process that can affect the rate, period etc. Therefore, we also analyzed the behavior of voltage gated $Na_V, k_V \; and \; Ca_V$ channels and compared signaling condition when the TRPV1 channels are distributed in the membrane.

Our TRPV1 model describe these channel function under electrical stimulation at different fixed temperatures. Nevertheless, it does not describe the gating process of TRPV1 channels when the membrane temperature changes (without involving electrical stimulation). The new mathematical model that we suggested for the contribution of temperature on opening probability of channels enables us to calculate the effect of heating phenomenon.

In the ne, thermodynamic model, mathematical expressions are proposed for the first time to measure the ionic flux generated by heating the membrane. In addition, this expression explains the effect of temperature and voltage on the ionic flux through voltage gated and temperature sensitive TRPV1 channels. This means that using this formula, it is possible to construct devices to stimulate and treat the nervous system by temperature. In addition, this expression can be important for devices used for electrical stimulation therapies, in the context of deep brain stimulation or pain.

Further research

The following list presents a compilation of ideas, and future directions that would be very interesting to pursue,and can benefit from the work developed in this thesis:

1. This research evaluates the effect of physical inputs on the function of voltage gated and TRPV1 channels on a single soma. Further study is required to measure the propagation of the spikes throughout a neuron or a number of neurons.

2. COMSOL software could be used to simulate the thermal stimulation condition in 2-D scale. We consider the soma as a cylinder and the nano particles as small heating sources. A dense distribution of nano particles in one side of cell results in temperature difference in different soma parts.

3. The simulations designed in this thesis by NEURON software can also be studied experimentally.

4. Since the mathematical model is constructed theoretically by considering a heat capacity for the channel, several experiments are required to find the value for related parameters. Experimental data about TRPV1 channels was recorded only for a fixed initial temperature and was not changed during the electrical stimulations. In some other experiments that thermal stimulation causes TRPV1 impulses, the parameters required to indicate in our model was not measured or the difference between the values of a parameter were high because of different environmental condition of TRPV1 channels.

5. It is possible to use the computational model introduced in this study to explore possible therapeutic strategies to address diseases and pathologies such as pain, Parkinson, among other neurological diseases.

References

1. *Huang, H., et al., Remote control of ion channels and neurons through magnetic-field heating of nanoparticles. Nat Nanotechnol, 2010.* ***5****(8): p. 602-6.*
2. *Hodgkin, A.L. and A.F. Huxley, A quantitative description of membrane current and its application to conduction and excitation in nerve. J Physiol, 1952.* ***117****(4): p. 500-44.*
3. *Carnevale, F. and F. Capacci, [The occupational carcinogenic risk at present time in Italy. Continuity and discontinuity with the past: emerging issues and perspectives]. Epidemiol Prev, 2009.* ***33****(4-5 Suppl 2): p. 6-16.*
4. *Voets, T., et al., The principle of temperature-dependent gating in cold- and heat-sensitive TRP channels. Nature, 2004.* ***430****(7001): p. 748-54.*
5. *Sterratt, D., et al., Principles of Computational Modelling in Neuroscience. 2011: Cambridge University Press.*
6. Goldman D. E., Potential, impedance, and rectification in membranes. 1943: *J. Gen.Physiol.* 27, 37–
7. Hodgkin A. L. and Katz B. (1949). The effect of sodium ions on the electrical activity of the giant axon of the squid. *J. Physiol.* 108, 37–77.
8. *Kandel, E., Principles of Neural Science, Fifth Edition. 2013: McGraw-Hill Education.*
9. Nernst W. (1888). Zur Kinetik der Lösung befindlichen Körper: Theorie der Diffusion. *Z. Phys. Chem.* 2, 613–637.
10. Fick A. (1855). Über Diffusion. *Ann. Phys. Chem.* 94, 59–86.
11. *Planck M. (1890). Über die Erregung von Electricität und Wärme in Electrolyten. Ann. Phys. Chem. Neue Folge 39, 161–186.*
12. *Hodgkin, A. L., et al. (1952). "Measurement of current-voltage relations in the membrane of the giant axon of Loligo." J Physiol 116(4): 424-448.*
13. *Hodgkin, A. L. and A. F. Huxley (1952). "The components of membrane conductance in the giant axon of Loligo." J Physiol 116(4): 473-496.*
14. *Hodgkin, A. L. and A. F. Huxley (1952). "Currents carried by sodium and potassium ions through the membrane of the giant axon of Loligo." J Physiol 116(4): 449-472.*
15. *Hodgkin, A. L. and A. F. Huxley (1952). "The dual effect of membrane potential on sodium conductance in the giant axon of Loligo." J Physiol 116(4): 497-506.*
16. *Hodgkin, A. L. and A. F. Huxley (1952). "A quantitative description of membrane current and its application to conduction and excitation in nerve." J Physiol 117(4): 500-544.*
17. *Marmont M. (1949). Studies on the axon membrane. J. Cell. Comp. Physiol. 34,351–382*
18. *Cole K. S. (1968). Membranes, Ions, and Impulses: A Chapter of Classical Biophysics(University of California Press, Berkeley).*
19. *Siciliano, Ryan, The Hodgkin-Huxley Model.2012: Conference Proceedings*
20. *Hille, B. (2001). Ionic Channels of Excitable Membranes, Sinauer.*
21. *Rodriguez, B. M., et al. (1998). "Voltage gating of Shaker K+ channels. The effect of temperature on ionic and gating currents." J Gen Physiol 112(2): 223-242.*

22. *Reuter, H. (1979). "Properties of two inward membrane currents in the heart." Annu Rev Physiol 41: 413-424.*

23. *Tsien, R. W. (1983). "Calcium channels in excitable cell membranes." Annu Rev Physiol 45: 341-358.*

24. *Catterall, W. A. (1991). "Excitation-contraction coupling in vertebrate skeletal muscle: a tale of two calcium channels." Cell 64(5): 871-874.*

25. *Tanabe, T., et al. (1993). "Structure and function of voltage-dependent calcium channels from muscle." Ann N Y Acad Sci 707: 81-86.*

26. *Tsien, R. W., et al. (1988). "Multiple types of neuronal calcium channels and their selective modulation." Trends Neurosci 11(10): 431-438.*

27. *Dunlap, K., et al. (1995). "Exocytotic Ca2+ channels in mammalian central neurons." Trends Neurosci 18(2): 89-98.*

28. *Catterall, W. A. (2011). "Voltage-gated calcium channels." Cold Spring Harb Perspect Biol 3(8): a003947.*

29. *Johnston, D. and S. M.-s. Wu (1995). "Foundations of cellular neurophysiology.*

30. *Hodgkin A. L. and Katz B. (1949). The effect of sodium ions on the electrical activity of the giant axon of the squid. J. Physiol. 108, 37–77.*

31. *Arrhenius S. (1889). Über die Reaktionsgeschwindigkeit bei der Inversion von Rohrzucker in Säuren. Z. Phys. Chem. 4, 226–248.*

32. *Eyring H. (1935). The activated complex in chemical reactions. J. Chem. Phys. 3, 107–115.*

33. *Pollak E. and Talkner P. (2005). Reaction rate theory: what it was, where is it today, and where is it going? Chaos 15, 26116*

34. Julius, D. & Basbaum, A. I. Molecular mechanisms of nociception. Nature 413, 203–210 (2001).

35. *Patapoutian, A., Peier, A. M., Story, G. M. & Viswanath, V. ThermoTRP channels and beyond:mechanisms of temperature sensation. Nature Rev. Neurosci. 4, 529–539 (2003).*

36. *Clapham, D. E. TRP channels as cellular sensors. Nature 426, 517–524 (2003).*

37. *Voets, T. & Nilius, B. TRPs make sense. J. Membr. Biol. 192, 1–8 (2003).*

38. *(2006). "Ca2+ Signaling, TRP Channels, and Endothelial Permeability." Microcirculation 13(8): 693-708.*

39. *Cosens, D. J. and A. Manning (1969). "Abnormal electroretinogram from a Drosophila mutant." Nature 224(5216): 285-287.*

40. *Minke, B., et al. (1975). "Induction of photoreceptor voltage noise in the dark in Drosophila mutant." Nature 258(5530): 84-87.*

41. *Watanabe, H. et al. Heat-evoked activation of TRPV4 channels in a HEK293 cell expression system and in native mouse aorta endothelial cells. J. Biol. Chem. 277, 47044–47051 (2002).*

42. *Gu¨ler, A. D. et al. Heat-evoked activation of the ion channel, TRPV4. J. Neurosci. 22, 6408–6414 (2002).*

43. *Xu, H. et al. TRPV3 is a calcium-permeable temperature-sensitive cation channel. Nature 418,181–186 (2002).*

44. *Smith, G. D. et al. TRPV3 is a temperature-sensitive vanilloid receptor-like protein. Nature 418, 186–190 (2002).*
45. *Peier, A. M. et al. A heat-sensitive TRP channel expressed in keratinocytes. Science 296, 2046–2049(2002).*
46. *Caterina, M.J., et al., The capsaicin receptor: a heat-activated ion channel in the pain pathway. Nature, 1997. 389(6653): p. 816-24.*
47. *Caterina, M. J. (2007). "Transient receptor potential ion channels as participants in thermosensation and thermoregulation." Am J Physiol Regul Integr Comp Physiol 292(1): R64-76.*
48. *Caterina, M.J., et al., A capsaicin-receptor homologue with a high threshold for noxious heat. Nature, 1999. 398(6726): p. 436-41.*
49. *McKemy, D. D., Neuha¨usser,W.M. & Julius, D. Identification of a cold receptor reveals a general role for TRP channels in thermosensation. Nature 416, 52–58 (2002).*
50. *Peier, A. M. et al. A TRP channel that senses cold stimuli and menthol. Cell 108, 705–715 (2002).*
51. *Story, G. M. et al. ANKTM1, a TRP-like channel expressed in nociceptive neurons, is activated by cold temperatures. Cell 112, 819–829 (2003).*
52. *Voets, T., et al., The principle of temperature-dependent gating in cold- and heat-sensitive TRP channels. Nature, 2004. 430(7001): p. 748-54.*
53. *Clapham, D.E. and C. Miller, A thermodynamic framework for understanding temperature sensing by transient receptor potential (TRP) channels. Proc Natl Acad Sci U S A, 2011. 108(49): p. 19492-7.*
54. *A.M. Phillips, A. Bull, L.E. Kelly, Identification of a Drosophila gene encoding a calmodulin-binding protein with homology to the trp phototransduction gene, Neuron 8 (1992) 631–642.*
55. *Minke, B. and B. Cook (2002). "TRP channel proteins and signal transduction." Physiol Rev 82(2): 429-472.*
56. *Montell, C. (2005). "The TRP superfamily of cation channels." Sci STKE 2005(272): re3.*
57. *Nilius, B. and T. Voets (2005). "TRP channels: a TR(I)P through a world of multifunctional cation channels." Pflugers Arch 451(1): 1-10.*
58. *S.F. Pedersen, G. Owsianik, B. Nilius, TRP channels: an overview, Cell Calcium 38 (2005) 233–252*
59. *T. Voets, K. Talavera, G. Owsianik, B. Nilius, Sensing with TRP channels, Nat. Chem. Biol. 1 (2005) 85–92.*
60. *George, M. S., E. M. Wassermann, and R. M. Post. 1996. Transcranial magnetic stimulation: a neuropsychiatric tool for the 21st century.J. Neuropsychiatry Clin. Neurosci. 8:373–382.*
61. *Hallett, M. 2000. Transcranial magnetic stimulation and the human brain. Nature. 406:147–150.*
62. *Sack, A.T. and D.E. Linden, Combining transcranial magnetic stimulation and functional imaging in cognitive brain research: possibilities and limitations. Brain Res Brain Res Rev, 2003. 43(1): p. 41-56.*
63. *Hodgkin, A. L., and W. A. Rushton. 1946. The electrical constants of a crustacean nerve fiber. Proc. R. Soc. Lond. B. Biol. Sci. 133:444–479.*
64. *Roth, B. J., and P. J. Basser. 1990. A model of the stimulation of a nerve fiber by electromagnetic induction. IEEE Trans. Biomed. Eng. 37:588–597.*
65. *Irwin, D.A. and C.S. Rebert, Slow potential changes in cat brain during classical appetitive conditioning of jaw movements using two levels of reward. Electroencephalogr Clin Neurophysiol, 1970. 28(2): p. 119-26.*
66. *Malmivuo, J. and R. Plonsey (1995). Bioelectromagnetism: principles and applications of bioelectric and biomagnetic fields, Oxford University Press, USA.*
67. *Rotem, A. and E. Moses (2008). "Magnetic Stimulation of One-Dimensional Neuronal Cultures." Biophysical Journal 94(12): 5065-5078.*

68. *Meyer, E., C. O. Muller, and P. Fromherz. 1997. Cable properties of dendrites in hippocampal neurons of the rat mapped by a voltagesensitive dye. Eur. J. Neurosci. 9:778–785.*
69. *Feinerman, O., M. Segal, and E. Moses. 2005. Signal propagation along unidimensional neuronal networks. J. Neurophysiol. 94:3406–3416.*
70. *Barker, A. T., C. W. Garnham, and I. L. Freeston. 1991. Magnetic nerve stimulation: the effect of waveform on efficiency, determination of neural membrane time constants and the measurement of stimulator output. Electroencephalogr. Clin. Neurophysiol. Suppl. 43:227–237.*
71. *Rovira, C., and Y. Ben-Ari. 1999. Developmental study of miniature IPSCs of CA3 hippocampal cells: modulation by midazolam. Brain Res. Dev. Brain Res. 114:79–88.*
72. *Tuckwell, H. C. 1988. Introduction to Theoretical Neurobiology. Cambridge University Press, Cambridge, New York.*
73. *http://neuron.duke.edu/*
74. *https://www.humanbrainproject.eu/ [HBP2012] The Human Brain Project,*
75. *https://www.humanbrainproject.eu/documents/10180/17648/TheHBPReport_LR.pdf*
76. *Hines, M. L. and N. T. Carnevale (2001). "NEURON: a tool for neuroscientists." Neuroscientist 7(2): 123-135.*
77. *http://web.mit.edu/neuron_v7.3/nrntuthtml/tutorial/tutA.html*
78. *David Sterratt, Neural Computation Practical 1: Getting to grips with Neuron and passive properties*
79. *David Sterratt, Neural Computation 2001/2002 Practical 2: The Hodgkin-Huxely model*
80. *http://web.mit.edu/neuron_v7.3/nrntuthtml/tutorial/tutB.html*
81. *Chapman, D. (1975). "Fluidity and phase transitions of cell membranes." Biomembranes 7: 1-9.*
82. *Kimura, J. E. and H. Meves (1979). "The effect of temperature on the asymmetrical charge movement in squid giant axons." J Physiol 289: 479-500.*
83. *Schauf, C. L. (1973). "Temperature dependence of the ionic current kinetics of Myxicola giant axons." J Physiol 235(1): 197-205.*
84. *Schwarz, W. (1979). "Temperature experiments on nerve and muscle membranes of frogs. Indications for a phase transition." Pflugers Arch 382(1): 27-34.*
85. *van Lunteren, E., et al. (1993). "Effects of temperature on calcium current of bullfrog sympathetic neurons." J Physiol 466: 81-93.*
86. *Yang, F. & Zheng, J.Aldrich, R. (Ed.) High temperature sensitivity is intrinsic to voltage-gated potassium channels, eLife, eLife Sciences Publications, Ltd, 2014, 3, e03255*
87. *Sigworth, F. J. Voltage gating of ion channels. Q. Rev. Biophys. 27, 1–40 (1994).*
88. *Dickerson, R.E. and I. Geis, Chemistry, matter, and the universe: an integrated approach to general chemistry. 1976: Addison Wesley Longman.*
89. *Liu, B., Hui, K. & Qin, F. Thermodynamics of heat activation of single capsaicin ion channels VR1.Biophys. J. 85, 2988–3006 (2003).*
90. *Baldwin RL (1986) Temperature dependence of the hydrophobic interaction in protein folding. Proc Natl Acad Sci USA 83:8069–8072.*
91. *Kauzmann W (1959) Some factors in the interpretation of protein denaturation. Adv Prot Chem 14:1–63.*
92. *Schellman JA, Lindorfer M, Hawkes R, Grutter M (1981) Mutations and protein stability. Biopolymers 20:1989–1999.*
93. *Privalov PL (1997) Thermodynamics of protein folding. J Chem Thermo 29:447–474.*

94. *Borg-Graham L. J. (1989). Modelling the somatic electrical response of hippocampal pyramidal neurons. Technical Report AITR-1161, MIT AI Laboratory.*
95. *Irvine L.A., Jafri M. S. and Winslow R. L. (1999). Cardiac sodium channel Markov model with temperature*
96. *Magee J.C. and Johnston D. (1995). Characterization of single voltage-gated Na+ and Ca2+ channels in apical dendrites of rat CA1 pyramidal neurons. J. Physiol.487, 67–90.*
97. *Hoffman D.A., Magee J.C., Colbert C.M. and Johnston D. (1997). K+ channel regulation of signal propagation in dendrites of hippocampal pyramidal neurons. Nature 387, 869–875.*
98. *Magistretti J. and Alonso A. (1999). Biophysical properties and slow voltage-dependent inactivation of a sustained sodium current in entorhinal cortex layer-II principal neurons: a whole-cell and single-channel study. J. Gen. Physiol. 114, 491–509.*
99. *Köhling R. (2002). Voltage-gated sodium channels in epilepsy. Epilepsia 43, 1278–1295.*
100. *Jaffe D. B., Ross W.N., Lisman J. E., Lasser-Ross N., Miyakawa H. and Johnston D. (1994). A model for dendritic Ca2+ accumulation in hippocampal pyramidal neurons based on fluorescence imaging measurements. J. Neurophysiol. 71, 1065–1077.*
101. *Fox A. P., Nowycky M.C. and Tsien R.W. (1987). Kinetic and pharmacological properties distinguishing three types of calcium currents in chick sensory neurones. J. Physiol. 394, 149–172.*
102. *Gillies A. and Willshaw D. (2006). Membrane channel interactions underlying rat subthalamic projection neuron rhythmic and bursting activity. J. Neurophysiol. 95, 2352–2365.*
103. *Brown A.M., Schwindt P.C. and Crill W.E. (1993). Voltage dependence and activation kinetics of pharmacologically defined components of the high-threshold calcium current in rat neocortical neurons. J. Neurophysiol. 70, 1530–1543.*
104. *Wigmore M.A. and Lacey M.G. (2000). A Kv3-like persistent, outwardly rectifying, Cs+-permeable, K+ current in rat subthalamic nucleus neurones. J. Physiol. 527, 493–506.*
105. *Heinemann S.H., Rettig J., Graack H.R. and Pongs O. (1996). Functional characterization of Kv channel beta-subunits from rat brain. J. Physiol. 493 (3), 625–633.*
106. *Halliwell J.V. and Adams P.R. (1982). Voltage-clamp analysis of muscarinic excitation in hippocampal neurons. Brain Res. 250, 71–92.*
107. *Storm J. F. (1988). Temporal integration by a slowly inactivating K+ current in hippocampal neurons. Nature 336, 379–381.*
108. *Sah P., Gibb A. J. and Gage P.W. (1988). Potassium current activated by depolarization of dissociated neurons from adult guinea pig hippocampus. J. Gen. Physiol. 92, 263–278.*
109. *Borg-Graham L. J. (1999). Interpretations of data and mechanisms for hippocampal pyramidal cell models. In Cerebral Cortex, Volume 13: Models of Cortical Circuits, eds P. S. Ulinski, E.G. Jones and A. Peters (Plenum Publishers, New York), pp. 19–138.*
110. *Moran, M.M., H. Xu, and D.E. Clapham, TRP ion channels in the nervous system. Curr Opin Neurobiol, 2004. 14(3): p. 362-9.*
111. *Tominaga, M., et al. (1998). "The cloned capsaicin receptor integrates multiple pain-producing stimuli." Neuron 21(3): 531-543.*
112. *Hellwig, N., et al. (2004). "TRPV1 acts as proton channel to induce acidification in nociceptive neurons." J Biol Chem 279(33): 34553-34561.*
113. *Gunthorpe, M. J., Harries, M. H., Prinjha, R. K., Davis, J. B. & Randall, A. Voltage- and timedependent properties of the recombinant rat vanilloid receptor (rVR1). J. Physiol. (Lond.) 525,747–759 (2000).*

114. Vlachova, V. et al. Functional role of C-terminal cytoplasmic tail of rat vanilloid receptor 1. J.Neurosci. 23, 1340–1350 (2003).

115. ?

116. Collins, C.A. and E. Rojas, Temperature dependence of the sodium channel gating kinetics in the node of Ranvier. Q J Exp Physiol, 1982. 67(1): p. 41-55.

117. Rosen, A.D., Nonlinear temperature modulation of sodium channel kinetics in GH(3) cells. Biochim Biophys Acta, 2001. 1511(2): p. 391-6.

118. Plakhova, V.B., et al. Infrared light irradiation diminishes effective charge transfer in slow sodium channel gating system. in Fourth International Workshop on Nondestructive Testing and Computer Simulations in Science and Engineering. 2001. International Society for Optics and Photonics.

119. Behrens, M.I., et al., Batrachotoxin-modified sodium channels from squid optic nerve in planar bilayers. Ion conduction and gating properties. The Journal of general physiology, 1989. 93(1): p. 23-41.